Universidade de Aveiro Departamento de Química
2017

Universidad Autónoma de Madrid Departamento de Química Orgánica
2017

Wioleta Borzęcka

Synthesis of novel photosensitizer-silica nanoparticle hybrids for controlled $^1O_2$ release in cancer photodynamic therapy

Síntese de novos híbridos do tipo fotossensibilizador-nanopartículas de sílica para libertação controlada de $^1O_2$ para tratamento de cancro por terapia fotodinâmica

Síntesis de nuevos materiales híbridos basados en fotosensibilizadores inmobilizados en nanopartículas de sílice para la liberación controlada de $^1O_2$ en terapia fotodinámica para el cáncer

Universidade de Aveiro Departamento de Química
2017

Universidad Autónoma de Madrid Departamento de Química Orgánica
2017

Wioleta Borzęcka

Synthesis of novel photosensitizer-silica nanoparticle hybrids for controlled $^1O_2$ release in cancer photodynamic therapy

Síntese de novos híbridos do tipo fotossensibilizador-nanopartículas de sílica para libertação controlada de $^1O_2$ para tratamento de cancro por terapia fotodinâmica

Síntesis de nuevos materiales híbridos basados en fotosensibilizadores inmobilizados en nanopartículas de sílice para la liberación controlada de $^1O_2$ en terapia fotodinámica para el cáncer

Doctoral thesis submitted to the Universidade de Aveiro and Universidad Autónoma de Madrid to fulfill the requirements to obtain the degree of Doctor of Nanosciences and Nanotechnology form Universidade de Aveiro, Doctor of Chemistry from Universidad Autónoma de Madrid and European Doctoral Degree under cotutelle agreement between both institutions. Doctoral thesis was prepared under the supervision of Professor João Paulo Costa Tomé, Associate Professor at the Centro de Química Estrutural, Instituto Superior Técnico, Universidade de Lisboa, Professor Tito Trindade, Associate Professor at the CICECO, Department of Chemistry, University of Aveiro and Professor Tomas Torres, Professor Catedrático at the Department of Organic Chemistry, Autonóma University of Madrid.

Financial support came from the FCT/MEC to QOPNA (FCT UID/QUI/00062/2013), CICECO-Aveiro Institute of Materials (FCT UID/CTM/50011/2013), IBILI (FCT UID/NEU/04539/2013) and CQE (FCT UID/QUI/0100/2013) research units, through national funds and where applicable cofinanced by the FEDER, within the PT2020 Partnership Agreement. The work was also supported by the Spanish MINECO (CTQ-2014-52869-P), Comunidad de Madrid (FOTOCARBON, S2013/MIT-2841), the Portuguese COMPETE (POCI-01-0145-FEDER-007440) and the Seventh Framework Programme (FP7-People-2012-ITN, SO2S project with grant agreement number: 316975).

To my husband, for his infinite patience.

o júri
presidente

Prof. Doutor Manuel António Assunção
Professor Catedrático e Reitor da Universidade de Aveiro

Doutor João Paulo Costa Tomé
Professor Associado – Departamento de Engenharia Química – Instituto Superior Técnico - Universidade de Lisboa

Doutor Tomás Torres Cebada
Professor Catedrático - Departamento de Química Orgânica - Universidade Autónoma de Madrid

Doutor António Jorge Dias Parola
Professor Associado com Agregação - Departamento de Química - Faculdade de Ciências e Tecnologia - Universidade Nova de Lisboa

Doutora Ana Luísa Daniel da Silva
Investigadora Auxiliar - Departamento de Química - Universidade de Aveiro

Doutora Rosa Cristina Simões Fernandes
Investigadora Auxiliar – Faculdade de Medicina – Universidade de Coimbra

Doutora Vanda Isabel Roldão Canelas Vaz Serra
Investigadora de Pós-doutoramento – Centro de Química Estrutural, Departamento de Engenharia Química – Instituto Superior Técnico - Universidade de Lisboa

Doutora Victoria Martínez Díaz
Professora Associada - Departamento de Química Orgânica - Universidade Autónoma de Madrid

agradecimentos

I would like to thank Professor João Tomé, Professor Tito Trindade and Professor Tomas Torres for their support and encouragement during my PhD studies. This work would not have been possible without you.

I would like to thank Professor Rosa Fernandes and Doctor Patrícia Pereira for their help and advice with all *in vitro* studies of my nanoparticles.

keywords Porphyrins, Phthalocyanines, Photosensitizers, Silica Nanoparticles, Photodynamic Therapy, Cancer

abstract

Cancer is one of the biggest health problem for humans. Until now, there is no efficient therapy for most cancers. An alternative method to conventional cancer treatments, including chemotherapy, radiotherapy and surgery, could be photodynamic therapy (PDT), which combines three components: a photoactive drug (photosensitizer, PS), a particular type of light and oxygen. In PDT, the severe side effects of chemotherapy or radiotherapy are minimized. However, as all clinical protocols, PDT still has some problems to solve. One of the difficulties in PDT is to find an ideal PS for the different tumors.

Recently, nanoparticle-based delivery systems have been explored as efficient vehicles to deliver PSs in PDT. In particular, silica nanoparticles (SNPs) are attracting great attention in PDT due to their biocompatibility, large surface area, controllable size formation, hydrophilic surface and ability for surface functionalization. The possibility for tumor targeting through surface modification is a key to successful cancer treatment. As such, this dissertation describes the synthesis and characterization of novel photosensitizer-silica nanoparticle hybrids for controlled singlet oxygen ($^1O_2$) release in cancer PDT. The work is divided into three chapters in which novel nanoformulations are presented as third generation PSs for PDT. In the first part, S-glycoside porphyrins (Pors) were prepared and encapsulated into SNPs by Stöber method. In the next part, the same Pors were grafted on the surface of sphere-shaped and rod-shaped mesoporous silica nanoparticles (MSNPs). Finally, NPs encapsulating phosphonate phthalocyanine (Pc) or covalently appended with Pc were prepared after slight modification of the reverse microemulsion method.

These new nanomaterials show relatively homogeneous morphological characteristics, such as size and shape. The new nanocarriers are able to produce $^1O_2$ after light irradiation and have been employed for *in vitro* studies with two human bladder cancer epithelial cell lines, HT-1376 and UM-UC-3. The results showed that the new nanoparticle-based systems could be successfully used as novel PSs in PDT of bladder cancer which is the fourth most commonly diagnosed cancer with the high rate of recurrence.

palavras-chave

Porfirinas, Ftalocianinas, Fotossensibilizadores, Nanopartículas de Sílica, Terapia Fotodinâmica, Câncer

resumo

O cancro é um dos maiores problemas de saúde para os humanos. Até agora, não há terapia eficiente para a maioria dos cancros. A terapia fotodinâmica (PDT) tem surgido como um método alternativo aos tratamentos convencionais de cancro, nomeadamente a quimioterapia, radioterapia e cirurgia. A PDT combina três componentes: uma droga fotoativa (fotossensibilizador, PS), luz e oxigênio. Os efeitos secundários observados em quimioterapia ou radioterapia são minimizados na PDT. No entanto, como em todos os protocolos clínicos, a PDT apresenta também limitações, nomeadamente a utilização de um PS aplicável a diferentes tumores.

Recentemente, as nanopartículas têm sido exploradas como veículos do PS a administrar em PDT. Em particular, as nanopartículas de sílica (SNPs) têm merecido uma especial atenção devido à sua biocompatibilidade, elevada área de superfície específica, quase monodispersidade e superfícies hidrofílicas com possibilidade de funcionalização química. Um aspeto crucial para um bem sucedido tratamento do cancro prende-se com a adequada modificação superficial vdas SNPs tendo o tumor como alvo. Como tal, esta dissertação descreve a síntese e caracterização de novos híbridos do tipo fotossensibilizador-nanopartículas de sílica para libertação controlada de oxigénio singleto ($^1O_2$) na PDT aplicada ao cancro.

O trabalho é dividido em três capítulos que descrevem nanoformulações para PDT em que o PS é de terceira geração. Na primeira parte, descreve-se a preparação de porfirinas de S-glicosídeo (Pors) e sua encapsulação em SNPs. A secção seguinte descreve a ligação dessas Pors à superfície de nanopartículas de sílica mesoporosa (MSNPs). Finalmente, descreve-se o encapsulamento de fosfonato ftalocianina (Pc) em sílica e também nanopartículas com Pc ligada covalentemente, utilizando uma adaptação do método de microemulsão inversa.

Estes novos nanomateriais apresentam características morfológicas relativamente uniformes, nomeadamente em termos de tamanho e forma. Estes sistemas apresentam capacidade para produzir $^1O_2$ após exposição à luz e foram utilizados em estudos *in vitro* envolvendo duas linhas de células epiteliais de cancro da bexiga humana, HT-1376 e UM-UC-3. Os resultados demonstram que as SNPs podem ser usados com sucesso como novos PSs em PDT de cancro da bexiga, sendo este o quarto cancro diagnosticado com a mais alta taxa de recorrência.

palabras clave

Porfirinas, Ftalocianinas, Fotosensibilizadores, Nanopartículas de Sílice, Terapia Fotodinámica, Cáncer

resumen

En los últimos años, el cáncer es uno de los principales problemas de salud para el ser humano. Hasta ahora no se ha desarrollado una terapia eficiente para la mayoría de los tipos de cáncer. Un método alternativo a las opciones convencionales de tratamiento del cáncer, como la quimioterapia, la radioterapia y la cirugía, podría ser la terapia fotodinámica (PDT), que combina tres componentes: un medicamento (fotosensibilizador o sustancia fotosensibilizadora, PS), un tipo particular de luz y oxígeno. En PDT los efectos secundarios de la quimioterapia o radioterapia se minimizan. Sin embargo, como es habitual en los protocolos clínicos de este campo, PDT todavía tiene algunos problemas por resolver. Una de las dificultades en PDT es encontrar un PS específico para los diferentes tumores.

Recientemente, las nanopartículas están siendo exploradas como vehículos para la administración de PS en PDT. Concretamente, las nanopartículas de sílice (SNPs) están atrayendo una gran atención en PDT debido a su biocompatibilidad, elevada área superficial, obtención controlada en cuanto a tamaño, poro y forma, superficie hidrófila y capacidad para la funcionalización superficial. La posibilidad de modificar la superficie del PS para dirigirse al tumor puede ser la clave del éxito en el tratamiento del cáncer. En base a esto, esta disertación describe la síntesis y caracterización de nuevos materiales híbridos basados en fotosensibilizadores immobilizados en nanopartículas de sílice para la liberación controlada de oxígeno singlete ($^1O_2$) en PDT para tratamiento de cáncer. El trabajo se divide en tres capítulos en los que se presentan nuevas nanoformulaciones como PS de tercera generación para PDT. En la primera parte, derivados *S*-glicósidos de porfirinas (Pors) fueron preparados y encapsulados en SNPs mediante el método de Stöber. En la siguiente parte, estas Pors fueron fijadas a la superficie de nanopartículas mesoporosas de sílice (MSNPs). Finalmente, ftalocianinas (Pc) funcionalizadas con grupos fosfonato fueron encapsuladas o fijadas covalentemente a NPs mediante ligeras modificaciones del método de microemulsión inversa.

Estos nuevos nanomateriales tienen una distribución de tamaños uniforme y son regulares en tamaño y forma. Además, todos ellos son capaces de producir $^1O_2$ después de la irradiación con luz. Tras su completa caracterización, se realizaron estudios in vitro con dos líneas de células epiteliales de cáncer de vejiga humana, HT-1376 y UM-UC-3. Los resultados mostraron que estos nuevos sistemas basados en nanopartículas podrían ser utilizados con éxito como nuevos PSs en PDT de cáncer de vejiga, que es el cuarto cáncer más comúnmente diagnosticado con alta tasa de recurrencia.

Abbreviations

Ad - adamantane

AlC_4Pc - tetra-substituted carboxyl aluminum phthalocyanine

AOT - bis(2-ethylhexyl)sulfosuccinate sodium salt

APS - 3-aminopropyltrimethoxysilane

APTS - 3-aminopropyltriethoxysilane

C18 - hydrocarbon octadecyltrimethoxysilane

CDI - *N,N′*-carbonyldiimidazole

Ce6 - chlorin e6

DCC - dicyclohexylcarbodiimide

DMF - *N,N*-dimethylformamide

DMSO - dimethyl sulfoxide

DOX - doxorubicin

CTAB - cetyltrimethylammonium bromide

EDC - 1-ethyl-3-(3-dimethylaminopropyl)carbodiimide

EDS - energy-dispersive X-ray spectroscopy

EPR - enhanced permeability and retention effect

FA - folic acid

FITC - fluorescein isothiocyanate

FT-IR - Fourier transform infrared spectroscopy

HP - hematoporphyrin

HPPH - 2-(1-hexyloxyethyl)-2-devinyl pyropheophorbide-a

LED - light-emitting diode

MB - methylene blue

MC 540 - merocyanine 540

MEF - metal-enhanced fluorescence

MRI - magnetic resonance imaging

MSNP - mesoporous silica nanoparticle

MSNR - mesoporous silica nanorod

MTT - 3-(4,5-dimethylthiazol-2-yl)-2,5-diphenyltetrazolium bromide

NHS - *N*-hydroxysuccinimide

NIR - near-infrared

NP - nanoparticle

NR - nanorod

ORMOSIL NPs - organically modified silica nanoparticles

Pc - phthalocyanine

PDT - photodynamic therapy

PEG - poly(ethylene glycol)

PEI - polyethylenimine

Por - porphyrin

PpIX - protoporphyrin IX

PS - photosensitizer

PTT - photothermal therapy

RITC - rhodamine isothiocyanate

ROS - reactive oxygen species

SNP - silica nanoparticle

TEM - transmission electron microscopy

TEOS - tetraethyl orthosilicate

TMPyP - meso-tetrakis(*N*-methylpyridinium-4-yl)porphyrin tetratosylated

THPMP - 3-(trihydroxylsilyl)propyl methylphosphonate

UCNPs - upconversion nanoparticles

UV-Vis - ultraviolet-visible spectroscopy

W/O - water-in-oil

VTES - vinyltriethoxysilane

ZnPc - zinc phthalocyanine

Table of Contents

CHAPTER 1: Targeting cancer cells with photoactive silica nanoparticles

Wioleta Borzęcka,[1,2,3] Tito Trindade,[2] Tomás Torres[3,4] and João Tomé[1,5]

[1]QOPNA and [2]CICECO, Department of Chemistry, University of Aveiro, 3810-193 Aveiro, Portugal; [3]Department of Organic Chemistry, Autonoma University of Madrid, 28049 Madrid, Spain; [4]IMDEA-Nanociencia, Campus de Cantoblanco, c/Faraday 9, 28049 Madrid, Spain; [5]Centro de Química Estrutural, Departamento de Engenharia Química, Instituto Superior Técnico, Universidade de Lisboa, Av. Rovisco Pais, 1049-001 Lisboa, Portugal

Keywords: Porphyrins, Phthalocyanines, Photosensitizers, Silica Nanoparticles, PDT, Cancer

Abstract: This introduction highlights recent advances in the preparation of silica nanoparticles (SNPs) functionalized with porphyrins and phthalocyanines for application in cancer photodiagnostic and photodynamic therapy (PDT). The use of photosensitizer-SNP formulations has emerged recently as new nanomedicines for cancer research owing to their unique physicochemical properties, which make them useful for photo-biomedical applications. In order to study their photobiological properties, diverse chemical strategies involving covalent and non-covalent bonding have been used to load photosensitizers in/on SNPs. This revision is an update of our previous published revision, covering the last 5 years in this hot area of photoactive nanoformulations to target and to kill cancer cells.

Chapter 1 was published in the following journal: Targeting cancer cells with photoactive silica nanoparticles, Borzęcka W., Trindade T., Torres T., Tomé J. P. C.; *Current Pharmaceutical Design*, **2016**, *22*, 6021–6038

Introduction

In recent years Nanosciences has evolved as an exciting and important scientific domains, with interdisciplinary approaches that involve topics of chemistry, biology, physics and engineering, among others. However, some of the approaches that today we recognize as belonging to Nanosciences share well-established processes identified in Nature or in conventional Science. For example, many years ago humans took advantage of nanomaterials by using them in several contexts, including therapeutic practices. Nevertheless, it is unquestionable that the progress observed in this area has opened a number of possibilities that rely, among other factors, on engineered nanoparticles with unique properties and innovative instrumentation that allows exploring nanoscale phenomena.

An early example on the use of nanomaterials is the well-known Lycurgus cup, a dichroic glass cup that can be appreciated in The British Museum (London) and that was manufactured during the Roman civilization. The Lycurgus cup exhibits a color (red or greenish) depending on the way that is illuminated, due to the presence of metal nanoparticles (e.g. gold and silver) used as pigments dispersed in the glass matrix. Other well-known examples on the use of metal nanoparticles as pigments can be appreciated by the great variety of colors in glass stained windows in European cathedrals from the Middle Ages. The optical effects exhibited by metal nanoparticles, namely those of colloidal gold, have been the subject of interest by Michael Faraday (1897) and Gustav Mie (1908), who explained scientifically these observations. Colloidal gold was also explored in therapeutics since early times, noteworthy it has been reported that the alchemist Paracelsus prescribed a gold colloid, termed as Aurum Potabile, as the elixir of life. Currently, gold nanoparticles form the basis of several nanomedicines, including their use in association with silica materials. Although there has been an unprecedented progress on the association of nanosciences and medicine, the above examples indicate the existence of old practices in this context.

Cancer is a major public health problem for humans, being the second leading cause of death in developing countries, just behind the heart diseases.[1] On nanomedicine, one of the therapies that has explored this concept is cancer PDT, an alternative method to the conventional cancer treatment options, including chemotherapy, radiotherapy, and

surgery.[2-5] Chemotherapy uses drugs that can damage or kill cancerous cells but also cause side effects (e. g. immunodeficiency, anaemia, hair loss, organ damage). On the other hand in radiotherapy malignant cells are controlled or killed by ionizing radiation which is limited by the cumulative radiation dose and is itself painless. PDT is an emergent therapeutic procedure used in cancer treatment. This technique combines three components: drug, visible or near-infrared (NIR) light and oxygen, which on its own do not have any toxic effects on the biological systems. This drug, called photosensitizer (PS) or photosensitizing agent, when in contact with molecular oxygen and exposed to light can produce reactive oxygen species (ROS) that are strongly cytotoxic to the target cells.[6-9]

A PS is activated by light of a particular wavelength, which determines how deeply light can penetrate the body. In this way, the application of PDT combine a PS, oxygen and light in a certain wavelength range. Most of the PSs used in cancer therapy and other tissue diseases are based on a tetrapyrrole structure, such as: porphyrins (Pors)[10-13], chlorins[14-19], bacteriochlorins[20-22] and phthalocyanines (Pcs)[23-27] (**Figure 1**). However, there are also other dyes with different molecular frameworks such as methylene blue (MB). MB is already a promising drug for PDT and methemoglobinemia treatments. In methemoglobinemia an abnormal amount of methemoglobin, a form of hemoglobin, is produced. Due to this disorder, hemoglobin can carry oxygen but is unable to release it effectively into the tissues.[28]

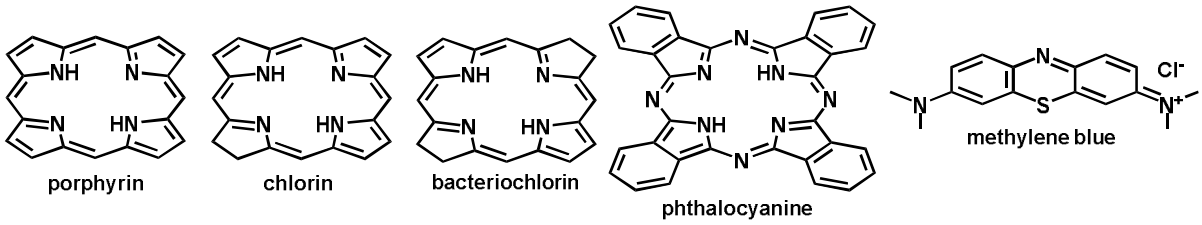

Figure 1. Molecular backbone of porphyrin, chlorin, bacteriochlorin, phthalocyanine and methylene blue.

An ideal PS should be a chemically pure compound, photostable and stable in water, should have a high absorption peak between 600 and 800 nm, should have no dark toxicity, and relatively rapid clearance from normal tissues and organs.[29-33] Red and infrared light penetrate more deeply into human tissues than blue light (**Figure 2**). The portion of the

visible and infrared spectrum between 600 and 800 nm is the ideal optical window for PDT. Absorption of photons with wavelength longer than approximately 800 nm does not provide sufficient energy to excite oxygen to its singlet state and to form a sufficient amount of ROS. Thus, irradiation with longer wavelength has insufficient energy to initiate a photodynamic reaction.

Therefore, PSs with strong absorbance in the near infrared region, such as chlorins, bacteriochlorins, and phthalocyanines, often improve cancer PDT results. But there are also many different factors which need to be taken into consideration when choosing a PS and the light source/type, such as: PS λ_{max} absorption, disease location, size and type of tumour, accessibility and cost.

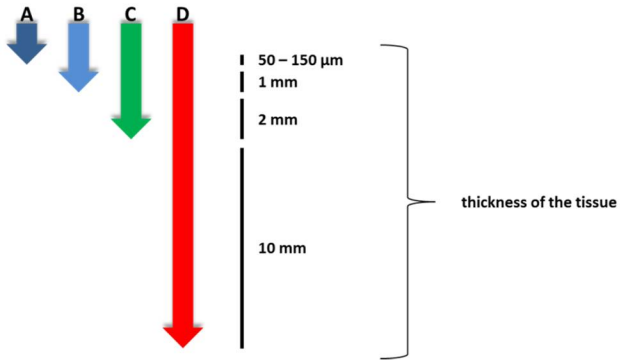

Figure 2. Light penetration through the tissues for light of distinct wavelength range (**A**: indigo light, **B**: blue light, **C**: green light, **D**: red and infrared lights)

How is PDT used to treat cancer?

The photodynamic action or damage in cancer PDT takes place close to the intracellular location of the PS. The reason why this damage occurs only close to PS's position is because the lifetime of singlet oxygen ($^1O_2$) in biological media is very short, approximately 10-320 ns. Therefore, the lifetime of $^1O_2$ limits its diffusion to more or less 10 to 55 nm in cells.[29] This makes PDT a selective treatment with much less secondary effects than conventional therapies. Apart from the first mechanism where ROS directly kill tumor cells, there are other two cell death mechanisms. In the second mechanism, PDT damages the tumor-associated vascular system, leading to tumor infarction. Finally, PDT can activate an immune response against tumor cells. Furthermore, these three mechanisms can influence each other, whose relative relevance for the overall tumor response is yet to

be defined. Nevertheless, long term tumor control requires the combination of all those components.[34]

Although PDT was established 20 years ago as a clinical protocol for cancer treatment, there are still limitations in its use as a general protocol to treat cancer. For instance, the light needed to activate most photosensitizers cannot pass through more than about 1 cm of tissue that is why PDT is usually used to treat tumors either located on (or under) the skin or on the lining of internal organs. Because light cannot pass far into large tumors PDT is also less effective in treating these tumors. As result of this 'light penetration limitation', PDT has been mostly applied in localised cancer treatments. Some of the PSs make skin and eyes sensitive to light after treatment. For example, porfimer sodium,[35] one of the PSs which is already available on the market, makes the skin and eyes sensitive to light over approximately 6 weeks after treatment. So, there is need to study alternatives to improve the efficiency of PDT and eliminate such limitations, which include low effectiveness in treating large tumors, burns, swelling, pain, and scarring in nearby healthy tissues or a persistent skin photosensitization. Therefore it is crucial to improve equipment and more effective ways of light activation. Also it is important to develop new powerful PSs, more specifically to target cancer cells, and activated by light that can penetrate tissue and treat deep or larger tumors. In the context of all these limitations, NPs have recently emerged as promising vehicles for PDT giving the possibility to successfully improve cancer treatment.[36-38]

Why to use SNPs for PDT?

PSs have been used in PDT by employing different nanoformulations. This can improve PDT treatment by increasing the biocompatibility of the hydrophobic photosensitizers' core and their blood circulation. Also selective accumulation in tumor tissues can be improved because particles of certain size tend to accumulate in tumor tissue much more than they do in normal tissue which is called enhanced permeability and retention effect (EPR).[39-41] In this field, silica nanoparticles (SNPs) have emerged as promising vehicles for PDT owing to their potential biocompatibility, large surface area, controllable size formation, hydrophilic surface and ability for surface functionalization, hence the possibility for tumor targeting through surface modification.[42] These unique physico-chemical properties make SNPs ideal platforms for bioimaging[43-48] and drug delivery

applications.[49-51] Also a number of applications of SNPs take advantage of their properties as protecting shells for photoactive compounds and magnetic cores. Hence, amorphous silica shells can protect against chemical and biochemical degradation, release of toxic ions, and activation of immune response.[52] SNPs could be combined with therapeutic drugs for chemotherapy[53-55] or with PSs for cancer PDT.[56-58] Both PS and chemotherapeutic drug can be stored in a single SNP to improve the cancer treatment.[59-61] Moreover, metal core can be incorporated inside SNP which allows the combination of therapies[60,62,63] and facilitates the removal and reutilization of the PS.[64,65] Building a silica layer on a magnetic NP could enhance hyperthermia treatment[66,67] and magnetic resonance image (MRI).[68-70]

In order to develop better NPs for specific cancer treatment, it is crucial to acquire knowledge on the NPs biodistribution and cell targeting. For example, particles of a range size between 5-100 nm are able to penetrate the brain, but with an uptake efficiency that decreases exponentially by increasing size. Besides, in order to penetrate the lung, the NPs should be smaller than 200 nm. If the size of NPs is less than 100 nm, they can be taken up by Kupffer cells in liver and if NPs are bigger than 100 nm, they can cross liver fenestrae and target hepatocytes.[71]

The discovery, in the early 1990s, of the new family of molecular sieves (M41S) contributed for a rapid advancement of research on mesoporous silica materials.[72] In 2001, a MCM-41-type mesoporous silica material was first reported as a drug delivery system. Perez-Pariente *et al.*[73] developed a MCM-41 materials showing capability for accepting and delivering organic compounds. This property is evidenced by using MCM-41 samples as hosts and the ibuprofen molecule as the guest. It was shown that ibuprofen occupies partially the MCM-41 mesopores, and it could diffuse out of them when the ibuprofen-loaded samples were immersed into a simulated body fluid, thus leading to new studies on the use of SNPs for drug delivery applications.[74,75]

Targeted delivery NPs can help to obtain chemical specificity to target binding sites presented in cancer cell.[76-78] Surface modification is a promising strategy to improve the efficacy and safety of therapeutic agents. Usually the ligands employed for targeted nanocarriers are small molecules (e.g. folic acid and carbohydrates), vitamins, peptides (RGD), nucleic acids (aptamers), proteins, antibodies and their fragments, between others.[76]

Folic acid has been used as a targeting ligand for selective delivery of attached imaging and therapeutic agents to cancer tissues. It is easy to conjugate folic acid to both therapeutic and diagnostic agents and it has high affinity for folate receptors. Folate receptor is often overexpressed in a number of human tumours while not expressed in most normal tissues. Due to all of these features folic acid can be used as a highly selective tumor marker. It has been shown that the conjugation of folic acid to liposomes or polymers, facilitates tumour specific delivery of anticancer drugs.[79,80] For example, Liu *et al.*[81] investigated folate-conjugated fluorescent silica nanoparticles for targeting delivery to folate receptor-positive tumors. They demonstrated that these nanomaterials can be internalized into KB cells bearing folate receptors with relatively high efficiency. Yong *et al.*[82] reported the synthesis of dye-loaded and folic acid conjugated organically modified silica NPs as targeted optical nanoprobes for *in vitro* and *in vivo* imaging. The authors have observed that the functionalization of FA to the NPs surface led to a strong cellular uptake of FA-conjugated NPs for pancreatic cancer MiaPaCa-2 cells and hepatoma SMMC-7721 cells with FA receptors overexpressed.

Mesoporous silica nanoparticles (MSNPs) have attracted great attention in recent years as drug delivery platforms, mostly because of their high biocompatibility.[83,84] Tamanoi *et al.*[85] proved that MSNPs are not only promising material for drug delivery but they are also biocompatible. These authors have shown its high tolerance, by serological, hematological, and histopathological examination of blood samples and mouse tissues after MSNPs injection. Tamonoi group[86] previously demonstrated that some type of MSNPs can store anticancer drugs, such as camptothecin (**Figure 3**), and can deliver them to human cancer cells. They successfully incorporated hydrophobic anticancer drug, camptothecin, into the pores of fluorescent MSNPs with the size~130 nm. Moreover, they delivered the drug into human cancer cells, PANC-1, AsPC-1, Capan- 1 (pancreatic), MKN45 (gastric) and SW480 (colon) to induce cell death. In the same research it was suggested that MSNPs might be used as nanocarriers to overcome limitations due to insolubility of many anticancer drugs. Secondly, they prepared nanocarriers *via* a sol–gel method incorporating fluorescein isothiocyanate (FITC), by a APTS linkage, for biodistribution fluorescence tracking experiments.[85] These NPs were decorated with phosphonate groups and were roughly spherical in shape and 100-130 nm in diameter, with hexagonal arrays of pores. Later these MSNPs were decorated with folic-acid conjugates to allow their targeting to

cancer cells, and then camptothecin was loaded (**Figure 3**). *In vivo* studies using human breast cancer cell lines, MCF-7, MCF10F, and SK-BR-3, have proven the biocompatible attribute of MSNPs and their capability to preferentially accumulate in cancer cells and to deliver the loaded drugs.

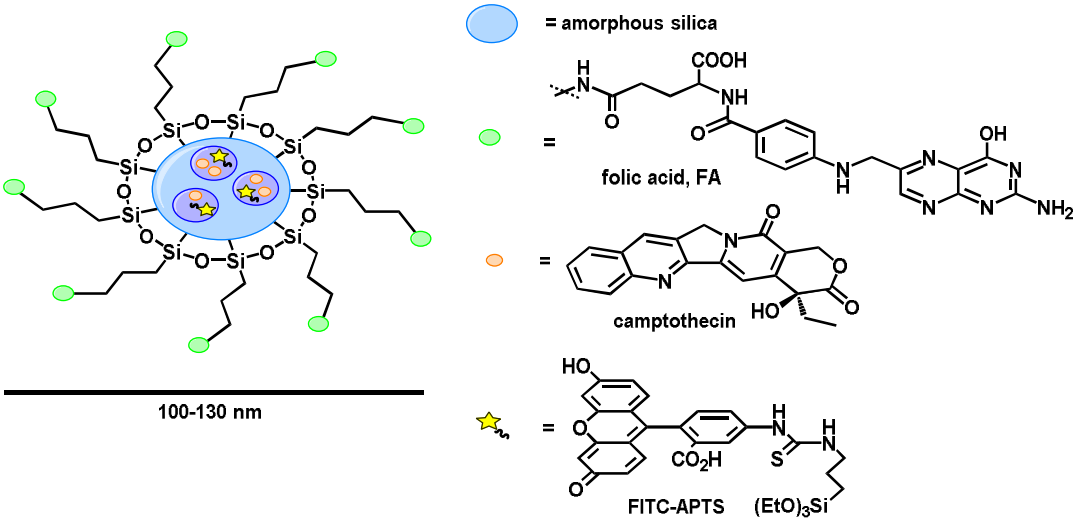

Figure 3. Fluorescent MSNPs modified with folic-acid-targeting ligands on the surface and loaded with camptothecin drug.

In the case of amorphous SNPs, which can be also biocompatible as MSNPs, Jian *et al.*[87] developed a bifunctional SNPs for simultaneous *in vivo* imaging and PDT by encapsulating MB (**Figure 1**) in the phosphonate-terminated silica matrix [87]. MBe ncapsulated phosphonated-terminated SNPs were synthesized using the synchronous hydrolysis of tetraethyl orthosilicate (TEOS) and 3-(trihydroxylsilyl)propyl methylphosphonate (THPMP) in water-in-oil microemulsion. *In vivo* studies were performed with subcutaneous-Hela-tumor-xenografted mice and showed that the bioeffects of SNPs on cancer cells and normal cells were both concentration-dependent. Which means that cytotoxicity is increased by increasing SNPs concentration. Furthermore, this study demonstrated that MB can be effectively protected by the phosphonate-terminated silica matrix from the dye leakage and enzymatic reduction and can effectively induce cell death.

Azzawi *et al.*[88] investigated the direct influence of SNPs uptake on the vasodilator responses of rat aortic vessels, *in vitro*, using SNPs (100 and 200 nm sized) and distinct surface attributes (positive and non-modified). Thus, monodispersed fluorescent SNPs of defined diameter were synthesized using a modified Stöber sol-gel method using TEOS,

aqueous ammonia solution, and water in absolute ethanol. First rhodamine isothiocyanate (RITC, **Figure 4**) was stirred with 3-aminopropyltrimethoxysilane (APS). Then, the reaction vessel was filled with nitrogen gas and mechanically stirred in the absence of light. Then to the mixture of ammonia, absolute ethanol, water, and TEOS, APS coupled with RITC was added. These SNPs presented no detrimental effect on biocompatibility (viability, proliferation, and differentiation)

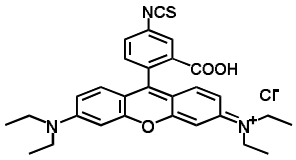

Figure 4. Rhodamine isothiocyanate (RITC).

Preparation of silica nanoparticles

Two main approaches have been used to prepare SNPs, one relies on the Stöber and Fink sol–gel method; the second one uses reverse microemulsions. In 1968 Werner Stöber and Arthur Fink reported the sol–gel synthesis of monodisperse solid SNPs ranging in size from 50 nm to 2 mm.[89] This method involves the controlled hydrolysis of a silica precursor (e.g. TEOS) and the condensation of silica oligomers, in an alcoholic solvent (ethanol) using a base (ammonia) as catalyst (**Figure 5**).

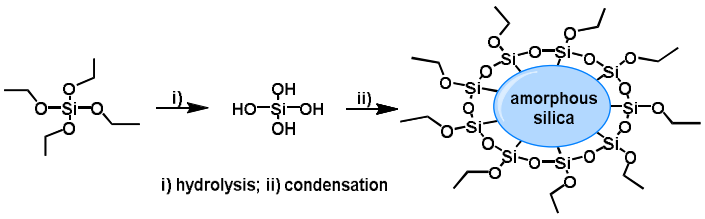

Figure 5. Stöber-Fink method (sol–gel synthesis) in which the hydrolysis and condensation of tetraethyl orthosilicate (TEOS) are facilitated by base in ethanol/water.

The size of the particles can be controlled by adjusting the reaction conditions. In 1992 Bogush *et al.* investigated the mechanisms behind the formation and growth of silica particles prepared from tetraalkoxysilanes in alcoholic solutions of water and ammonia.[90] According to them “the growth proceeds through a surface reaction-limited condensation of hydrolyzed monomers or small oligomers. The particle formation (or particle

nucleation) proceeds through an aggregation process of siloxane substructures that is influenced strongly by the surface potential of the silica particles and the ionic strength of the reaction medium".[90] The final SNP size strongly depends on the ratio between tetraalkoxysilanes, alcohol, water, and ammonia mixtures.[42]

The reverse phase microemulsion method

An alternative method for the synthesis of monodisperse SNPs involves the use of reverse microemulsions (reverse phase, or water-in-oil microemulsions, W/O, **Figure 6**).

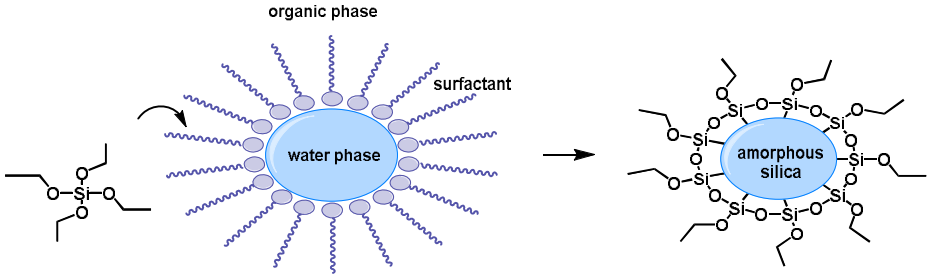

Figure 6. General idea of reverse phase microemulsion method in which TEOS is hydrolyzed at the micellar interface and enters the aqueous droplet to form a silica nanoparticle within the micelle.

Reverse phase microemulsions consist of nanometer-sized water droplets stabilized by a surfactant in an organic phase. The micelles in the microemulsion act as nanoreactors that assist in controlling the kinetics of particle nucleation and growth. The size and number of micelles within the microemulsion can be regulated by varying the water to surfactant ratio. This approach works particularly well for monodispersed NPs smaller than 100 nm in diameter and allows the encapsulation of active molecules in the reverse micelles during NP formation.[91] Water-in-oil microemulsions are stable systems composed of aqueous and organic phases, and a surfactant. It has many advantages, such as mild conditions for encapsulation procedures and it offers straightforward control over particle size and shape by simple varying the microemulsion parameters.[92]

Silica nanoparticles in PDT

PDT with Por-SNPs

In this area, few reviews have been published, one of them being ours.[93] In here we are revising the last 5 years of works that have been coming out in this hot area.

Ximing *et al.*[94] prepared novel SNPs with controllable fluorescence intensity from porphyrin-bridged silsesquioxane. To study the properties of tetrakis(*p*-chloroacetyloxy)phenylporphyrin incorporated in SNPs, firstly they covalently linked porphyrin to (3- aminopropyl)triethoxysilane (APTS) and by using the selfassembly of porphyrin linked covalently to silsesquioxane, incorporated porphyrin into the silica matrix (**Figure 7**). Using the same procedure, Por without covalently linked (3-aminopropyl) triethoxysiane was not effectively encapsulated, most probably because this Por forms aggregates in water.[94] This procedure results in NPs with a narrow size-distributed region and a regular spherical structure with a size of 100 nm. Here, Por was entirely entrapped into SNPs due to the covalent attachment in the system and formed core-shell structures, which efficiently prevents aggregation, leakage and fluorescence quenching effects. This research gives an efficient synthetic example to a family of PS and mesoporous core-shell materials with excellent optical properties and good stability in aqueous solution, thus novel platforms for many applications.

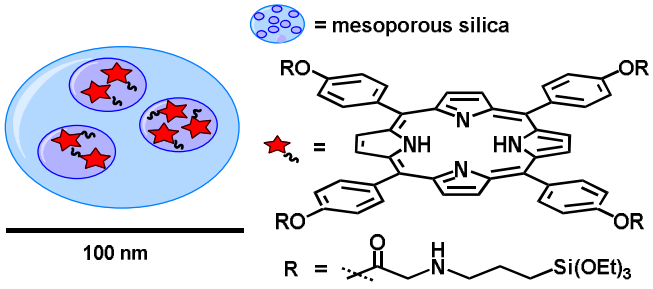

Figure 7. Silica nanoparticles doped with photostable porphyrin.

Gao *et al.*[95] presented a simple method to enhance photodynamic selectivity of Pors attached to SNPs against breast cancer cells. This straightforward system was achieved directly upon the interaction of cationic meso-tetrakis(*N*-methylpyridinium-4-yl)porphyrin tetratosylated (TMPyP, **Figure 8**) with bare SNPs. The final NPs' size were 5–7 nm and an average of one TMPyP molecule was loaded per SNP.

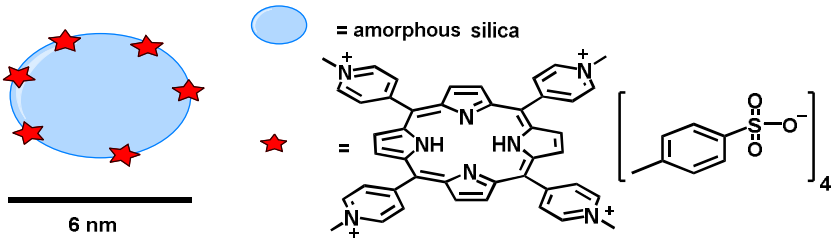

Figure 8. Silica nanoparticles with adsorbed meso-tetrakis(*N*-methylpyridinium-4-yl)porphyrin tetratosylated (TMPyP) on the surface.

Morphological uniform SNPs were prepared with quaternary microemulsion method, leading to ~70% of the nanoparticles having diameters between 3 nm and 5 nm. Later, TMPyP was adsorbed onto SNPs by stirring SNPs and TMPyP at pH 8 for 48 hours under dark conditions. Such prepared SNPs-TMPyP were then separated from the solution by centrifugation, followed by washing with NaOH solution (pH 8) and drying in a vacuum desiccator.

In weak acidic solutions, the adsorption of TMPyP from SNPs surface result production of $^1O_2$. By monitoring $^1O_2$ luminescence at 1270 nm, quantum yields of $^1O_2$ production were found to be pH-dependent, decreasing from 0.45 in a pH 3-6 to 0.08 at pH 8-9, which was also consistent with pH-dependent adsorption attitude of TMPyP on SNPs surface. This pH-controllable photosensitization makes SNPs-attached cationic Por a promising candidate for use in PDT. Thus, the enhanced therapeutic selectivity in the human adenocarcinoma breast cell line SK-BR-3 was checked at both physiological pH 7.4 and acidic tumor extracellular pH 6.0. The photodynamic selectivity test revealed that when the pH was reduced from 7.4 to 6.0, the cell viability decreased from 60% to 35% which means that SNPs-TMPyP exhibited pH-sensitive responses. This easy procedure gives a simple nanocarriers with pH-triggered therapeutic selectivity.

He *et al.*[96] developed organically modified silica (ORMOSIL) nanoparticles encapsulated with protoporphyrin IX (PpIX, **Figure 9**) for direct two-photon photodynamic therapy. PpIX, is a naturally occurring Por which can be found in haemoglobin, cytochrome c and other biologically relevant molecules. Similar to other Por-based PSs, PpIX has several disadvantages, such as low water compatibility or reduced selectivity for targeted tissues. ORMOSIL NPs have big pores in their matrix, which can then be loaded with either

hydrophilic or hydrophobic molecules. These molecules can be released from the matrix into selected targets.

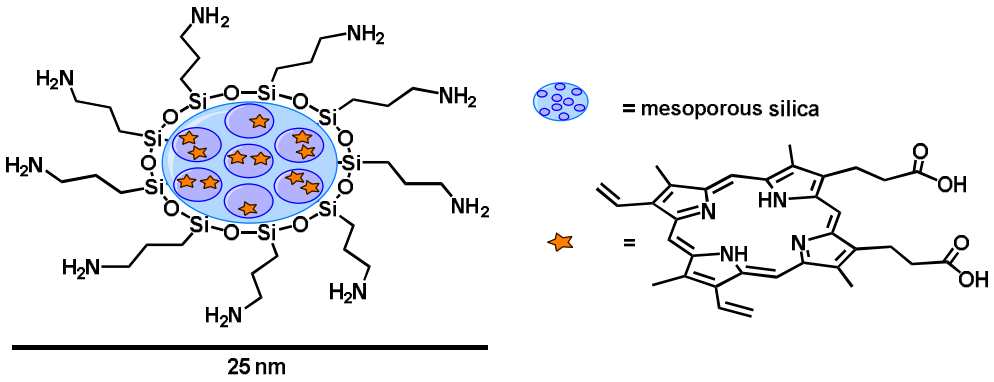

Figure 9. PpIX doped ORMOSIL nanoparticles.

ORMOSIL NPs with PpIX were synthesized in the nonpolar core of Aerosol-OT/ dimethyl sulfoxide (DMSO)/water micelles. The final NPs have an average diameter of about 25 nm and spherical morphology with a narrow distribution of sizes. Two-photon upright confocal microscope confirmed their uptake in tumor cells (HeLa cells). Also, two-photon PDT towards HeLa cells by using PpIX doped ORMOSIL NPs showed that the death of HeLa cells was induced by the $^1O_2$, which was generated by two-photon excited PpIX. Because of meso-porosity of ORMOSIL NPs, oxygen could easily contact the encapsulated PS and further be stimulated to a reactive state. And later, the ROS could be released from the meso-pores of ORMOSIL nanoparticles to destroy HeLa cells. These experiments revealed that this nanomaterial is very promising in cancer PDT.

Ho *et al.*[97] synthetized and studied phospholipid-functionalized mesoporous silica nanocarriers for selective PDT of cancer. These highly efficient, non-cytotoxic drug delivery platforms designed for PDT are phospholipid-capped, PpIX-loaded and fluorescein FITC-sensitized mesoporous silica nanocarriers derivatized with folate (**Figure 10**).

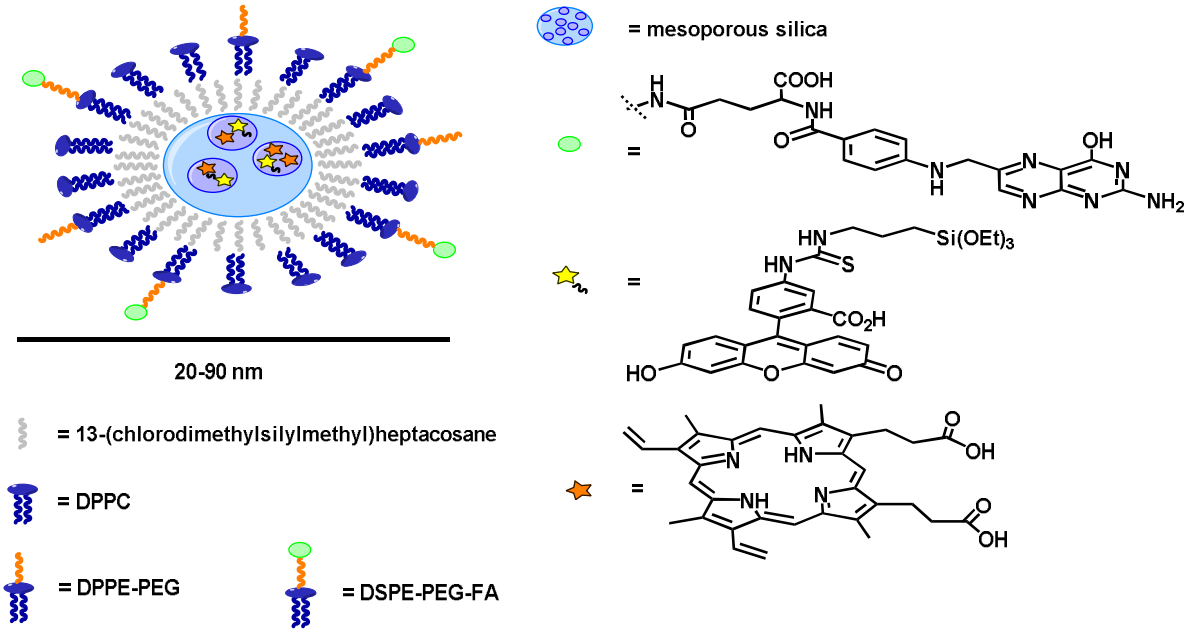

Figure 10. Phospholipid-capped, PpIX-loaded and fluorescein FITC-sensitized mesoporous silica nanocarriers derivatized with folate.

The synthesis of the final MSNPs included steps of preparation of FITC-sensitized MSPNs (FMSNPs), hydrophobization of FMSNPs, encapsulation of PpIX, and surface modification of phospholipid molecules onto the PpIX-loaded hydrophobic FMSNPs. The same authors[98] have reported previously that phospholipid-modification of MSNPs can improve colloidal stability in water and also decrease nonspecific binding with proteins commonly presented in physiological fluids, which was also observed for these new nanosystems. After incorporation of the folate-ligand onto the PpIX-loaded MSNPs, it was confirmed that these nanocarriers offer good biocompatibility and present selective targeting of the folic acid (FA) receptor-overexpressed HeLa cells. In comparison to free PS, the NPs decreased dark toxicity and their cellular uptake was higher. Upon irradiation with visible light, nanocarriers generated $^1O_2$ effectively in aqueous environments which was a good signal for *in vitro* photocytotoxicity. For the *in vitro* studies HeLa and A549 cells as two cancer cell lines were chosen and it was demonstrated that neither light irradiation nor the MSNPs alone causes cytotoxicity. Only the combination of both was effective to kill the targeted cells *in vitro* and prevent tumor growth *in vivo*. This was proved by *in vivo* study of subcutaneous melanoma in nude mice inoculated with B16F10 cells which revealed the capability for those NPs to mitigate nearly 65% of tumor growth.

This nanomaterial with excellent targeting ability, can be used both in fluorescence imaging and PDT.

Vivero-Escoto *et al.*[99] synthetized stimuli-responsive protoporphyrin IX silica-based nanoparticles for *in vitro* PDT. To overcome problems such as leaking, aggregation and self-quenching of PpIX inside of the SNPs they designed SNPs with the surface modified with PpIX attached through a redox-responsive linker (RR-PpIX-SNPs, **Figure 11A**). They assumed that after internalization by cancer cells, the disulfide bond would be broken (because of the reducing conditions present in cancer cells) and PpIX in monomeric form would be released and upon light exposure the PS generate $^1O_2$, which results in cell death (**Figure 11B**). All this should eliminate aggregation of the PpIX, self-quenching and consequently increase the PDT efficiency.

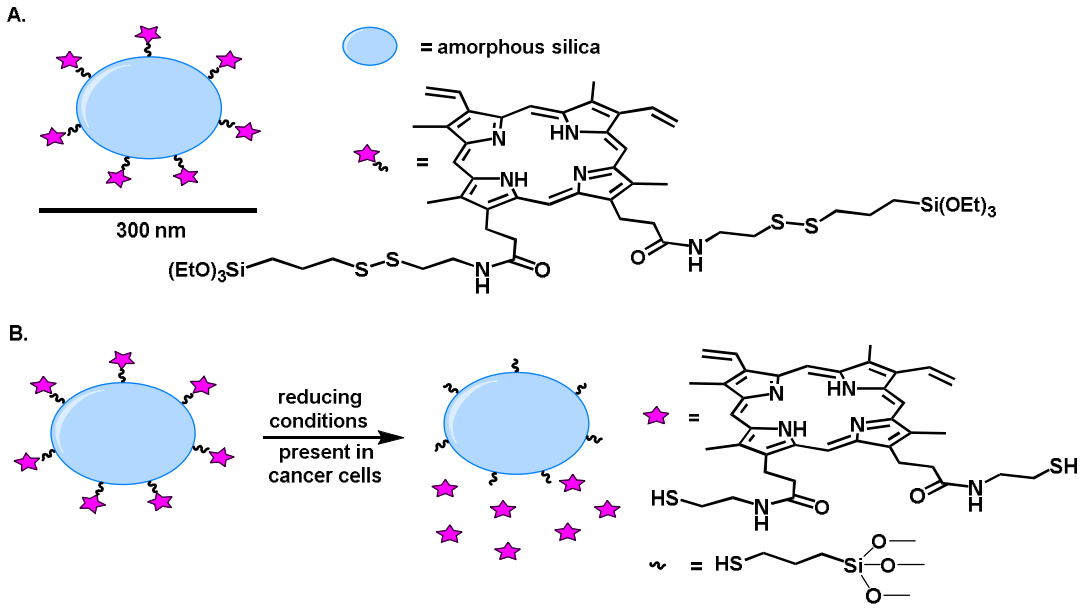

Figure 11. A) Stimuli-responsive PpIX silica-based nanoparticles; **B)** Redox-responsive release of PpIX in monomeric form under reducing conditions present in cancer cells.

RR–PpIX–SiNPs were prepared by modifying the surface of SNPs with redox-responsive silyl-functionalized protoporphyrin IX ligand (RR–PpIX silane ligand, **Figure 11A**) *via* a grafting method. Firstly, SNPs were synthetized *via* a Stöber method and then previously prepared RR–PpIX silane ligand was grafted onto the SNPs (1:10 wt) by stirring and refluxing the mixture in ethanol. The final RR–PpIX–SiNPs showed sizes typically of 300 nm in diameter and contained 85.7 μmol of PS per gram of NPs.

The biocompatibility and phototoxicity of these NPs were investigated in human cervical cancer (HeLa) cells. Cell viability measurements showed that RR–PpIX–SNPs were more phototoxic than a control sample which did not contain a redox-responsive linker (PpIX–SNPs). Probably, intracellular release of PS avoids the aggregation and self-quenching. Confocal microscopy shows that these nanocarriers were mainly localized in lysosomes. Moreover, they were biocompatible in the absence of light as was proved by MTS assay. Release experiments demonstrated that PpIX–SNPs and RR–PpIX–SNPs are stable in the absence of reducing agents under normal physiological conditions. However, in the reducing conditions, PpIX molecules were quickly released from the RR– PpIX–SNPs which was demonstrated in solution and *in vitro*. These nanoplatforms still need improvement to be used in *in vivo* application but seems to be a very interesting alternative for conventional PS formulations used in PDT.

Miao X. *et al.*[100] prepared hollow SNPs loaded with polyhematoporphyrin (Photosan-II, **Figure 12**) and examined its effect in killing QBC939 cells. Due to the hydrophobic nature of Photosan- II, two problems arise: the difficult delivery in physiological environment and the low photophysical properties due to the aggregation of PSs, which decreased the production of $^1O_2$ for PDT. In order to overcome this problem, they decided to encapsulate it in SNPs.

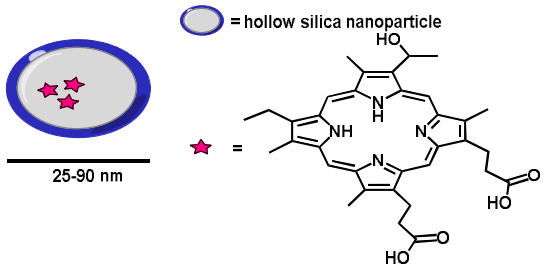

Figure 12. Polyhematoporphyrin (Photosan-II) loaded hollow SNPs.

Photosan-II loaded NPs were prepared by one-step wet chemical-based synthetic route, using TEOS, polyacrylic acid (or sodium polyacrylate), Photosan-II, ammonia and anhydrous ethanol. DLS measurements showed that the size of NPs was in the range of 25-90 nm. The photobiological activity of these PS-loaded NPs was evaluated on human cholangiocarcinoma QBC939 cells. In MTT assay, NPs and free PS at the same

concentration destroyed about 95.3% ± 2.0% and 55.7% ± 1.9% of QBC939 cells, respectively. This demonstrates that these NPs enhance the photoactivity of the PS.

In 2013, Wen *et al.*[101] also evaluated *in vitro* and *in vivo* cytotoxic effects of Photosan-II loaded hollow SNPs, but on liver cancer. NPs loaded with Photosan-II were prepared as indicated above (**Figure 12**)[100]. In this case, it was compared the inhibitory effects of PSs loaded in hollow SNPs and conventional photosensitizers on HepG2 human hepatoma cell proliferation. Firstly, free Photosan-II and NPs containing Photosan-II were administered to *in vitro* cultured HepG2 hepatoma cells and treated by PDT in the same conditions. Then both systems were evaluated in *in vivo* experiments on liver cancer in nude mice. Under the same experimental conditions NPs loaded with Photosan-II performed better then free PS. In both cases, *in vitro* and *in vivo* studies, hollow SNPs loaded with PS were more efficient than the PS alone.

Mancin *et al.*[102] studied targeted delivery of photosensitizers, their efficacy and selectivity issues revealed by multifunctional ORMOSIL nanovectors in cellular systems. PEGylated and non-PEGylated ORMOSIL nanoparticles were prepared by microemulsion condensation of VTES. To investigate the photophysical properties of the embedded dye in NPs, first PSs **1**, **2** and **3** were synthetized (**Figure 13**).

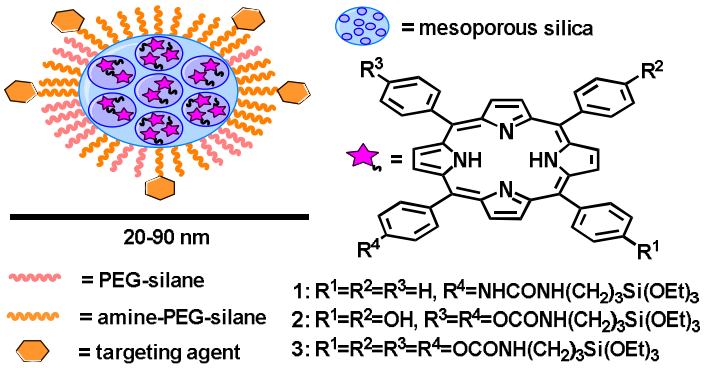

Figure 13. Doped, PEGylated and functional ORMOSIL NPs.

For the PDT studies Stöber silica nanoparticles and VTES-ORMOSIL NPs (both PEGylated and not) doped with the alkoxysilane porphyrin derivative **1** were selected (**Figure 13**). ORMOSIL NPs containing the alkoxysilane derivatives **2** and **3** were also prepared (**Figure 13**). Photophysical properties, fluorescence lifetimes and singlet oxygen quantum yields of these NPs were examined. After this study the most promising were **2**-

doped ORMOSIL NPs and they were chosen with the intention of being decorated with functional groups for targeting cancer cells (**Figure 13**). As targeting agents folic acid, biotin, the cyclic RGD peptide and the antibody Cetuximab were chosen.

Dye-doped, PEGylated and targeted NPs can be prepared by a simple one-pot procedure which allows the rapid preparation and screening of multifunctional nanosystems for PDT. The NPs were prepared by adding to the reaction mixture PEG derivatives. FA and biotin were directly linked to the NPs' amino groups *via* the formation of an amide bond. Thus, decoration with targeting agents was performed by directly adding its *N*-hydroxysuccinimide ester derivatives to the reaction mixture before the purification.

The ability of the PEGylated ORMOSIL NPs to internalize cancer and healthy cells was investigated. For this research A549 (human lung carcinoma cells), CCD-34Lu (human normal lung fibroblasts), KB (folate receptor positive cells derived *via* HeLa contamination), HeLa (human malignant cervical cells expressing low amounts of EGF receptor), A431 (human epidermoid carcinoma cells, expressing high amounts of EGF receptor) and HUVEC (human umbilical vein endothelial cells, overexpressing αvß3 integrin) cells were selected. Next, the phototoxicity of NPs loaded with PS was determined in the case of both RGD- and Cetuximab-conjugated nanoparticles. Final results suggest the disturbance of the PEG layer with small targeting agents, but not with bulky antibodies. It was also concluded that dense PEGylation minimizes toxicity and helps the uptake by cells.

Durand *et al.*[103] prepared mannose-functionalized porous silica-coated magnetic nanoparticles for two-photon imaging or PDT of cancer cells. One of the concepts of this work was to prepare hybrid NPs containing a Fe_3O_4 magnetic core surrounded by a silica shell containing Por derivative and grafted targeted molecules on the surface of the NPs. The preparation of this nanomaterial started by forming a structured silica shell around magnetite NPs with the simultaneous incorporation of the PS in the silica shell. Then mannose moieties were grafted on the surface by covalent bond (**Figure 14**). Previously prepared aqueous solution of magnetite NPs were added to a diluted solution of TPP[pSO_3^-, NH_4^+]$_3$pNHCON$(CH_2)_3$Si$(OEt)_3$ in ethanol and in the presence of NaOH. After stirring at 70 ºC for a while, TEOS and 3-(trihydroxysilyl) propylmethylphosphonate were added and the resulting solution was stirred for 2 h. After workup and treated with an ethanolic

solution of NH_4NO_3 and heated at 60 ºC the suspension was collected by centrifugation and washed with ethanol. Based on the UV–Vis spectra, the quantity of PS encapsulated in NPs (**Figure 14A**) were 6.13 µmol/g and according to TEM measurement the size of NPs was 148 nm. In the following step, APTS was grafted on the surface of NPs by dispersing NPs in water and adding a solution of APTS in ethanol. In the last step of NPs preparation, mannose was grafted on the surface of NPs (**Figure 14B**). TEM measurements showed uniform-sized spherical NPs with visible metal-oxide core and silica shell. To study the efficacy of mannose targeting cells in PDT experiments, MDA-MB-231 breast cancer cells were treated with both NPs, with and without mannose functionalization. This experiment showed that NPs without mannose functionalization induced 26% of cell death and NPs functionalized with mannose induced 43% of cell death. It was proved that, the higher efficiency of mannose-functionalized NPs was due to an active endocytosis *via* mannose receptors.

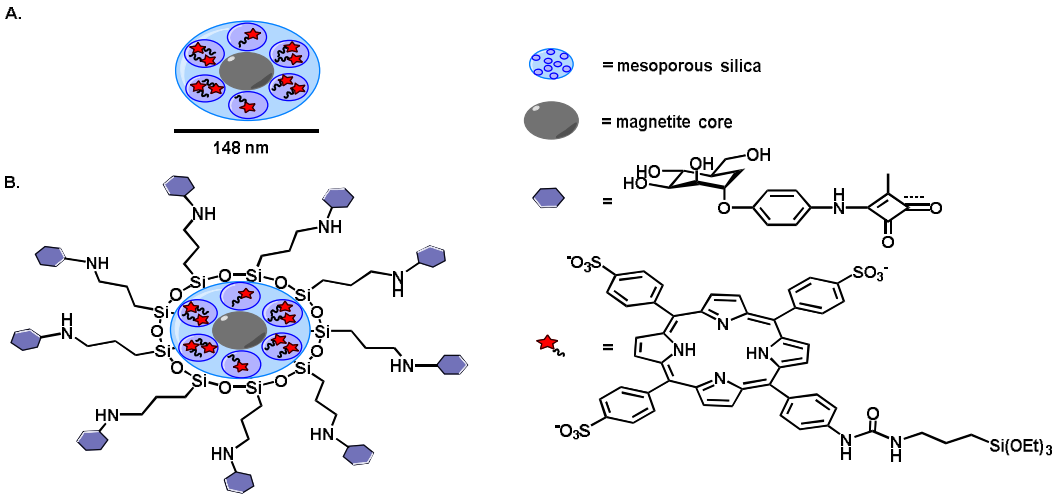

Figure 14. A) Magnetic NPs with the PS incorporated in the silica shell; **B)** Hybrid Fe_3O_4 core-SiO_2 shell nanoparticles functionalized with mannose moieties.

Qian *et al.*[104] demonstrated photosensitizer doped colloidal mesoporous silica nanoparticles for three-photon photodynamic therapy. Hence, HPPH (2-(1-hexyloxyethyl)-2-devinyl pyropheophorbide-a) doped MSNPs have been prepared (**Figure 15**), by mixing HPPH in DMF, and then neat VTES were stirred in Pluronic F127, 1-butanol and water. Neat APTS was then added when the micellar system appeared optically clear. After stirring for 24 h the surfactant pluronic F127 and cosurfactant 1-butanol were removed by dialysis and the

final NPs, with an average diameter of about 20 nm, were then filtered through a membrane.

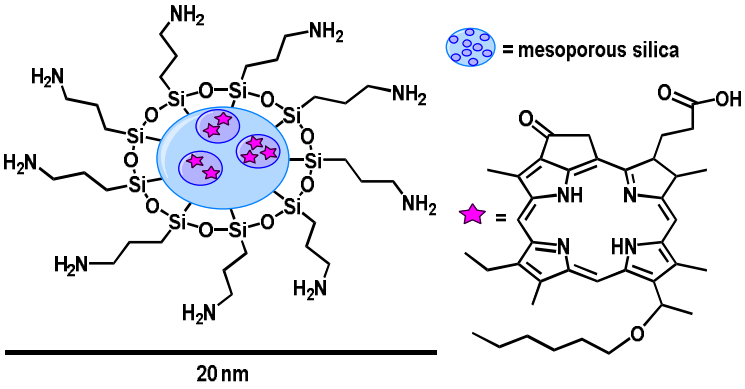

Figure 15. HPPH doped SNPs.

This research combined two technologies, multiphoton microscopy and NPs-assisted PDT. Based on an upright confocal microscope equipped with a 1560 nm femtosecond laser, the direct three-photon luminescence imaging and cytotoxicity caused by PDT towards HeLa cells, which were uptaken by HPPH doped SNPs were proved.

Unlike the porphyrin loaded SNP, there are few reports on the use of corroles as PS. Corroles are aromatic tetrapyrrolic macrocycles bearing a direct pyrrole–pyrrole linkage. Barata *et al.*[105] have reported hybrid particles by covalent linking of a gallium(III)(pyridine) complex of 5,10,15-tris(pentafluorophenyl)corrole (GaPFC) at the surface of surface modified SNP. Although these systems did not show high efficiency in terms of singlet oxygen generation, it is one of the first examples of corrole-silica hybrid materials explored as an alternative for photodynamic therapy.

PDT with Pc-SNPs

In this area, more recently, Lei Ren *et al.*[106] prepared multifunctional ZnPc-loaded MSNPs for enhancement of PDT efficacy by endolysosomal escape. Since zinc phthalocyanine (ZnPc, **Figure 16**) is hydrophobic species and undergo self-aggregation in aqueous solutions, which drastically reduce its photosensitizing efficiency, the preparation of ZnPc-loaded MSNPs can help to maintain ZnPc molecules as monomers and enhance PDT effect. ZnPc in monomeric state has higher production of $^1O_2$ thus acts as a better PS then in aggregate state.[106]

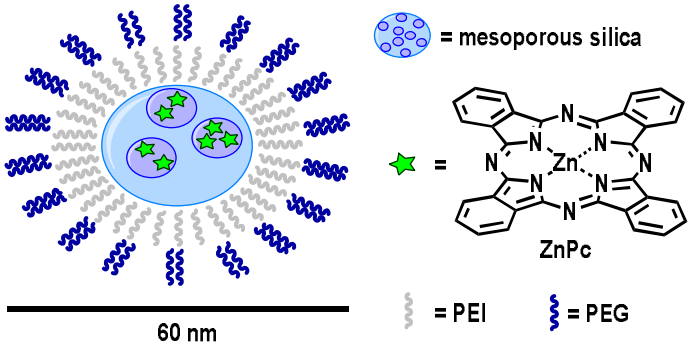

Figure 16. Poly(ethylene glycol) (PEG)- and polyethylenimine (PEI)-functionalized ZnPc-loaded MSNPs.

To prepare poly(ethylene glycol) (PEG)- and polyethylenimine (PEI)-functionalized ZnPc-loaded MSNPs, first the MSNPs were synthesized using an organic template method in O/W phase. This procedure results in MSNPs with a specific surface area of about 632 m^2/g, with an average pore size of 3.3 nm. These NPs had a large surface area and suitable pore size for loading ZnPc (1.4 nm). Then, CDI (N,N′-carbonyldiimidazole) surface activation method was used to functionalize MSNPs with PEI and PEG. The as prepared MSNPs were dispersed by sonication in CDI solution and purified with ethanol by centrifugation. Then, the CDI activated MSNPs were dispersed in the ZnPc-saturated solution. The amount of ZnPc in CDI-activitated MSNPs/ZnPc (0.8 wt%) was determined spectrophotometrically at 670 nm.

To modify the surface of the above NPs, CDI activated MSNPs/ZnPc were dispersed in water by sonication and then an aqueous solution of PEI was added. After 12 h of stirring, the PEI functionalized MSNPs/ZnPc (PEI-MSNPs/ZnPc) were purified by centrifugation, washed with water, and freeze-dried. Similar protocol was used to immobile PEG on the surface of these NPs. The final NPs were about 60 nm (**Figure 16**).

In these nanocomposites (PEG-PEI-MSNPs/ZnPc), MSNPs acts as a nanocarrier of the encapsulated ZnPc, which is the PDT agent, PEI facilitates endosomal escape and PEG enhances biocompatibility. *In vitro* study with the mouse ascitic hepatoma cell line H22 showed that the phototoxicity of the PEG-PEI-MSNPs/ZnPc is greatly enhanced compare with the ZnPc loaded MSNPs. Also these NPs presented high tumor specificity and therapeutic efficacy *in vivo*. After intravenous injection of PEG-PEI-MSNs/ZnPc in tumor-bearing mice followed by light exposure, these nanoplatforms exhibited the ultra-efficient

passive tumor targeting and great PDT efficacy. All these attributes make the PEG- and PEI-functionalized MSNPs a promising multifunctional nanocarrier for PDT.

Zhao *et al.*[107] showed a spacer intercalated disassembly and photodynamic activity of ZnPc inside nanochannels of MSNPs. As was mentioned previously, ZnPc suffers severe aggregation in aqueous environments, thus losing its $^1O_2$ generation efficiency. So, they decided to overcome this problem by loading ZnPc into the nanochannels of adamantine-functionalized MSNPs (**Figure 17**). In these nanocomposites, adamantane (Ad) serves as a hydrophobic spacer which, functionalized inside the mesopores of MSNPs could help avoid the aggregation of ZnPc. Amino-substituted β-cyclodextrin (CD-2NH_2) could enhance the dispersibility of these NPs in physiological environment, promoting NPs to be endocytosed by cancer cells. But also the CD-2NH_2 ring could block PS inside the NPs preventing leakage. Additionally, the conjugation of a targeting ligand FA, with the amino groups of CD-2NH_2 gives the possibility of targeting cancer cells. In this conditions ZnPc can generate cytotoxic $^1O_2$ upon light irradiation at 675 nm in aqueous conditions.

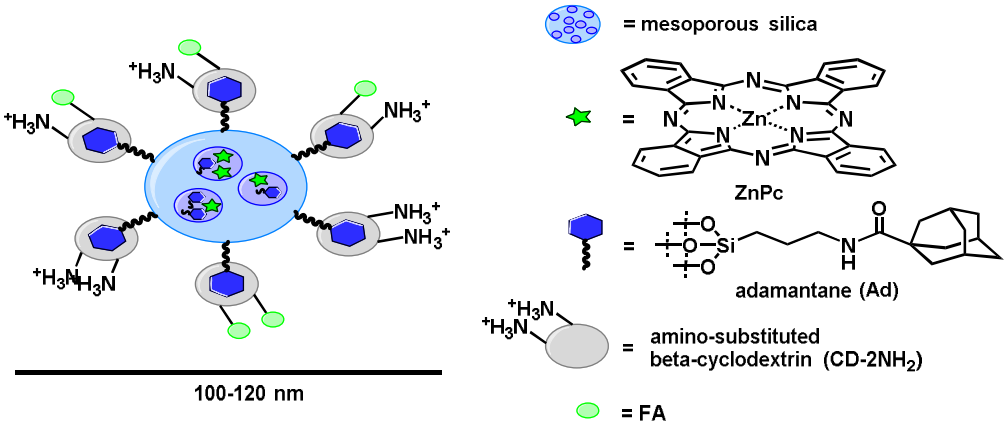

Figure 17. Schematic illustration for the ZnPc-loaded MSNP-Ad and its complex with CD-2NH_2 (MSNPs-Ad+ZnPc+CD-2NH_2-FA).

In the beginning MSNPs-NH_2 were synthesized *via* a co-condensation method [108]. Then, Ad was covalently conjugated with amino groups of MSNPs-NH_2, both onto the NPs surface and nanochannels to form MSNPs-Ad. Later, ZnPc was loaded into the nanochannels of MSNP-Ad and the MSNPs-Ad+ZnPc+CD-2NH_2 hybrid was prepared by making use of strong inclusion complexation between Ad and β-cyclodextrin. The amount of ZnPc loaded in MSNP-Ad was determined spectrophotometrically (0.6 wt %). In the

end, FA was conjugated through amide bond formation between the carboxylic acid group on FA and the amino group on CD-2NH_2. After structural characterization, the first photochemical studies were the photoinduced $^1O_2$ generation capability of the hybrid. The promising results provide a proof-of-concept that the strategy used in immobilized PSs inside the nanochannels of MSNPs prevents ZnPc from aggregation.

To examine the PDT efficiency of this new nanomaterial, the MTT cell viability assay on HeLa cancer cell lines was performed. Comparing MSNP-Ad+ZnPc+CD-2NH_2 hybrid with free ZnPc in solution, using the same amount of PS in both experiments, was observed a more effective apoptosis effect by the hybrid after light irradiation, indicating high PDT efficiency. These ZnPc loaded NPs exhibit stability in aqueous solution and low cytotoxicity in the dark. All this together make these NPs a promising platform for the next generation of photodynamic therapeutics towards specific cancer treatment.

Dennis K. P. Ng *et al.*[109] described the preparation of amorphous SNPs of mono-PEGylated zinc(II) phthalocyanines and their *in vitro* photodynamic activity. PEGylated ZnPc was prepared by substitution reactions of polyethylene glycol monomethyl ether monotosylate with 2-hydroxyphthalocyaninatozinc(II) in the presence of K_2CO_3 in DMF (**Figure 18**). This compound is built of hydrophilic PEG chain and the hydrophobic macrocyclic core thus, it is amphiphilic. Therefore these aspects enhance the cellular uptake and intracellular localization.

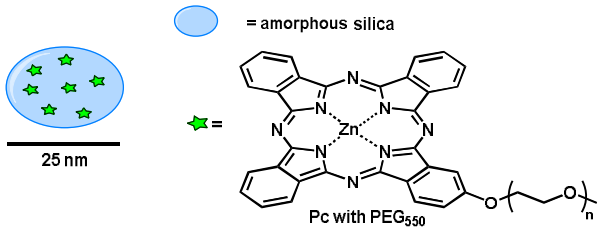

Figure 18. Mono-PEGylated zinc(II) Pc NPs.

The encapsulation of mono-PEGylated zinc(II) Pc into organically modified silica-based NPs was based on controlled hydrolysis of VTES in micellar media. The final 25 nm NPs were highly monodispersed in size and stable in aqueous media. These NPs presented high $^1O_2$ production efficiency so the photodynamic activity of these systems toward HepG2 human hepatocarcinoma cells was also studied. In the conditions used for this experiment,

more than 97% of the cells were killed. Later, cellular uptake of these nanosystems was examined by confocal fluorescence microscopy. After incubation for 2 h, these NPs showed strong intracellular fluorescence which indicated that it was taken up effectively into the cells. These characteristics make these NPs promising PDT agents, because of their uniform size, stability in aqueous media, high $^1O_2$ generation efficiency and high cellular uptake.

Ren *et al.*[110] presented co-enhancement of fluorescence and singlet oxygen generation by silica-coated gold nanorods (AuNRs) core-shell nanoparticles (**Figure 19**). They combined silica-coated AuNRs with tetra-substituted carboxyl phthalocyaninatealuminum(II) (AlC_4Pc). In this work AlC_4Pc worked in the same time as both fluorophore and PS to get distance-dependent metal-enhanced fluorescence (MEF) and metal-enhanced singlet oxygen generation phenomenon.

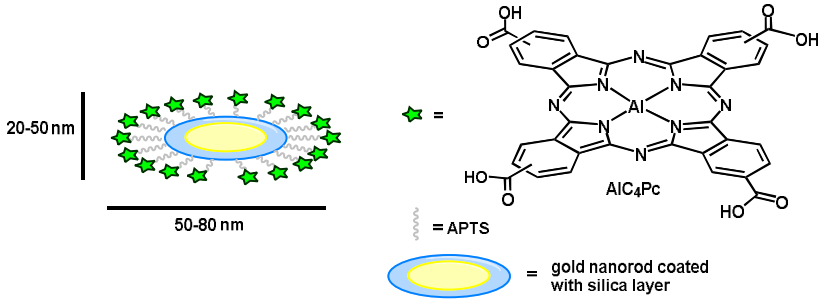

Figure 19. Silica-coated gold nanorods core-shell nanoparticles decorated with tetrasubstituted carboxy AlC_4Pc.

To prepare silica-coated AuNRs core-shell structure first, AuNRs were made by well-known seed-mediated growth process [110,111]. Subsequently, to coat AuNRs with silica, modified Stöber method was used (**Figure 19**) [112]. Silica layers with different thicknesses were obtained by adding varying amounts of TEOS. After removal of CTAB surfactant form AuNRs solution, NRs were re-dispersed in pure water and pH was adjusted to 10. Then, TEOS in methanol together with APTMS in methanol were injected to form the silica shell. After 24 h, the colloidal solution was centrifuged twice to remove the unreacted TEOS and APTMS to afforded amine-capped silica-coated AuNRs.

The covalent binding of AlC_4Pc to the surface of above NPs was performed by using EDC and NHS cross-linking procedure to create amide bonds between AlC_4Pc and APTS. For

this, AlC_4Pc was pre-activated by an EDC/NHS solution and then added into silica-coated AuNRs solution, affording AuNRs-AlC_4Pc hybrid. The average length and diameter of AuNRs core were measured to be 46.8 ± 3.2 and 19.4 ± 1.1 nm. The uniform amorphous silica spacer shells had thickness from 2.1 to 28.2 nm.

It was observed that when the AlC_4Pc was bound to the surface of NRs, the fluorescence intensity and $^1O_2$ generation varied with the thickness difference of silica shell. Thus, amorphous silica shell could serve as a spacer layer between the AuNRs and AlC_4Pc to get an optimum fluorescence enhancement effect. Co-enhancement of fluorescence intensity and $^1O_2$ production were highest when the distance between AlC_4Pc and AuNRs was 10.6 nm. These unique characteristics make the prepared AuNRs-based silica shell promising for MEF- fluorescence imaging and PDT.

Zheng *et al.*[113] synthesised magnetic, fluorescent and mesoporous core-shell-structured nanoparticles for simultaneous magnetic resonance imaging (MRI) and fluorescence imaging, cell targeting and PDT. The core of the NPs was made from a single Fe_3O_4 NP encapsulated in fluorescent dyes co-doped nonporous silica (**Figure 20**). This core was covered by ordered mesoporous silica containing PSs. To gain the targeting capacity the surface of NPs were functionalized with folic acid. FITC was used as fluorescence imaging agent which was covalently incorporated into the silica core. Their location and covalent bonds can isolate the dyes from the external environment and protect them from photobleaching. AlC_4Pc was chosen as a PS, and it was covalently linked in the rigid porous structure of the mesoporous silica to avoid the degradation of PS in biological environments, and overcome their premature release. Moreover, the mesoporous structure of the shell allows the easy diffusion of O_2 which can react with the PS for $^1O_2$ generation.

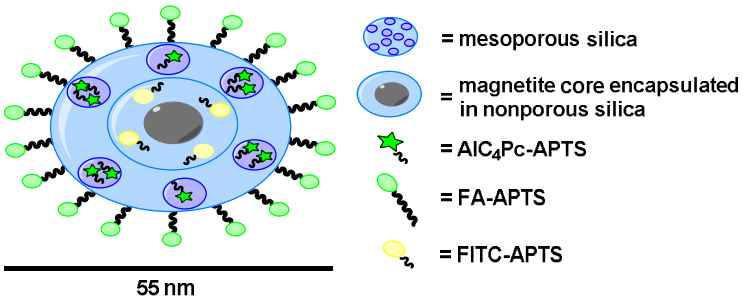

Figure 20. NPs with magnetic core encapsulated in FITC co-doped nonporous silica. The core is covered by ordered mesoporous silica containing PSs. The surface of NPs were functionalized with folic acid (FA).

Monodispersed superparamagnetic Fe_3O_4 NPs with an average size of 6 nm, were prepared using a solvothermal reaction [113,114]. The NPs were then coated with nonporous silica layer through a reverse micelle method. To covalently incorporate FITC into these NPs, FITC was reacted with APTS and then co-hydrolyzed with TEOS during the reverse micelle encapsulation process. The resulting NPs had uniform diameter of 40 ±5 nm. Subsequent NPs were coated with a mesoporous silica layer by base-catalyzed hydrolysis of TEOS in the presence of CTAB. To covalently bind AlC_4Pc in the mesoporous silica layer, AlC_4Pc was firstly treated with APTS and then supplied together with TEOS during the coating process. Lastly, folic acid was covalently anchored on the surface of these NPs to recognize the over-expressed folate receptors presented in many cancer cells. The amount of AlC_4Pc conjugated into the final material was about 0.51 wt%. The NPs had a uniform layer of mesoporous silica with a thickness of about 9 nm and uniform mesopores with an average pore size of 2.5 nm. Fluorescence imaging and magnetic resonance imaging were examined with human hepatoma cells (QGY-7703) and human hepatocytes (QSG-7701). Due to the introduction of fluorescence molecules it was possible to directly monitor the cellular uptake of the NPs by fluorescence microscopy. The surface modification with folic acid enhanced the delivery of PSs molecules to the targeting cancer cells that overexpress the folate receptor. These NPs presented much higher $^1O_2$ production than the same amount of free AlC_4Pc in solution which suggests that these nanovehicles act as a nanoreactor to facilitate the photo-oxidation reaction. *In vitro* studies proved that these nanocomposites effectively killed cancer cells through the PDT process. All these experiments proved the bio-applicability of these theranostic nanomaterials for MRI, fluorescence imaging and PDT.

PDT with assistance of UCNPs

One of the biggest limitations of PDT is the small penetration depth of visible light needed for its activation. To overcome this problem Yong Zhang *et al.*[37] have used mesoporous-silica-coated upconversion fluorescent nanoparticles that in a remote-controlled mode converted the penetrating NIR light to visible wavelength for simultaneous activation of two PSs in order to enhance PDT (**Figure 21**). Nowadays upconversion nanoparticles (UCNPs), that emit high-energy photons upon excitation by low-energy NIR radiation, have attracted considerable attention for their application in biomedicine. One of the problems in using UCNPs as a PDT agent in the clinical setting is that the PSs are normally physically adsorbed onto their surface. This interaction is weak and has low attachment efficiency of the PSs to the UCNPs. The development of UCNPs coated with a layer of mesoporous silica shell can overcome this problem.

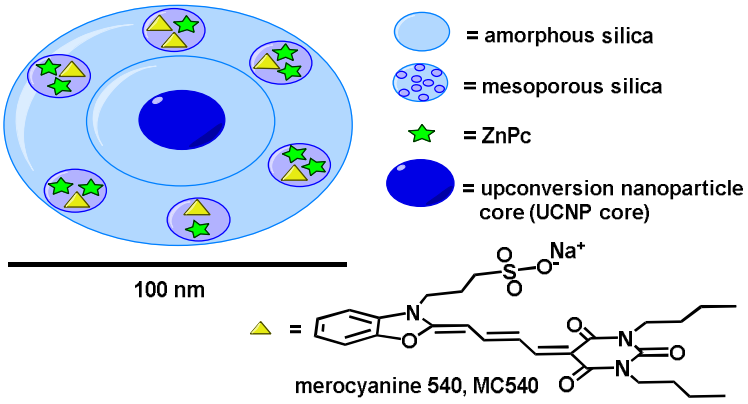

Figure 21. UCNPs coated with a layer of amorphous silica shell and mesoporous silica layer encapsulating ZnPc and MC 540 photosensitizers.

In this work mesoporous silica-coated $NaYF_4$:Yb,Er/silica UCNPs were synthesized in a multistep process and then FA and PEG conjugation to the UCNPs was performed based on EDC/NHS method. In the end, two PSs, merocyanine 540 (MC540) and ZnPc were loaded into the porous of silica shell to obtain final NPs smaller than 100 nm (**Figure 21)**. These UCNPs under irradiation with a 980 nm laser emitted upconversion visible fluorescence at two main peaks, which matched with the absorption of both PSs, MC 540 (green at~540 nm) and ZnPc (red at ~660 nm). This feature makes these two PSs a suitable pair for use in conjunction with the NaYF4:Yb,Er material. Their conjugates with FA and polyethylene glycol were intravenously administered into tumor-bearing mice to examine

their targeting ability and their PDT effect. Compared to approaches using a single PS, dual system showed much better PDT efficacy by enhanced generation of $^1O_2$ and reduced cell viability during *in vivo* studies with B16-F0 melanoma cells. These nanoplatforms may be used in the future in non-invasive deep-cancer therapy.

Nanfeng Zheng *et al.*[115] prepared multifunctional core-shell upconverting nanoparticles with AlC_4Pc covalently incorporated inside the silica shells for PDT and MRI of cancer cells (**Figure 22**).

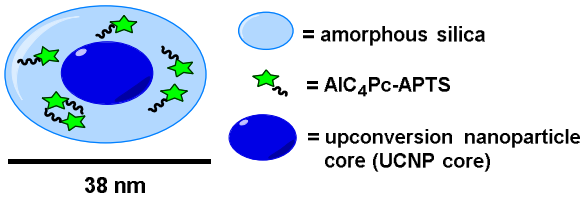

Figure 22. Silica-coated lanthanide-doped UCNPs with AlC_4Pc covalently incorporated in their interior.

Firstly, the synthesis of lanthanide-doped UCNPs ($NaGdF_4$:Yb/Er/$NaGdF_4$, UCNPs) with an edge-length of about 22 nm were performed.[115] Then, AlC_4Pc photosensitizer was covalently bind to the silica networks of the silica-coated UCNPs. AlC_4Pc was loaded into silica-coated UCNPs by co-hydrolysis of the AlC_4Pc silanization precursor with TEOS *via* W/O microemulsion method. In this method the thickness of the silica shell (3–10 nm) was controlled by varying the amount of TEOS in the reaction mixture. To improve cell-uptake efficiency, owing to the size-dependent uptake of cells on the particle, the nanocomposite with the size of 38 nm was chosen for further study. The covalent coupling of PSs in the silica network would prevent the degradation of PS in biological environments, and overcome their premature release. These UCNPs encapsulated inside the silica shell were able to convert NIR light to strong red-light emission, which then was captured by the PS covalently linked. The final NPs were stable against photosensitizer leaching and highly efficient in $^1O_2$ generation under NIR light. Moreover, *in vitro* studies with BNL 1ME A.7R.1 (MEAR), a mouse liver hepatoma cell line revealed that these NPs can enter cancer cells and successfully destroy them upon NIR irradiation. This nanosystem allowed a deeper light penetration than visible-light excitation. Additionally, the NPs showed good MRI contrast in aqueous solution and inside cells. These small size-controllable diameter

multifunctional NPs can be applied in versatile imaging diagnosis and as a therapy tool in cancer treatment.

Huichen Guo *et al.*[116] presented one pot facile synthesis, *in vitro* bioimaging and PDT of cancer cells with mesoporous silica-coated $NaYF_4$ nanocrystals with encapsulated ZnPc (**Figure 23**).

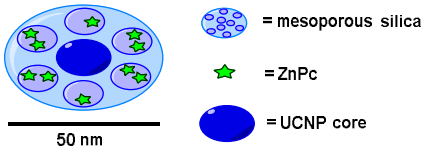

Figure 23. Mesoporous silica-coated UCNPs with encapsulated ZnPc.

The first step in this study was to prepare uniform $NaYF_4$:Yb/Er nanocrystals using the procedure for the high quality hexagonal phase $NaYF_4$:Yb/Er nanocrystals which can be found elsewhere.[116] Then, these nanocrystals were coated with mesoporous silica layer and finally ZnPc was loaded into the pores of the mesoporous silica by soaking the mesoporous silica-coated $NaYF_4$ NPs in a solution of ZnPc in pyridine for 24 h. The final NPs were spherical, highly monodispersed, stable in aqueous systems and had the size of less than 50 nm with an average pore size of 2.6 nm. Moreover, these NPs also displayed good biocompatibility and could be used for bio-labeling or bio-imaging and as PS carriers for tumor therapy. It was proved that upon excitation by a NIR laser, the NPs loaded with ZnPc converted NIR radiation to visible light, which later activates the PS to generate $^1O_2$ and destroy cancer MB49-PSA cells. This facile procedure for core-shell nanoparticles could be easily used in the potential applications of drug delivery and nanobiotechnology.

Chun-Hua Yan *et al.*[117] prepared triple-functional core-shell structured UCNPs covalently grafted with PS for luminescent, MRI and PDT *in vitro* (**Figure 24**).

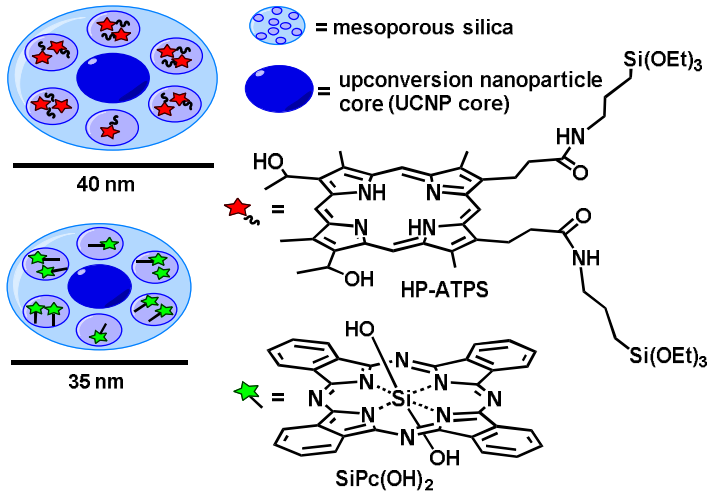

Figure 24. Triple-functional core–shell structured UCNPs covalently grafted with PS.

The 10 nm UCNPs were coated with mesoporous silica shell layer, in which PS, hematoporphyrin (HP) and silicon phthalocyanine dihydroxide, was covalently grafted. The silica shell improved the dispersibility of hydrophobic PSs in aqueous environment. To graft the PS onto the silica shell, carboxylic group of HP reacts with amino groups of APTS to form an amide bond to siloxane groups, which later hydrolyze with TEOS to form Si-O-Si covalent bonds. This process was not necessary in the case of Pc because it has two silanol hydroxyls for further hydrolysis reactions. Final NPs had 40 nm for Por-NPs and 35 nm for Pc-NPs. These NPs utilize NIR irradiation at 980 nm to emit luminescence at about 550 nm and 660 nm. The first one was used in fluorescence imaging and the other was absorbed by the PS molecules to generate singlet oxygen for killing cancer cells in PDT. Further, the Gd^{3+} ions with paramagnetic properties located in the core of NPs can be used as a contrast agent for MRI. This triple-function nanomaterial could have a bright future in the fields of minimally invasive therapy and rapid detection.

Pc-NPs showed better efficiency of $^1O_2$ generation than Por-NPs within the same irradiation time. Both nanomaterials exhibit excellent PDT efficiency in water solutions and in HeLa cells through an energy transfer process between the core and PS molecules under NIR laser irradiation. CaF_2 is well-known to be biocompatible therefore improving biological safety. The nanomaterial displayed low dark cytotoxicity and NIR image in HeLa cells. All these unique advantages make these new multifunctional materials promising for applications in clinical treatment and detection.

PDT with chemotherapy in combination treatment

What can enhance cancer therapy is the synergic anticancer effect of two active molecules such as a PS and a drug in the same nanocarrier. Having this in mind Jean-Olivier Durand *et al.*[118] improved cancer therapy with MSNPs combining targeting, drug delivery and PDT. They designed MSNPs loaded with camptothecin (**Figure 25**), possessing a PS in the walls, and functionalized with galactose to enhance the anti-cancer activity of these nanocarriers.

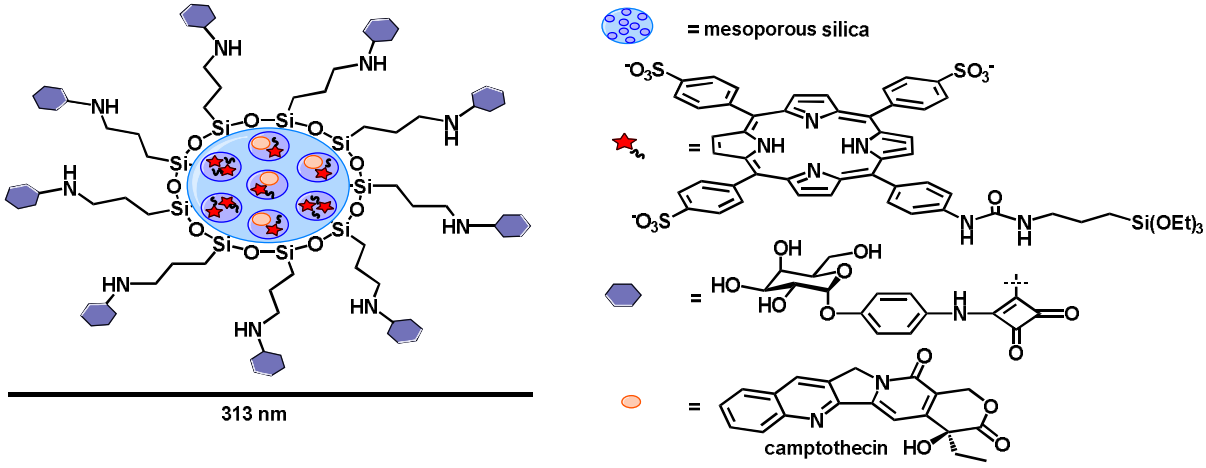

Figure 25. MSNPs covalently encapsulating PS, loaded with camptothecin and functionalized with galactose on the surface.

In this research two types of NPs were prepared, MSNPs covalently encapsulating fluoresceine functionalized with galactose and the same NPs but with PS instead of fluoresceine. MSNP-FITC and MSNP-FITC-NH_2 were synthesized and described,[119] and were used for confocal localization of fluorescent NPs decorated with galactose in living HCT-116 cancer cells. These MSNPs, which encapsulated water soluble PSs, were synthesized following previously described methods.[120] This procedure afforded NPs with a specific surface area of 728 m^2/g, volume of pores of 0.50 cm^3/g and pores diameter of 2.76 nm. Dynamic light scattering showed a hydrodynamic diameter of 245 nm and titration (UV–Vis) gave 9.76 µmol of PS per gram of NPs. Then, previously prepared p-[N-(2-ethoxy-3,4-dioxocyclobut-1-enyl)amino]phenyl-α-D-galactopyranoside[121] was grafted on the surface of the MSNPs through the APTS linker to get 313 nm final NPs. In the end, the anticancer drug camptothecin was loaded by stirring these NPs with

camptothecin in DMSO. After centrifugation NPs were washed with water and dried under vacuum. UV–vis titrations showed that camptothecin was loaded in the MSNPs in 7.11 μmol g^{-1}.

Confocal localization of fluorescent MSNPs loaded with FITC and decorated with galactose in living HCT-116 cancer cells indicated that these NPs were more efficiently internalized in comparison with unfunctionalized NPs. Which means that galactose functionalization is an efficient targeting of MSNPs to cancer cells. The accumulation of galactose-functionalized NPs in the endosomal and lysosomal compartments was mediated by galactose receptors present on the colorectal cancer cells.

MSNPs functionalized with a PS and sugar and containing camptothecin combined drug delivery and PDT were tested on three cancer cell lines, colorectal (HCT-116), pancreatic (Capan-1) and breast cancer (MDA-MB-231), selected for their high invasive and metastatic potentials. These nanoplatforms showed a dramatic improvement of cancer cell death, induced 79–100% cell death, compared to individual treatments. These data provide the proof of principle that synergic anticancer effect of two active molecules such as a PS (Por) and a drug (camptothecin) in the same nanocarrier enhance cancer therapy.

Zhuang Liu *et al.*[122] fabricated mesoporous silica nanorods intrinsically doped with a PS, chlorin e6 (Ce6), and loaded with doxorubicin (DOX), a widely used anti-cancer drug (**Figure 26**). This nanomaterial was applied as a multifunctional drug carrier for combination therapy of cancer. During the preparation of these NPs it was observed that by increasing the amount of Ce6 doped inside the silica matrix, the morphology of MSNPs changes from spheres to rod-like shapes.

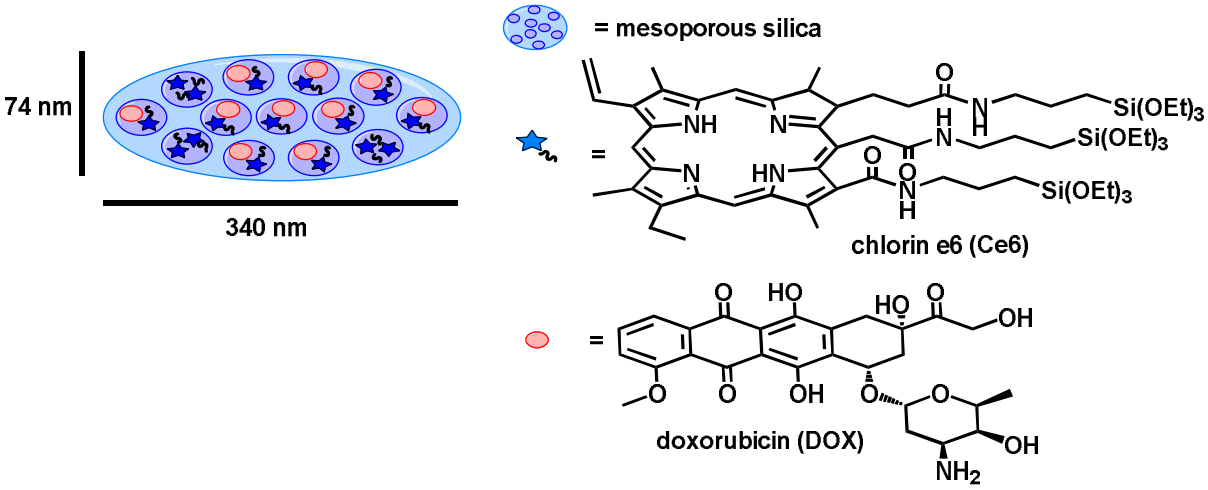

Figure 26. Mesoporous silica nanorods intrinsically doped with chlorin e6 and loaded with doxorubicin (DOX), a widely used anti-cancer drug.

Ce6-doped mesoporous silica nanorods were prepared first by formation of amide bonds between Ce6 and APTS. To prepare Ce6-doped mesoporous silica nanorods firstly, Ce6 was covalently conjugated to APTS by the formation of amide bonds. Then, nanorods were synthesized by co-condensation of TEOS together with different amounts of APTS-conjugated Ce6 in the presence of aqueous ammonia and CTAB. Different from spherical MSNPs prepared without addition of APTS-Ce6, the obtained nanorods showed various morphologies from spheres to rods. By increasing the amount of APTS-Ce6 it was possible to synthesized four types of nanorods with average dimensions of 208/170 nm, 307/108 nm, 311/90 nm and 340/74 nm.

In the end, all four new materials were loaded with DOX. The most promising nanamaterials were 340/74 nm nanorods because of its highest Ce6 loading, faster uptake by cancer cells, and similar DOX loading compared with other nanorods. The Ce6 loading on nanocarriers was stable thanks to covalent conjugation. On the other hand, DOX showed pH-dependent release because it was only non-covalently adsorbed into the mesoporous structure. Thus, this multifunctional nanosystem can be both use in PDT (without the need of Ce6 release) and in chemotherapy (after DOX is released from nanocarriers and entered cell nuclei).

It was observed that the nanorods with average dimensions of 340/74 nm are uptaken by cancer cells much faster than spherical NPs. Therefore, as a drug delivery platform for *in*

vitro and *in vivo* studies, these NPs were chosen. After successful combined PDT and chemotherapy of cancer in cellular experiments with 4T1, HeLa and 283T cells, *in vivo* animal studies were performed. Following *in vivo* study with Balb/c mice bearing 4T1 tumors it was observed that combined PDT/chemotherapy is much effective than each individual therapy.

Jianmei Lu *et al.*[123] studied amphiphilic copolymer coated upconversion nanoparticles for near-infrared light-triggered dual anticancer treatment. Like in the previous example they combined action of Ce6 and DOX in new core-shell nanocomposite for controlled release of anticancer drugs, DOX for chemotherapy and Ce6 for PDT treatment (**Figure 27**). To prepare these NPs first 20 nm Mn^{2+}-doped UCNPs were coated with a mesoporous silica layer *via* the hydrolysis of TEOS in a micro-emulsion system. Then, long chain hydrocarbonoctadecyltrimethoxysilane (C18) was attached for the self-assemble process combined with the amphiphilic copolymer. Later, Ce6 was grafted on the surface of silica shell *via* Ce6-(3-aminopropyl) triethoxysilane. These NPs had narrow distribution and a particle size of about 50 nm. In the end, the NIR light-responsive amphiphilic copolymer containing 9,10-dialkoxyanthracene groups was used to cover the NPs *via* self-assembly process. During the last step, DOX was introduced to the reaction mixture to load it into final NPs.

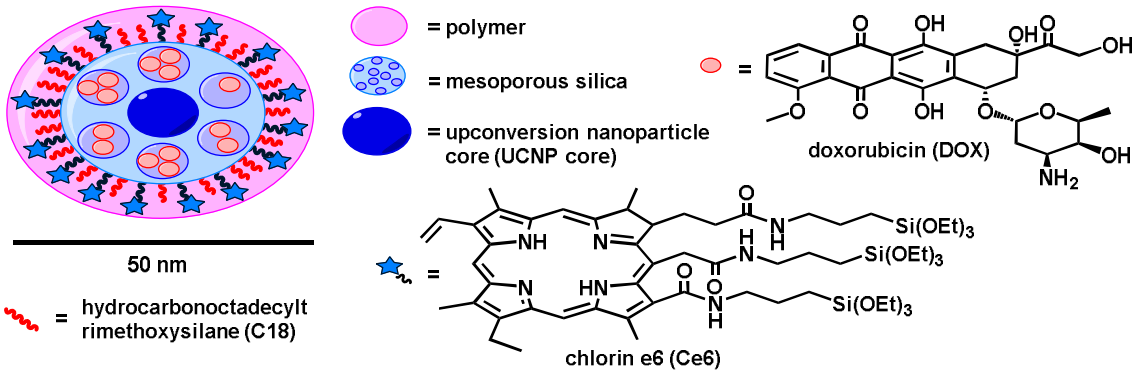

Figure 27. UCNPs coated with a mesoporous silica layer, decorated with C18 and Ce6, loaded with DOX and covered by amphiphilic copolymer.

The nanosystem worked as follow, upon irradiation with a 980 nm laser, NPs were able to absorb and convert the NIR light to higher-energy visible red light (660 nm). This process excited PS to generate $^1O_2$ which degraded dialkoxyanthracene group in the amphiphilic

copolymer. As soon as copolymer was detached from the surface of the NPs, the pre-loaded drug was released. Later, experiments demonstrated that in this system the NIR light-controlled chemotherapy and PDT could worked simultaneously. Like in the former case, *in vitro* and *in vivo* experiments with KB cells also proved that comparing NPs with and without DOX, the drug-loaded multifunctional NPs possessed better therapeutic efficacy, in synchronous NIR light triggered chemotherapy and PDT.

Another example how to make more efficient combination of chemotherapy and PDT presented Li Chena *et al.*[124] with dual pH-responsive MSNPs (**Figure 28**). They prepared NPs which can respond to the cancer extracellular and intercellular pH stimuli. On the surface of these NPs histidine was grafted to allow the acid sensitive PEGylated tetraphenylporphyrin zinc (Zn-Por-CA-PEG) behaved as a gatekeeper to prevent loaded-drug from leaching at health tissues. This operation closed the pores of MSNPs by the metallo-supramolecular-coordinated interaction between Zn-Por and histidine. To synthetize acid sensitive PEGylated Zn-Por in the beginning, Zn-Por-CA was prepared by reaction between Zn-Por-NH_2 and CA. Then, Zn-Por-CA was PEGylated by condensation between the carboxyl group of Zn-Por-CA and the hydroxyl group of PEG. PEG was used to enhance the biocompatibility and stability *in vivo*.

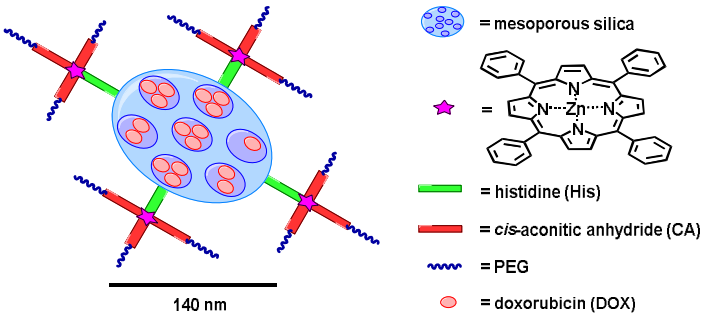

Figure 28. Dual pH-responsive MSNPs.

As a scaffold, MCM-41 type MSNPs with an average diameter of 140 nm were used. These NPs decorated with NH_2 groups were synthesized according to a reference procedure.[125] To prepare histidine modified NPs, MSNPs–NH_2 were dispersed in anhydrous DMSO, and then BOC-histidine, EDC·HCl and NHS were added into the solution. After workup these NPs reacted with earlier prepared Zn-Por-CA-PEG. In the end, DOX was loaded by a simple dialysis technique.

Particular tissues of the body, eg. endosomal and lysosomal cell compartments (pH ≈ 5.5) and cancers and inflammatory tissues (pH ~ 6.8), have a more acidic pH than blood or healthy tissues (pH ~ 7.4). To explore these pH-differences, these acid sensitive conjugated nanosystem cis-aconitic anhydride (CA) between Zn-Por and PEG which in cancer cells (pH ~ 6.8) will cleave. Moreover, the surface of Zn-Por will be amino positively charged to promote cell internalization. Additionally, at intracellular acidic microenvironments (~5.3) the metallo-supramolecular-coordination will fall apart and carried drug and Zn-Por will be realised due to the removal of gatekeeper. The cytotoxicities of final NPs in the dark against HeLa and MCF-7 cells were evaluated *in vitro* by a standard MTT assay. These experiments indicated that MSNPs had good biocompatibility and no toxicity towards the normal cells. Moreover, compared with the single chemotherapy of DOX or PDT of Zn-Por in MSNPs, dual pH-responsive MSPs showed higher *in vitro* cytotoxicity. All of this together showed a great potential of this new nanomaterial in cancer treatment.

Juan L. Vivero-Escoto *et al.*[126] loaded MSNPs with cisplatin and aluminum chloride phthalocyanine (AlClPc) for combination chemotherapy and PDT (**Figure 29**).

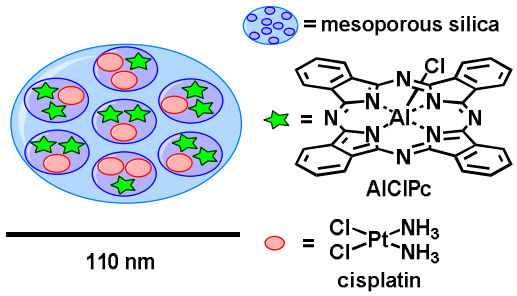

Figure 29. MSNPs with cisplatin and aluminum chloride phthalocyanine.

MSNPs were synthesized by surfactant-templated approach using CTAB as the surfactant.[127] When NPs were prepared, first AlClPc and then cisplatin molecules were loaded into MSNPs after stirring in DMSO. According to SEM and TEM the size of final NPs was 109.7 ± 13.3 nm.

Intracellular uptake and cytotoxicity were evaluated in human cervical cancer (HeLa). These experiments showed that the MSNPs can be internalized in HeLa cells. Furthermore, after light exposure, the combination of both AlClPc and cisplatin compounds in the same MSNPs produce higher cytotoxic effect against HeLa cells in comparison to the control

MSNPs loaded with AlClPc and MSNPs loaded with cisplatin. This is another good example of SNPs which simultaneously carry PS and anticancer drug for combination PDT and chemotherapy to treat cancer.

Double action of PDT and PTT

Another way to improve PDT is to combine it with photothermal therapy (PTT) to get a double action of both treatments. Koichiro Hayashi *et al.*[128] combined photodynamic and photothermal therapies using a single light source with photostable iodinated silica/porphyrin hybrid NPs with heavy-atom effect. The combination of PDT and PTT can lead to a synergistic effect. Unfortunately, in that kind of systems two light sources of different wavelengths usually are required, and PDT and PTT are separately carried out. It is difficult to focus the two light beams at the same position thus, this sequential irradiation complicates the treatment process. Here, it was decided to develop nanoplatforms that generate $^1O_2$ and heat by irradiation with a light source of single wavelength.

For this reason iodinated silica/Por hybrid NPs with high Por content were synthesized *via* covalent linkage by a sol-gel method using Por-containing silicon alkoxide and (3-iodopropyl)trimethoxysilane as precursors (**Figure 30**). The surface of NPs were modified with PEG and FA. PEG was used to prevent phagocytosis by the reticuloendothelial system (RES) and extend the retention time in blood. Consequently, PEG promote the enhanced permeability and retention effect and FA increases NPs' accumulation in tumors. Final NPs were spheres with rough surfaces and mean diameter of 47 ± 12 nm.

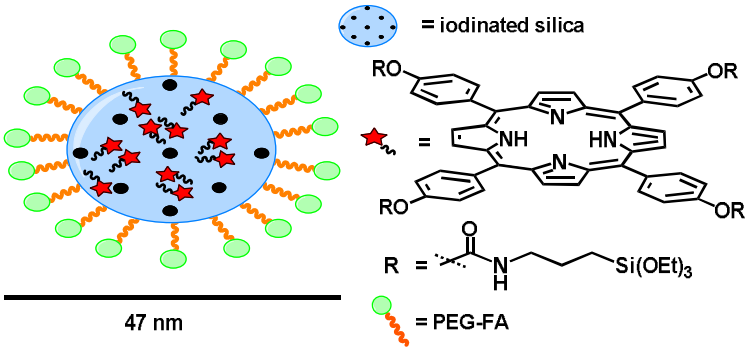

Figure 30. Silica/porphyrin hybrid NPs decorated with PEG and FA.

These NPs under LED irradiation can generate both $^1O_2$ and heat, acting as PSs in PDT and as nanoheaters in PTT. Additionally, they exhibit the external heavy atom effect,

which considerably enhances the quantum yield for $^1O_2$ generation and the light-to-heat conversion efficiency.

For the biological study human myeloma RPMI 8226 cell line was chosen. The *in vivo* fluorescence imaging demonstrated that NPs with FA and PEG on its surface, were locally accumulated in the tumor cells into tumor-bearing mice. Moreover, the LED irradiation on the tumor area effects necrosis to the tumor tissues. The synergetic effect of both PDT and PTT treatment results in the inhibition of tumor growth and higher mice survival rate. This easy to prepare nanosystem could be employed in the PDT/PTT combination therapy against multiple myeloma, which is resistant to conventional chemotherapy.

Z. X. Zhao *et al.*[129] prepared novel mesoporous silica composite NPs of AlC_4Pc and Pd nanosheet which were used as a dual carrier system to combine PDT with PTT (**Figure 31**). This combination is possible because Pd nanosheets and PS display matched maximum absorptions in the range of 600–800 nm, thus the final nanomaterials can produce $^1O_2$ and heat upon 660 nm single continuous wavelength laser irradiation.

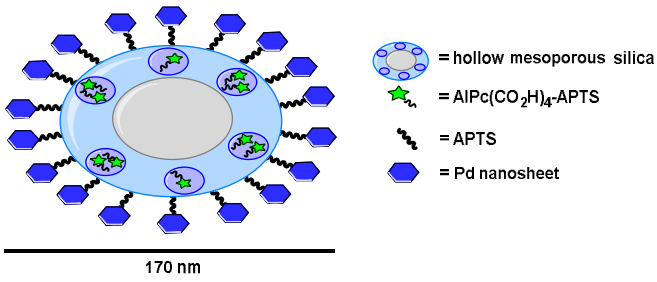

Figure 31. Hollow mesoporous silica composite NPs consists of AlC_4Pc and Pd nanosheet.

To prepare these materials first, water soluble PS was synthetized and covalently linked to a mesoporous silica network. In the next step, Pd nanosheet covered the surface of mesoporous silica by both coordination and electrostatic interaction. Initially SNPs were prepared using a modified Stöber method and then these NPs were coated with CTAB/SiO_2 shell *via* base-catalyzed hydrolysis of TEOS and condensation of silica onto the surface of CTAB pre-coated SNPs. Simultaneously, the AlC_4Pc-APTS conjugate was also covalently incorporated into the silica shell. To obtain NPs with hollow cores and penetrating pore channels, Na_2CO_3 was utilized to remove silica core-generating templates and NH_4NO_3 was used to remove CTAB pore-generating templates. Finally, small Pd nanosheets were deposited onto the surface of amino-modified NPs to get final NPs.

The obtained hollow mesoporous silica structure not only improved the hydrophilic property of the PS, but also generated $^1O_2$ that can be easily released from the matrix. After confirmation of $^1O_2$ generation by these NPs, photothermal effect of these materials under the irradiation of a 660 nm laser (0.5 Wcm^{-2}), that is used for the PDT, were investigated. It was observed that the temperature of the NPs' solution (200 μg of NPs in 1.0 ml of water) rapidly increased from 26.4 °C to 37.4 °C after 4 min of 660 nm irradiation. This proved the possibility of using this novel material in PDT and PTT simultaneously. The prepared NPs exhibited good biocompatibility and were easily up taken by cancer cells. *In vitro* results with HeLa cells showed that the cell-killing efficacy by using these NPs together with PDT and PTT was higher than PDT or PTT individual.

Conclusions

Considerable efforts have been made toward the research and development of nanoplatforms for cancer photodiagnostic and photodynamic therapy. Among the nanoparticle platforms, SNPs show particular promise. In this review, we highlighted the major research advances involving cancer photodiagnostic and photodynamic therapy based on PS-SNPs. We summarized the recent use of Por and Pc in PDT, but also the application of PS-SNPs in PDT with assistance of UCNPs, PDT with chemotherapy in combination treatment, and double action of PDT and PTT. Overall, the research advances in PS-SNPs delivery systems are exciting and hold great potential for future PDT applications.

Acknowledgements

Thanks are due to FCT/MEC for the financial support to QOPNA (FCT UID/QUI/00062/2013), CICECO-Aveiro Institute of Materials (FCT UID/CTM/50011/2013) and CQE (FCT UID/QUI/0100/2013) research units, through national funds and where applicable cofinanced by the FEDER, within the PT2020 Partnership Agreement. The work was also supported by the Spanish MINECO (CTQ-2014-52869-P) and Comunidad de Madrid (FOTOCARBON, S2013/MIT-2841). We further wish to thank the Seventh Framework Programme (FP7-People-2012-ITN) for funding the SO2S project (grant agreement number: 316975).

CHAPTER 2: Encapsulation of glycosylated porphyrins in silica nanoparticles for photodynamic therapy *in vitro*

Wioleta Borzęcka,[1,2,3] Patrícia M. R. Pereira,[1,4] Rosa Fernandes,[4,5] Tito Trindade,[2] Tomás Torres,[3,6] and João Tomé[1,7]

[1]QOPNA and [2]CICECO, Department of Chemistry, University of Aveiro, 3810-193 Aveiro, Portugal; [3]Department of Organic Chemistry, Autonoma University of Madrid, 28049 Madrid, Spain; [4]Laboratory of Pharmacology and Experimental Therapeutics, Institute for Biomedical Imaging and Life Sciences (IBILI), Faculty of Medicine, University of Coimbra, Azinhaga de Santa Comba, Coimbra, Portugal; [5]CNC.IBILI, University of Coimbra, 3000 Coimbra, Portugal; [6]IMDEA-Nanociencia, Campus de Cantoblanco, c/Faraday 9, 28049 Madrid, Spain; [7]Centro de Química Estrutural, Departamento de Engenharia Química, Instituto Superior Técnico, Universidade de Lisboa, 1049-001 Lisboa, Portugal

Keywords: Porphyrins, Photosensitizers, Silica Nanoparticles, PDT, Cancer

Abstract: In this study, we report the preparation, characterization and *in vitro* studies of amorphous silica nanoparticles encapsulating porphyrins (Pors). *S*-glycoside porphyrins were prepared and encapsulated into silica nanoparticles (SNPs) by Stöber method. These new materials were fully characterized and their *in vitro* properties were examined in two human bladder cancer cell lines, HT-1376 and UM-UC-3. The results shows that these new nanoformulations could be successfully used as novel photosensitizers (PSs) for photodynamic therapy (PDT).

Introduction

Cancer is a major public health problem for humans, being the second leading cause of death in developing countries, just behind the heart diseases.[130] Although we made improvements in healthcare, still more people have cancer today than ever before. According to trends in the lifetime risk of developing cancer in Great Britain, the biggest risk factor for most cancers is just getting older.[131] Up to now, to treat cancer we use surgery, chemotherapy, radiotherapy, and PDT. Unfortunately, these treatments for some patients are not efficient. Among the others, PDT is a promising therapeutic procedure used in cancer treatment which combines three components: drug, visible or NIR lights and oxygen. By its own these units do not have any toxic effects on the biological systems. They become strongly cytotoxic to the target cells only when they produce reactive oxygen species (ROS) which take place when the drug, called PS or photosensitizing agent is in contact with molecular oxygen under specific light irradiation. [132-135] Despite the fact that PDT was approved by Food and Drug Admnistration (FDA) 20 years ago as a clinical protocol for cancer treatment, the method still have limitations to use it as a general protocol to treat any type of cancer.

Thus, there is still need to study alternatives to improve the efficiency of PDT and eliminate its limitations, such as: low effectiveness in treating large tumors, burns, swelling, pain, and scarring in nearby healthy tissues or a persistent skin photosensitization. For that it is crucial to improve equipment and the delivery of the activating light. Also, it is important to develop new powerful PSs, which specifically target cancer cells, and activated by light that can penetrate tissue and treat large tumors. In the context of all limitations, NPs have recently emerged as promising vehicles for PDT giving the possibility to successfully improve cancer treatment.[38,136,137]

Most of the PSs that are used in cancer therapy and other tissue diseases are based on a tetrapyrrole structure, such as: porphyrins (Pors),[10,138,139] chlorins,[140-143] bacteriochlorins,[144-146] and phthalocyanines (Pcs).[147-150]

Using PSs in PDT as different nanoformulations can improve the treatment by increasing the biocompatibility of most of the hydrophobic PSs' and their blood circulation. Also selective accumulation in tumor tissues can be improved thanks to enhanced permeability

and retention effect (EPR).[39,40,151] Among others nanomaterials, silica nanoparticles (SNPs) have emerged as promising vehicles for PDT owing to their biocompatibility, large surface area, controllable size formation, hydrophilic surface and ability for surface functionalization, hence the possibility for tumor targeting through surface modification.[42] Moreover, amorphous silica shells can protect against chemical and biochemical degradation, release of toxic ions, and activation of immune response.[152] Already there are same nanoparticle-based drug delivery platforms which were approved by FDA and others under clinical trials.[153-155]

One of the main goals to advanced PDT is to design drugs which specifically can target the tumor cells with rapid cellular uptake but do not damage the healthy ones. In this field SNPs arrived as an outstanding platforms to covalently and non-covalently immobilize PS outside or inside them. Recent studies demonstrated that using SNPs combined with Pors could eliminate aggregation of the Pors, low water compatibility or reduced selectivity for targeted tissues and consequently increase the PDT efficiency.[93,156] The pioneering work in this field appeared in 2003 when Yan *et al.*[157] embedded meta-tetra(hydroxyphenyl)-chlorin into silica nanoparticle platforms and showed that it could generate singlet oxygen ($^1O_2$) while the PS effect is maintained. Moreover, the authors have shown that the $^1O_2$ production by the SNPs is higher than the one from the free PS. From that time scientist put a lot of effort to enhance PDT with PS-SNPs.

For instance, Gao *et al.*[95] in a simple method enhanced photodynamic selectivity of Pors adsorbed onto SNPs against breast cancer cells. In the same year, He *et al.*[96] developed organically modified silica (ORMOSIL) nanoparticles encapsulated with protoporphyrin IX (PpIX) for direct two-photon PDT. In this research ORMOSIL nanoparticles were able to successfully destroy HeLa cells. Ho *et al.*[97] also used PpIX with mesoporous silica nanocarriers for selective PDT of cancer. These highly efficient, non-cytotoxic drug delivery platforms designed for PDT were phospholipid-capped, PpIX-loaded and fluorescein FITC-sensitized mesoporous silica nanocarriers derivatized with folate. These complex SNPs were effective to kill targeted HeLa and A549 cells *in vitro* and prevent further tumor growth. Miao X. *et al.*[100] were able to overcome hydrophobic nature of Photosan-II by loading it into hollow SNPs. By this they eliminated the difficulties with the delivery in physiological environment and the low photophysical properties due to the

aggregation of PSs, which decreased the production of $^1O_2$ for PDT. These NPs enhance the photoactivity of the PS against QBC939 cells. Later, Wen *et al.*[101] proved that these NPs in *in vitro* and *in vivo* experiment on liver cancer in nude mice were more efficient than the PS alone. Qian *et al.*[104] went a little bit further and developed Por (HPPH) doped colloidal mesoporous silica nanoparticles for three-photon photodynamic therapy. The cytotoxicity of PDT towards HeLa cells, which were uptaken by HPPH doped SNPs were proved.

For cancer treatment applications, an ideal PS should be a chemically pure compound with good photostability and water solubility, should have a high absorption peak between 600 and 800 nm (red to deep red), should have no dark toxicity, and relatively rapid clearance from normal tissues and organs.[158-161] In this work 5,10,15,20-tetrakis(4-1'-thio-glucosyl-2,3,5,6-tetrafluorophenyl) porphyrin (Glu-Por, **PS 1**) and 5,10,15,20-Tetrakis(4-1'-thio-galactosyl-2,3,5,6-tetrafluorophenyl) porphyrin (Gal-Por, **PS 2**) were chosen as PSs (**Figure 1**). These Pors were chosen as PSs platforms because there are a number of reports on the potential of glycosylated porphyrins as PDT agents.[162-166] In our research it was decided to use Pors with *S*-glycoside bonds rather than *O*-glycoside because drugs bearing saccharides with *O*-glycoside linkages generally have short half-lives because this bond is readily hydrolyzed by a variety of enzymatic and nonenzymatic acid/base reactions.[167] It is known that aggregation of the PS decreases the efficiency of $^1O_2$ generation. Thus, we decided to deliver PSs inside cancer cells into nanovehicles which could also enhance stability of these PSs in the aqueous media. Hence, PSs were non-covalently encapsulated into amorphous silica matrix, and then these nanomaterials were studied on cancer PDT.

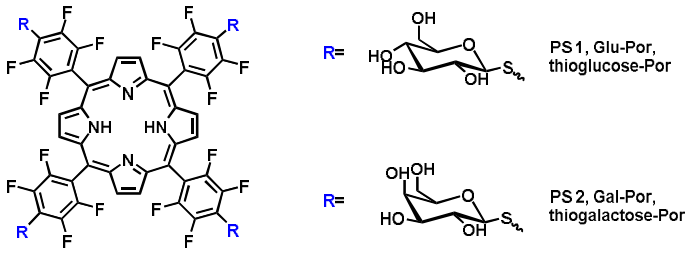

Figure 1. Structures of Glu-Por and Gal-Por used as free and encapsulated PSs.

Results and discussion

Synthesis of PSs

Porphyrins **PS 1** and **PS 2** were synthesized according to literature procedures present elsewhere.[162-166] By using the nucleophilic substitution of the p-fluorine of the corresponding free-base porphyrin 5,10,15,20-tetrakis(pentafluorophenyl)porphyrin ($TPPF_{20}$) with acetyl 2,3,4,6-tetra-*O*-acetyl-1-thio-D-glucopyranoside or acetyl 2,3,4,6-tetra-O-acetyl-1-thio-D-galactopyranoside were obtained the corresponding protected carbohydrate porphyrins. Applying simple click type synthesis these Pors bearing four carbohydrate moieties, conjugated *via* *S*-glycoside bond were obtained in very high yields. Final deprotection of the carbohydrate moieties using alkaline hydrolysis afforded the final *S*-glycoside porphyrins **PS 1** and **PS 2**.

Preparation of NPs and their PS-NP hybrids

SNPs and their Por-NP nanoformulations were prepared by Stöber method in which the hydrolysis and condensation of tetraethyl orthosilicate (TEOS) is facilitated by base in ethanol and water (**Figure 2**).[168]

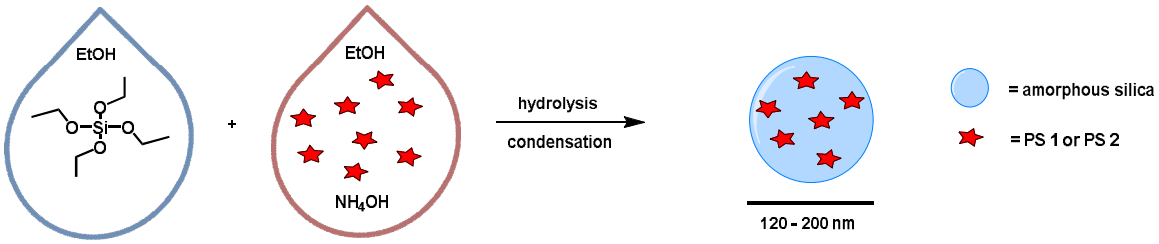

Figure 2. Schematic preparation of PSs encapsulated into SNPs.

To get high $^1O_2$ generation it is crucial to encapsulate as much as possible of PSs inside NPs and to keep or improve the photophysical properties of the PSs after encapsulation. Therefore, firstly the conditions of NPs' preparation were optimized by varying the amount of base, TEOS and PS (**Table 1, 2, 3**). Compound **PS 1** was chosen as the model to optimize reactions. Generally, in 15 mL falcon tube PS was dissolved in EtOH and then NH_4OH was added (total volume of this mixture was 6.250 mL). The mixture was sonicated for 5 min and TEOS dissolved in EtOH was added (total volume of this mixture was 1.250 mL). The reaction was incubated for 24 h at 25 °C under continuous agitation

(250 rpm) in laboratory incubator shaker (IKA KS 4000 i control) in horizontal position. After that time NPs were isolated by centrifugation (15 mL falcon tubes, 6000 rpm, 30 min) and washed 4 times with EtOH. The final NPs were dried at room temperature.

PSs encapsulation optimization studies

Keeping the amount of PS and TEOS constants, three reactions with different amounts of base were performed to determine the amount of encapsulated PS *versus* the amount of base (**Table 1**). In this case 5 mg of **PS 1** (2.977 µmol) were dissolved in EtOH and then NH_4OH was added. The mixture was sonicated for 5 min and 83.7 µL of TEOS (0.375 mmol) dissolved in EtOH was added. After 24 h reaction NPs were washed and dried at room temperature.

NP	NH_4OH [µL] [mol]	PS inside final NPs [mg] [µmol]	Total amount of final NPs [mg]	mg of PS/ mg of final NPs *100 [%]	Size of final NPs [nm]
NP 1	187.5 0.0012	-	-	-	-
NP 2	375 0.0024	1.59 0.95	20.0	7.95	58.4 ± 6.5
NP 3	750 0.0048	1.36 0.81	24.0	5.67	266.6 ± 24.4

Table 1. Detailed experimental data showing how amount of encapsulated **PS 1** depends on the amount of base.

From these results it is clear that higher concentrations of NH_4OH, give a smaller amount of encapsulated **PS 1** into NPs. However, too low concentration of base unable even the formation of NPs (**NP 1**). The concentration of base also influences the size of NPs. After increasing twice the concentration of NH_4OH, the size of NPs increased almost 5 times (**NP 2** *versus* **NP 3**). For the further synthesis, 0.0024 mol of NH_4OH was used.

Keeping the amounts of PS and base constants, the dependence on amount of encapsulated PS from amount of TEOS were determined. For this, 5 mg of **PS 1** (2.977 µmol) was dissolved in EtOH and then 375 µL of NH_4OH (0.0024 mmol) was added. The mixture

was sonicated for 5 min and TEOS dissolved in EtOH was added (**Table 2**). After 24 h reaction NPs were washed and dried at room temperature.

NP	TEOS [µL] [mmol]	PS inside final NPs [mg] [µmol]	Total amount of final NPs [mg]	mg of PS/ mg of final NPs *100 [%]	Size of final NPs [nm]
NP 2	83.7 0.375	1.59 0.95	20	7.95	58.4 ± 6.5
NP 4	500 2.239	1.7 1.01	134.6	1.27	57.5 ± 10.7

Table 2. Detailed experimental data showing how amount of encapsulated PS depends on amount of TEOS.

It was observed that the decrease of TEOS in the reaction medium by almost six times, increases the concentration of PS in final NPs by 6.3 times. Thus, the amount of TEOS was kept as 83.7 µL for the next studies.

Then, we determined how amount of encapsulated PS depends on amount of PS in the reaction mixture (keeping the amounts of TEOS and base constants). For this, **PS 1** was dissolved in EtOH and then 375 µL of NH_4OH (0.0024 mmol) was added. The mixture was sonicated for 5 min and 83.7 µL of TEOS (0.375 mmol) dissolved in EtOH was added (**Table 3**). After 24 h reaction NPs were washed and dried at room temperature.

NP	PS [mg] [µmol]	PS inside final NPs [mg] [µmol]	Total amount of final NPs [mg]	mg of PS/ mg of final NPs *100 [%]	Size of final NPs [nm]
NP 5	2.5 1.489	0.6713 0.4	19.7	3.41	48.1 ± 4.6
NP 2	5.0 2.977	1.59 0.95	20	7.95	58.4 ± 6.5
NP 6	20.0 11.909	6.7 3.989	25.5	26.27	104.1 ± 6.2
NP 7	50.0 29.77	11.2 6.66	23.0	48.7	197.3 ± 29.0

Table 3. Detailed experimental data showing how amount of encapsulated PS depends on amount of starting PS.

As it is shown in above table (**Table 3**), the higher the concentration of PS in reaction mixture, the more effective is encapsulation of PS into NPs. Moreover, the size of NPs is changing with the same tendency. This is probably due to the fact that when the amount of PS was increased in the reaction medium, silica forms bigger pores and NPs become bigger.

Selected PS-NPs formulation protocol

The most successful results were obtained with the preparation of **NP 7** and, consequently, NPs encapsulating compound **PS 2** (**NP 8**, **Table 4**) were prepared according to the same procedure. In both cases the amount of encapsulating PS were almost the same. The same protocol was used to synthetize silica nanoparticles in the absence of PS (**SNP**) for further comparison and characterization (for details, please go to the SI).

NP	PS 1 [mg] [µmol]	PS 2 [mg] [µmol]	PS inside final NPs [mg] [µmol]	Total amount of final NPs [mg]	mg of PS/ mg of final NPs *100 [%]	µmol of PS/ mg of final NPs	Size of NPs [nm]
NP 7	50.0 29.77	-	11.2 6.66	23.0	48.7	0.289	197.3 ± 29.0
NP 8	-	50.0 29.77	10.2 6.07	28.2	36.0	0.215	128.3 ± 22.2

Table 4. Detailed experimental data showing differences between encapsulation of **PS 1** (**NP 7**) and **PS 2** (**NP 8**).

SNPs and PS-NPs characterization

The selected NPs were morphologicaly and chemicaly characterized by several image and spectroscopic techniques. For details, please go to the SI.

The average size of all NPs was measured by transmission electron microscopy (TEM, **Figure SI 6-8**). For final materials, **NP 7** and **NP 8** dynamic light scattering (DLS) was also used to determine their size distribution (**Figure SI 9, 10**). The particle size distribution was measured after drying the sample (TEM) and in dispersion in water (DLS). The difference in particle sizes measured by TEM (**NP 7**, 197.3 ± 29.0 nm; **NP 8**, 128.3 ± 22.2 nm) and DLS (**NP 7**, 233.5 nm; **NP 8**, 133.2 nm) showed the common

difference between the mean hydrodynamic diameter (measured by DLS) and the size (measured by TEM). Typically the hydrodynamic diameter obtained by DLS is larger than the size gathered by TEM. These NPs have uniform size distribution and are regular in terms of the size and shape.

Among other parameters, NPs' interactions with cancer cells depends on NPs' size which influence its active and passive cellular internalization. Since cell-NP interactions are modulated by size of NPs hence the size of nanodrug can determine the therapeutic targeting.[169] Presented NPs have very good size for passive targeting to tumor tissues. Compare with healthy cells, tumor cells have poor lymphatic drainage and leaky vasculature. Because of that particles ranging from 10 to 500 nm accumulate inside tumor cells and lymphatic filtration allows them to stay there. In contrary, very often much smaller ordinary drugs cannot remain in tumors because they return to the circulation by diffusion process.[170,171]

The UV-Vis absorption spectra of **NP 7** and **NP 8** were collected after dispersing, respectively, 0.535 and 0.510 mg of them in 3mL of distilled water (**Figure SI 13**). It is clear that both show the typical spectra of a free base Por, with the Soret band at 403 nm (**NP 7**) and 407 nm (**NP 8**).

The EDS spectra show the chemical composition of **NP 7** and **NP 8**, where a small percentage of sulphur must be related to the thio-carbohydrate moieties of the Pors (**Figure SI 11, 12**). **PS 1**, **PS 2**, **SNP** and the corresponding **NP 7** and **NP 8** were also analysed by FT-IR (**Figure SI 14**). The spectra of both NPs formulations show some of the features of the porphyrins (**PS 1** and **PS 2**) and the solely silica nanoparticles (**SNP**).

The amount of encapsulated PS inside NPs was calculated by UV-Vis spectrophotometry. The final NPs were washed with EtOH until no typical Soret and Q bands were observed in the rinse solvent. **NP 7** (0.289 µmol/mg) have slightly higher concentration of PS per mg of final material than **NP 8** (0.215 µmol/mg).

Singlet oxygen generation study

Singlet oxygen ($^1O_2$) was determined by an indirect chemical method using 1,3-diphenylisobenzofuran (DPBF) as $^1O_2$ quencher (for details, please go to the SI). The $^1O_2$

was determined for both nanoformulations (**NP 7** and **NP 8**) and its corresponding PSs (**PS 1** and **PS 2**) (**Figure 3**). The free **PS 1** and **PS 2** were tested at concentrations of 0.5 µM. **NPs** composed of **PS 1** and **PS 2** were tested at concentrations of PS: 12.6 µM (**NP 7**) and 1.6 µM (**NP 8**). Both free PSs oxidized DPBF in the same way. In spite of the different amount of PS inside NPs and the different size of these nanoformulations, DPBF kinetic decay was similar in the two nanoformulations. From this study we can observe that 0.131 mg of **NP 7** could produce the same amount of $^1O_2$ as 0.022 mg of **NP 8**. Which means that **NP 8** are 6 times more efficient in terms of $^1O_2$ generation. Although **NP 8** (128.3 ± 22.2 nm) are smaller than **NP 7** (197.3 ± 29.0 nm) and have slightly lower amount of PS per mg of NPs (**Table 4**), these NPs produce higher amount of $^1O_2$. This could be due to the fact that in case of smaller NPs oxygen can penetrate better their pores and $^1O_2$ has shorter way to go out from nanoformulation than in bigger NPs. Thus, **NP 8** are more effective in $^1O_2$ production than **NP 7** while corresponding free Pors (**PS 1** and **PS 2**) are producing the same amount of $^1O_2$ under the equal experimental conditions.

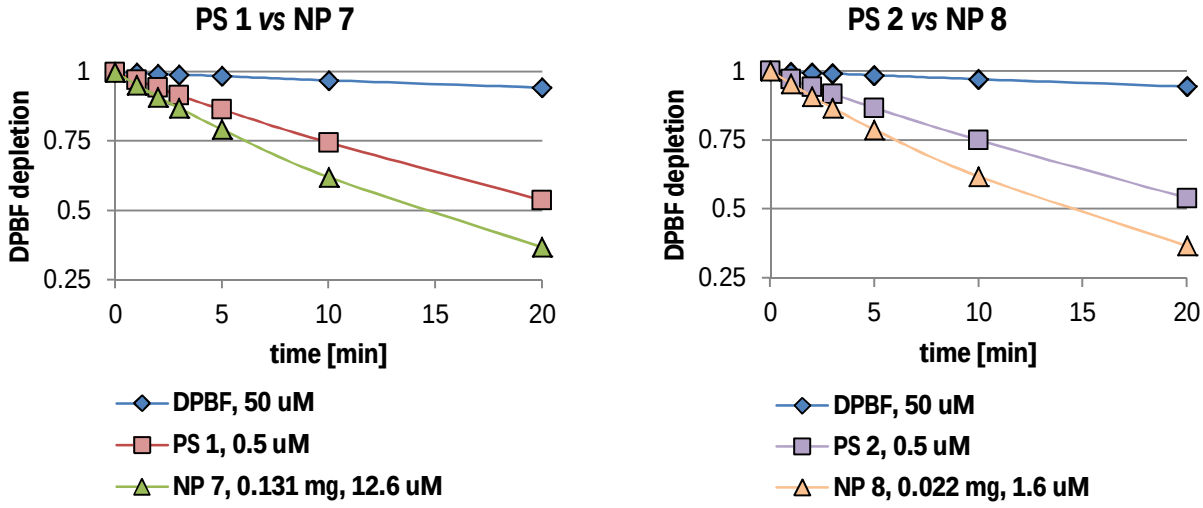

Figure 3. $^1O_2$ generation by **PS 1**, **PS 2** and its corresponding NPs (**NP 7** and **NP 8**) were each point represents the mean of at least three independent experiments, and has a standard deviation lower than 3%.

In vitro studies

In vitro studies were carried out into two human bladder cancer cell lines, HT-1376 and UM-UC-3. These cell lines are suitable *in vitro* cancer models for the evaluation of new glyco-porphyrinoids, since they express the glyco-binding proteins - glucose transporter

(GLUT1) and galactose-binding protein (galectin-1) - in different levels.[148] Previous studies have demonstrated that these two proteins have a key role on the uptake and further phototoxicity of galactodendritic PSs.[148,172-174] We have previously reported that UM-UC-3 and HT-1376 bladder cancer cells have high levels of the galactose-binding proteins, galectin-1 and GLUT1.[148]

Cellular uptake of PSs and its nanoformulations

Preliminary uptake studies were performed for glucosylated **PS 1** and galactosylated **PS 2** (**Figure 4**). Bladder cancer cells were incubated with increasing concentrations of PS (0, 2.5, 5 and 10 μM prepared in PBS, maximum 0.5% DMSO v/v) for 4 h in the darkness. Fluorescence spectroscopy studies demonstrated that **PS 1** accumulation was higher in HT-1376 than in UM-UC-3 cancer cells. On the other hand, the uptake of **PS 2** was higher in UM-UC-3 than in HT-1376 cancer cells.

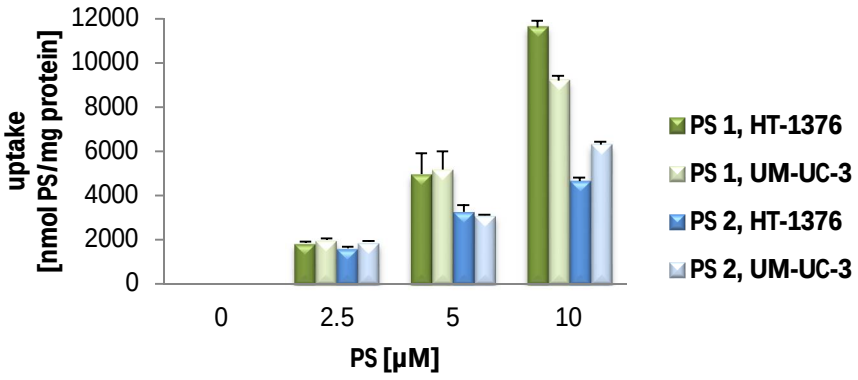

Figure 4. Intracellular uptake of **PS 1** and **PS 2** (0-10 μM in PBS) by UM-UC-3 and HT-1376 bladder cancer cells. Cells were incubated with **PS** for 4 h and uptake was determined by fluorescence spectroscopy. Data are means ± s.e.m. of at least three independent experiments performed in triplicates.

Next, the uptake of **NP 7** and **NP 8** was evaluated by fluorescence spectroscopy and fluorescence microscopy (**Figures 5** and **6**) after incubating UM-UC-3 and HT-1376 bladder cancer cells in dark with different concentrations of the new NPs.

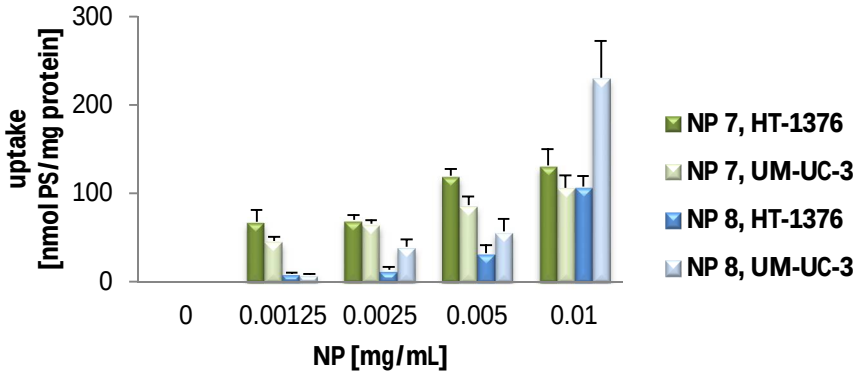

Figure 5. Cellular uptake of **NP 7** and **NP 8**. UM-UC-3 and HT-1376 bladder cancer cells were incubated with **NP 7** (0-0.010 mg/mL, 0-2.89 μM of **PS 1** in RPMI medium) and **NP 8** (0-0.010 mg/mL, 0-2.15 μM of **PS 2** in RPMI medium) overnight. Data are means ± s.e.m. of at least three independent experiments performed in triplicates.

Preliminary studies demonstrated that the uptake of both **NP 7** and **NP 8** (for concentrations ranging from 0 to 0.010 mg/mL) was negligible when cells where incubated with NPs for at least 4 h (data not shown). Further studies were performed by incubating cancer cells with PS nanoformulations overnight. When the cells were incubated overnight with RPMI medium containing NPs solutions there was uptake dependent on the concentration of the NPs and cell line. Interestingly, uptake of **PS 1** and **PS 2** performed with overnight incubation (PS solutions prepared in cell culture medium) was lower (data not shown) when compared with the uptake of 4 h (PS solutions prepared in PBS buffer). The uptake of **NP 7** was higher in HT-1376 cells (which contain high levels of GLUT1 protein) when compared with UM-UC-3 cancer cells (**Figure 5**). On the other hand, **NP 8** uptake was higher in UM-UC-3 cells (which contain high levels of galectin-1 protein) than in HT-1376 cancer cells. Considering the levels of galectin-1 and GLUT1 proteins, the uptake of **NP 7** is higher in HT-1376 cells because these **NPs** contain Por bearing glucose moieties. On the contrary, the higher uptake of **NP 8** in UM-UC-3 cancer cells was observed due to the presence of Por bearing galactose moieties in the pores of these nanoformulations.

Further studies performed by fluorescence microscopy (**Figure 6**) demonstrated a strong fluorescence of **NP 7** and **NP 8** in HT-1376 and UM-UC-3 bladder cancer cells,

respectively, incubated overnight with 0.010 mg/mL of NP formulations (2.89 μM of **PS 1** in case of **NP 7** and 2.15 μM of **PS 2** for **NP 8**).

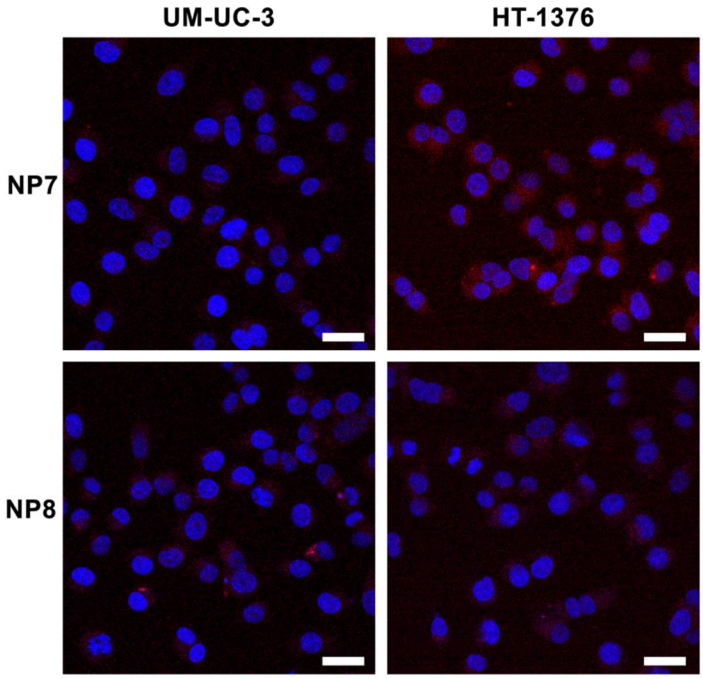

Figure 6. Representative fluorescence images of UM-UC-3 and HT-1376 bladder cancer cells after overnight incubation with **NP 7** (red, 0.010 mg/mL, 2.89 μM of **PS 1**) or **NP 8** (red, 0.010 mg/mL, 2.15 μM of **PS 2**) in darkness and cell nucleus stained with DAPI (blue). Scale bars, 20 μm.

Dark toxicity and phototoxicity

Toxicity of **PS 1**, **PS 2**, **NP 7** and **NP 8** in UM-UC-3 and HT-1376 bladder cancer cells in the dark was evaluated using the well-known MTT assay (**Figures SI 16** and **17**). This colorimetric assay determines the cell metabolic activity, by assessing the ability of living bladder cancer cells to reduce yellow 3-[4,5-dimethylthiazol-2-yl]-2,5-diphenyl-tetrazolium bromide (MTT), to a purple formazan. After overnight incubation of cancer cells (in dark) with NPs (0-0.010 mg/mL in RPMI medium) or 4 h incubation with PSs (0-10 μM in PBS), none of the PSs or new NPs induced dark toxicity in cancer cells (**Figures SI 16** and **17**). Moreover during $^1O_2$ generation studies we observed that NPs are very much stable in the solution of DMF:H_2O (9:1, by volume) in which all experiments were

held (**Figures SI 4** and **5)**. However, during biological experiments slow release of PS form the silica matrix was detected after 4 h and 18 h incubation in PBS buffer or RPMI medium (**Figure SI 15**). Higher release in case of **NP 8** was noted than in **NP 7**.

After confirming the uptake and non-dark toxicity of PSs and their new NP formulations in UM-UC-3 and HT-1376 bladder cancer cells, their toxicity after light irradiation was equally evaluated using the MTT assay (**Figures 7** and **8**). UM-UC-3 and HT-1376 bladder cancer cells were incubated for 4 h with PSs (0-10 µM in PBS) or overnight with NPs (**NP 7**: 0-0.010 mg/mL, 0-2.89 µM of **PS 1** and **NP 8**: 0-0.010 mg/mL, 0-2.15 µM of **PS 2**) and then irradiated with an optical fiber emitting white light for 40 min (12 mW/cm^2). No cytotoxicity was observed in the untreated (cells incubated in the absence of PSs or NPs) sham irradiated cells.

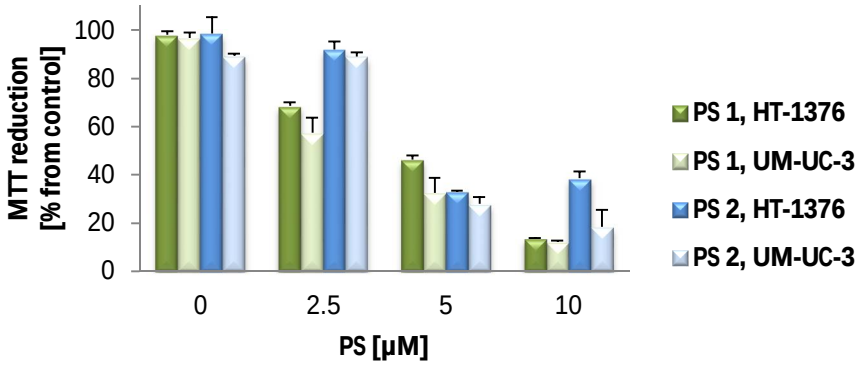

Figure 7. Phototoxicity of **PS 1** and **PS 2** (0-10 µM in PBS) determined 24 h after PDT treatment using the MTT assay. The percentage of cytotoxicity was calculated relatively to control cells (cells incubated with PBS and then irradiated). Data are means ± s.e.m. of at least three independent experiments performed in triplicates.

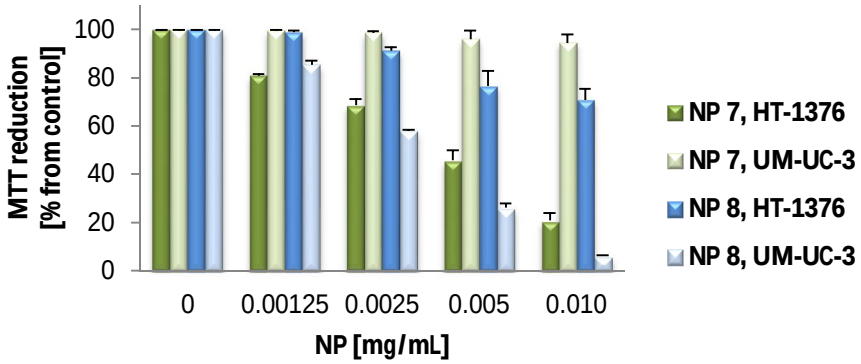

Figure 8. Phototoxicity of **NP 7** (0-0.010 mg/mL, 0-2.89 μM of **PS 1**) and **NP 8** (0-0.010 mg/mL, 0-2.15 μM of **PS 2**) determined 24 h after PDT treatment using the MTT assay. The percentage of cytotoxicity was calculated relatively to control cells (cells incubated with RPMI medium and then irradiated). Data are means ± s.e.m. of at least three independent experiments performed in triplicates.

Both PSs and NPs induced phototoxicity in UM-UC-3 and HT-1376 bladder cancer cells in a concentration- and cell line-dependent manner. However, in case of NPs the phototoxicity much more depends on cell line type than in case of PSs (**Figure 7** and **Figure 8**). **NP 7** led to a significantly higher phototoxicity on HT-1376 cells compared to UM-UC-3 cells (**Figure 8**). The phototoxicity of **NP 8** was higher in UM-UC-3 than in HT-1376 bladder cancer cells (**Figure 8**). Taking into account the levels of galectin-1 and GLUT1 proteins, the phototoxicity of **NP 7** is higher in HT-1376 cells because the uptake of these NPs was higher due to the presence of Por bearing glucose moieties. All the same, the higher phototoxicity of **NP 8** in UM-UC-3 cancer cells was due to their higher uptake by these cells because of Por bearing glucose moieties. SNPs without PSs do not induced phototoxicity in UM-UC-3 and HT-1376 bladder cancer cells (data not shown).

Phototoxicity was higher with NP formulations than with PS (**Figures 7-9**). From the below figure it is clear that these new nanomaterials are more efficient in PDT than corresponding free Pors (**Figure 9**). **NP 7** with 2.89 μM of **PS 1** were able to destroy almost the same amount of HT-1376 cells as 10 μM of free **PS 1**. Likewise **NP 8** with 2.15 μM of **PS 2** were able to damage almost equal amount of UM-UC-3 cells as 10 μM of free **PS 2**. Thus, these NPs are around 3-5 times more effective in photodynamic treatment than their free Pors.

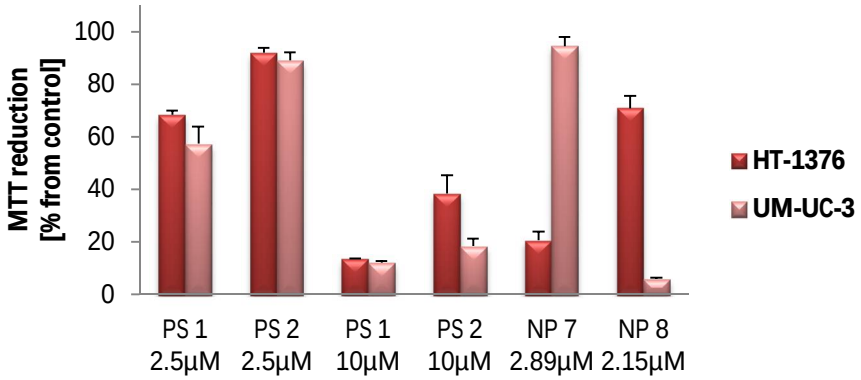

Figure 9. Phototoxicity of **PS 1** (2.5 µM, 10 µM), **PS 2** (2.5 µM, 10 µM), **NP 7** (2.89 µM of **PS 1**) and **NP 8** (2.15 µM of **PS 2**) determined 24 h after PDT treatment using the MTT assay. The percentage of cytotoxicity was calculated relatively to control cells (cells incubated with RPMI medium and then irradiated). Data are means ± s.e.m. of at least three independent experiments performed in triplicates.

The role of cytotoxic ROS generated after PDT with 0.010 mg/mL of **NP 7** (2.89 µM of **PS 1**) and **NP 8** (2.15 µM of **PS 2**) was evaluated using sodium azide, histidine[175] and cysteine[176] as ROS quenchers. When PDT experiments were performed with cells in the presence of non-toxic concentrations of ROS quenchers, there was reduction on the phototoxicity induced by the new NPs. Data show that $^1O_2$ should have a high effect on the phototoxicity induced by **NP 7** or **NP 8**, since phototoxicity was highly reduced when PDT experiments were performed with $^1O_2$ quenchers (sodium azide and histidine).

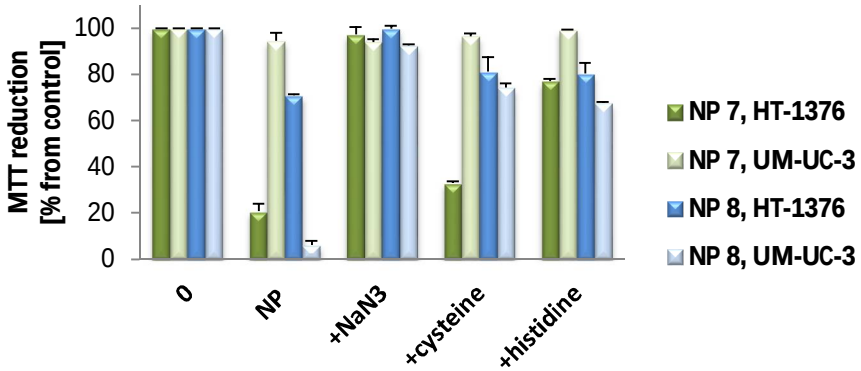

Figure 9. Phototoxicity after PDT with **NP 7** (0.010 mg/mL, 2.89 µM of **PS 1**) and **NP 8** (0.010 mg/mL, 2.15 µM of **PS 2**) in the presence of 50 nM of ROS quenchers (sodium

azide, histidine and cysteine) in HT-1376 and UM-UC-3 cells. Cytotoxicity was assessed 24 h after treatment using the MTT assay. The percentage of cytotoxicity was calculated relatively to control cells (untreated cells). Data are means ± s.e.m. of at least three independent experiments performed in triplicates.

Conclusions

In summary, two types of new PS-loaded silica nanoparticles were successfully prepared after modification and optimization of well-known Stöber method. Both novel materials were able to produce $^1O_2$ hence *in vitro* studies with two human bladder cancer cell lines, HT-1376 and UM-UC-3, were performed. Despite slightly lower efficiency in terms of singlet oxygen generation compered to non-immobilized PSs, the nanocarriers offer an alternative route to develop new platforms for PDT. Overall, these NPs presented 3-5 times higher therapeutic efficacy *in vitro* compering with corresponding free PSs. In the presented work, we demonstrated that *S*-glycoside Pors encapsulated into silica matrix by straightforward Stöber method were more efficient in *in vitro* PDT against two human bladder cancer cell lines, HT-1376 and UM-UC-3, than non-encapsulated PSs.

Acknowledgements

Thanks are due to FCT/MEC for the financial support to QOPNA (FCT UID/QUI/00062/2013), CICECO-Aveiro Institute of Materials (FCT UID/CTM/50011/2013), IBILI (FCT UID/NEU/04539/2013) and CQE (FCT UID/QUI/0100/2013) research units, through national funds and where applicable cofinanced by the FEDER, within the PT2020 Partnership Agreement. The work was also supported by the Spanish MINECO (CTQ-2014-52869-P), Comunidad de Madrid (FOTOCARBON, S2013/MIT-2841) and Portuguese COMPETE (POCI-01-0145-FEDER-007440). We further wish to thank the Seventh Framework Programme (FP7-People-2012-ITN) for funding the SO2S project (grant agreement number: 316975).

Supplementary Information

Encapsulation of glycosylated porphyrins in silica nanoparticlesfor photodynamic therapy *in vitro*

Experimental section

General methods

Absorption spectra were recorded using a Shimadzu UV-2501-PC. FT-IR spectra were recorded in KBr pellets using GRASEBY SPECAC. The irradiation system used to determine the production of $^1O_2$ and the phototoxicity during *in vitro* experiments was a Lumacare source, model LC-122, consisting on a 250 W halogen lamp coupled to an optical fiber (with a cutoff filter for wavelengths <540 nm). The radiation power was measured with a potentiometer bright Spectra Physics, model 407A and the sensor of the same brand, model 407A-2. The dynamic light scattering (DLS) measurements were taken by Zetasizer Nano ZS from Malvern Instruments. Transmission electron microscopy (TEM) images were obtained using a Hitachi H-9000 transmission electron microscope operatingat an acceleration voltage of 300 kV and JEOL 2200FS transmission electron microscope operating at an acceleration voltage of 200 kV.

All reagents were obtained from commercial sources and were used without further purification steps. Reverse phase column chromatography was carried out on Waters Sep-Pak C18 35 cm^3 cartridges. Analytical thin layer chromatography (TLC) was carried out on pre-coated silica gel sheets (Merck, 60, 0.2 mm).

Preparation of NPs

In a 15 mL falcon tube 50 mg of **PS 1** or **PS 2** (29.77 µmol) was dissolved in 5.875 mL of EtOH and then 0.375 mL of 25% NH_4OH (2.4 mmol) was added. The mixture was sonicated for 5 min and 83.7 µL of TEOS (0.375 mmol) in 1166.0 mL of EtOH was added. The reaction was incubated for 24 h at 25 °C under continuous agitation (250 rpm) in laboratory incubator shaker (IKA KS 4000 i control) in horizontal position. After that time NPs were isolated by centrifugation (15 mL falcon tubes, 6000 rpm, 30 min) and washed with EtOH. The final NPs were dried at room temperature.

The same method was used to synthetize silica nanoparticles in the absence of PS with the average size of 86.1 ± 10.3 nm (named as **SNP**).

Singlet oxygen generation study

Singlet oxygen ($^1O_2$) was determined by a chemical method using 1,3-diphenylisobenzofuran (DPBF). DPBF has an absorption maximum at 415 nm, thus it is possible to follow the ability of the NPs to generate $^1O_2$ by measuring the DPBF absorption decay, at this wavelength. The solutions were irradiated at RT and under magnetic stirring, with optical fiber (with a cutoff filter for wavelengths <540 nm) at a fluence rate of 10 mW/cm^2.

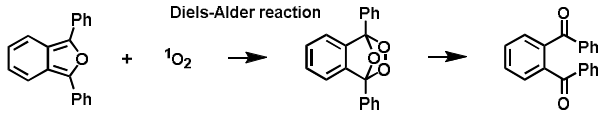

Figure SI 1. Reaction of DPBF with $^1O_2$.

PS 1 (0.5 μM), **PS 2** (0.5 μM), **NP 7** (0.131 mg, 12.6 μM of **PS 1**) or **NP 8** (0.022 mg, 1.6 μM of **PS 2**) were placed into 3 mL cuvette which contained solution of DMF:H_2O (9:1, by volume). Then, DPBF (50 μM) in solution of DMF:H_2O was added (total volume in cuvette 3 mL). The breakdown of DPBF was monitored by measuring the decrease in absorbance at 415 nm at pre-established irradiation intervals. The results were expressed by plotting the DPBF depletion against the irradiation time. The depletion of DPBF was calculated as follows: *DPBF depletion* = Abs_1/Abs_0. Abs_0 and Abs_1 are the absorbance values at 415 nm before and after irradiation, respectively.

Stability and photostability of PS-NPs during singlet oxygen generation study

Stability and photostability studies were carried out in the same conditions of irradiation of the singlet oxygen studies. Each point represents the mean of at least three independent experiments, and has a standard deviation lower than 3%. Nanoparticles were stable during singlet oxygen study.

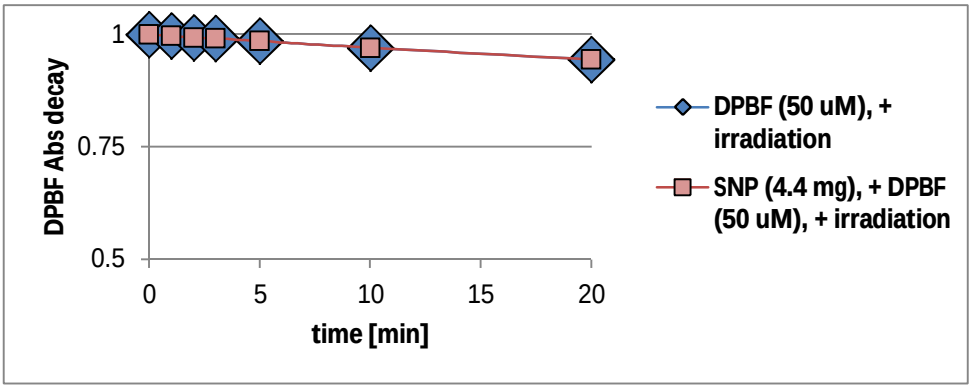

Figure SI 2. Stability of SNPs during singlet oxygen generation study.

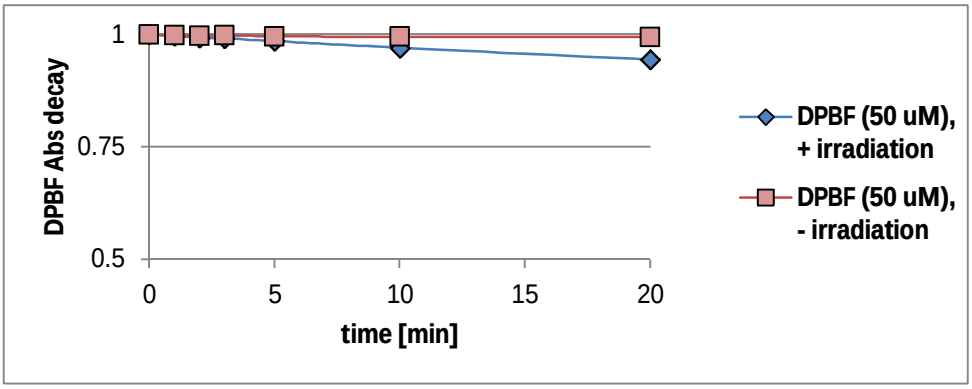

Figure SI 3. Stability of DPBF during singlet oxygen generation study.

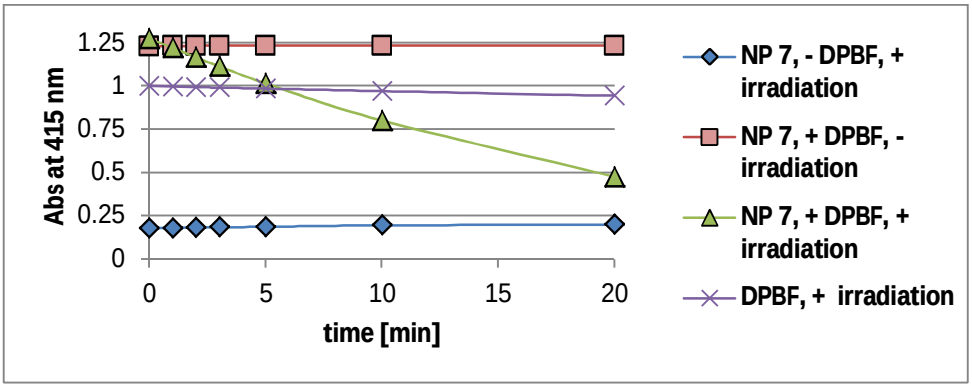

Figure SI 4. Stability of **NP 7** during singlet oxygen generation study.

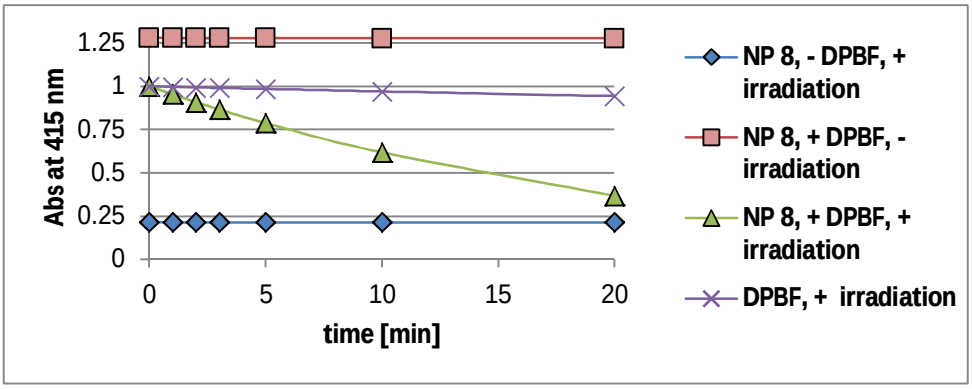

Figure SI 5. Stability of **NP 8** during singlet oxygen generation study.

Characterization of NPs

TEM

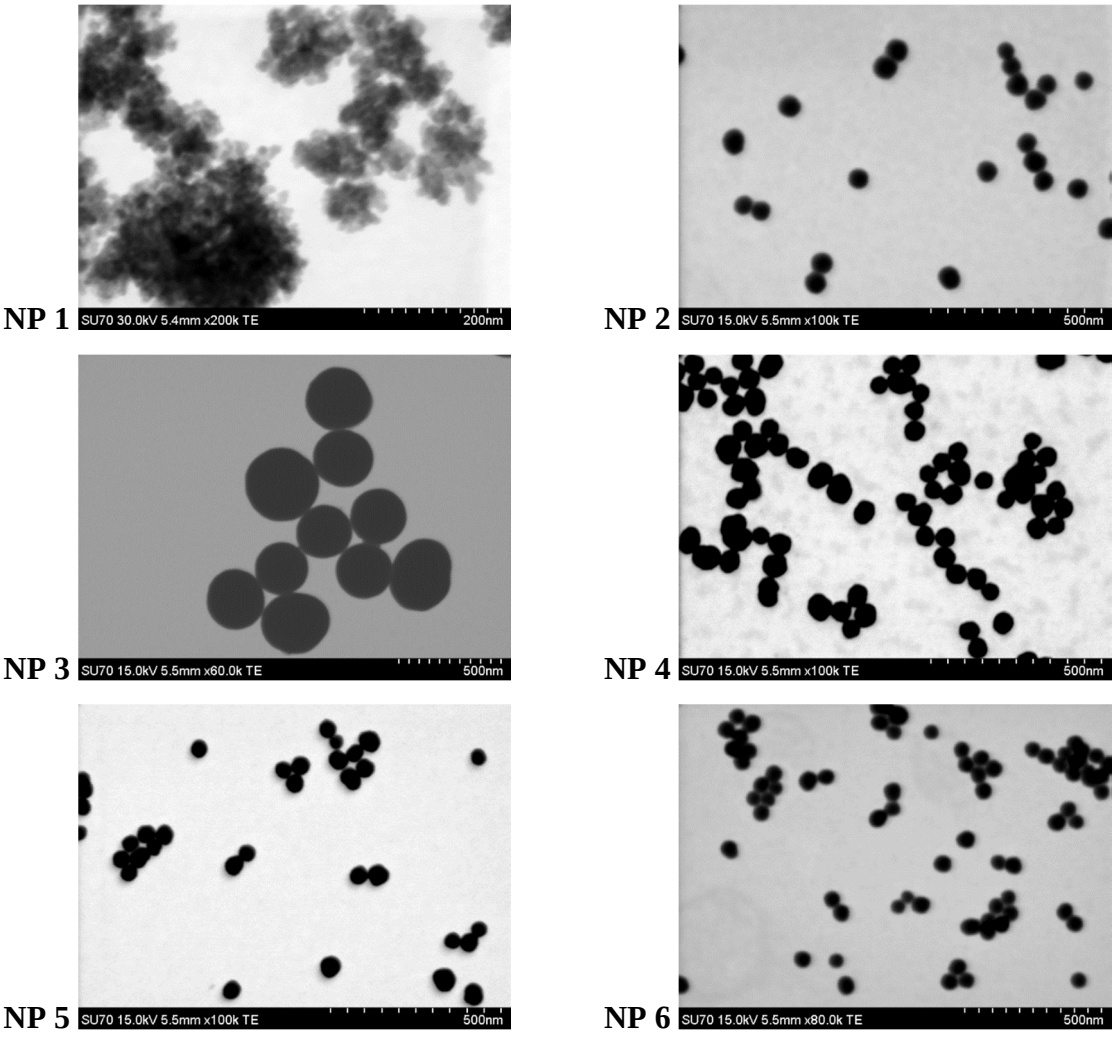

Figure SI 6. TEM images of **NP 1**-**NP 6**.

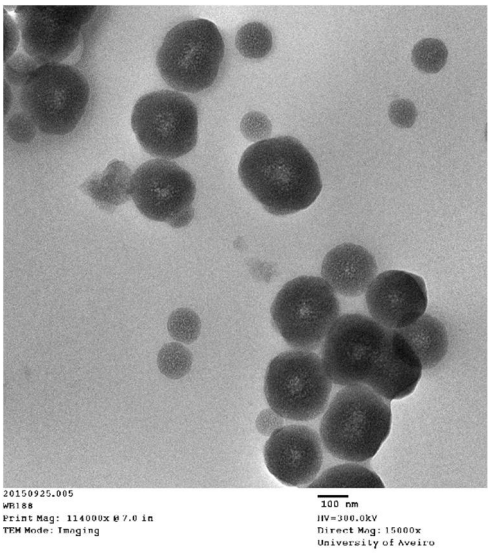

NP 7

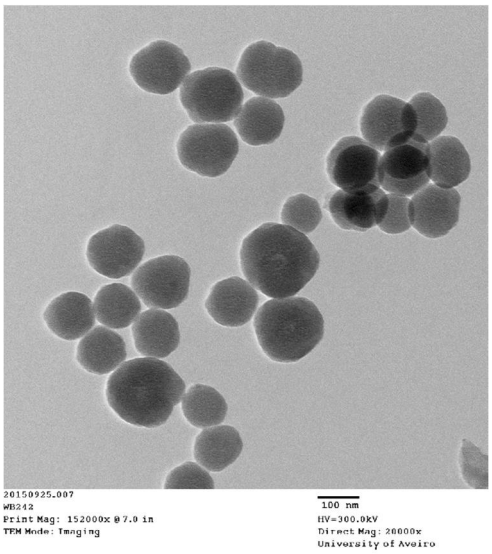

NP 8

Figure SI 7. TEM images of final **NP 7** and **NP 8**.

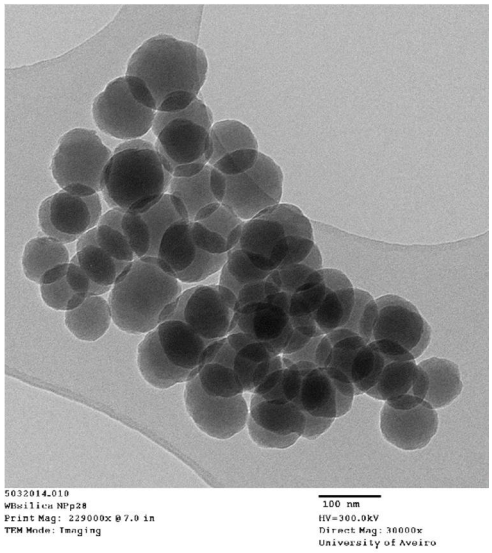

Figure SI 8. TEM image of SNPs without PS.

DLS

		Size (d.n...	% Number:	St Dev (d.n...
Z-Average (d.nm): 276.5	Peak 1:	233.5	100.0	33.42
PdI: 0.271	Peak 2:	0.000	0.0	0.000
Intercept: 0.953	Peak 3:	0.000	0.0	0.000
Result quality Good				

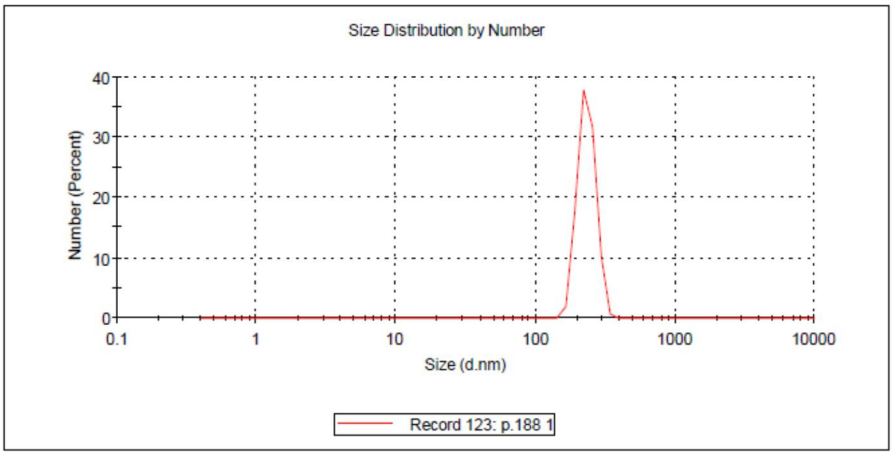

Figure SI 9. DLS size distribution of **NP 7** in water.

		Size (d.n...	% Number:	St Dev (d.n...
Z-Average (d.nm): 159.6	Peak 1:	133.2	100.0	26.32
PdI: 0.214	Peak 2:	0.000	0.0	0.000
Intercept: 0.876	Peak 3:	0.000	0.0	0.000
Result quality Good				

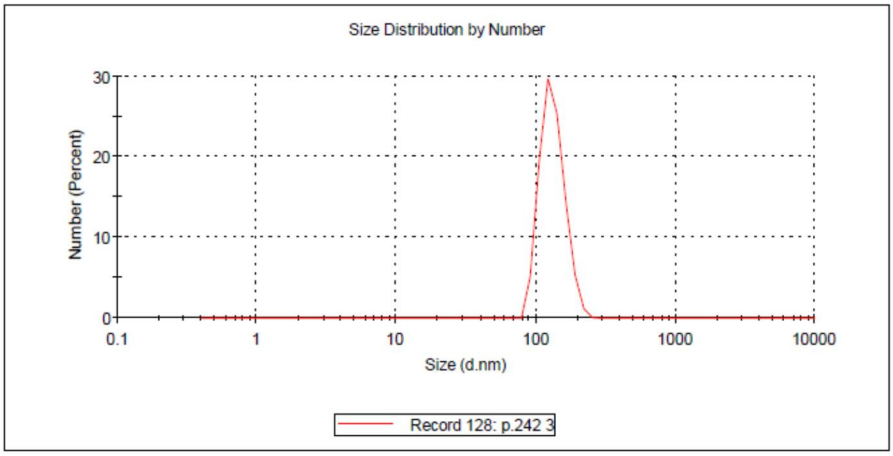

Figure SI 10. DLS size distribution of **NP 8** in water.

EDS

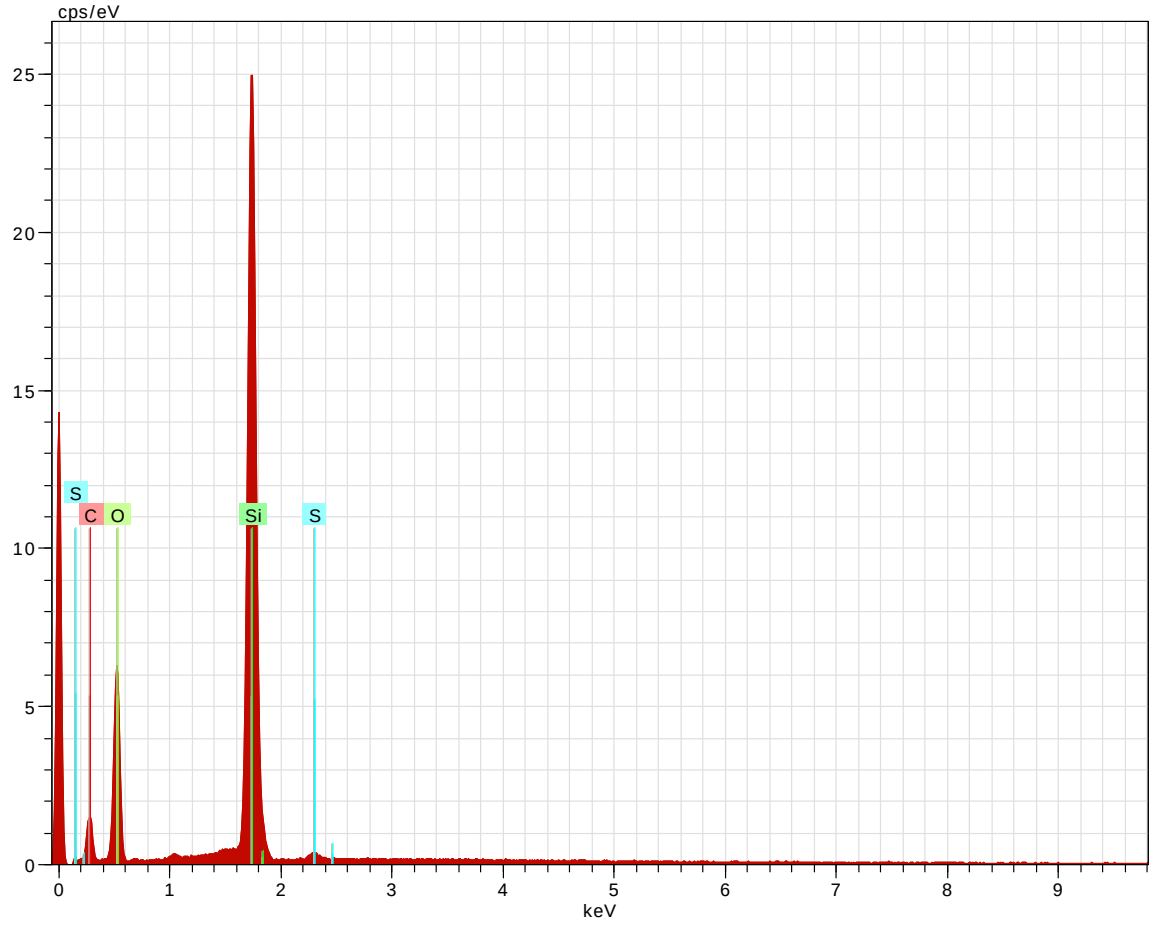

NP 7.spx Date:27-08-2015 18:14:01 HV:30.0kV Puls th.:4.70kcps

Spectrum: NP 7.spx

Element	Series	unn. C [wt.%]	norm. C [wt.%]	Atom. C [at.%]	Error (3 Sigma) [wt.%]
Oxygen	K-series	41.70	49.39	50.21	15.75
Carbon	K-series	22.35	26.47	35.85	10.29
Silicon	K-series	20.01	23.70	13.72	2.75
Sulfur	K-series	0.37	0.43	0.22	0.13
	Total:	84.42	100.00	100.00	

Figure SI 11. EDS of **NP 7**.

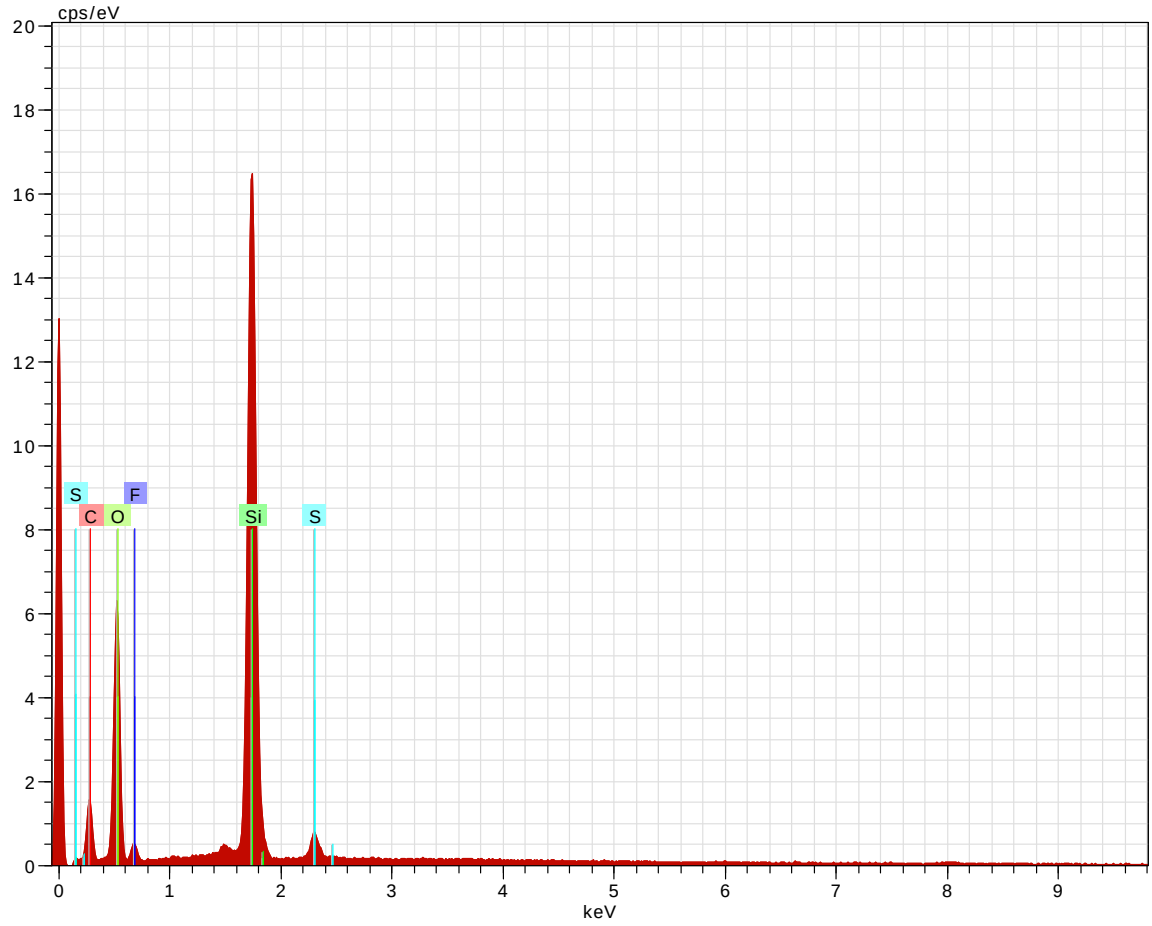

NP 8.spx Date:27-08-2015 18:10:23 HV:30.0kV Puls th.:3.83kcps

Spectrum: NP 8.spx

Element	Series	unn. C [wt.%]	norm. C [wt.%]	Atom. C [at.%]	Error (3 Sigma) [wt.%]
Oxygen	K-series	56.15	49.49	49.70	20.76
Carbon	K-series	29.40	25.91	34.67	13.04
Silicon	K-series	20.37	17.95	10.27	2.80
Fluorine	K-series	6.66	5.87	4.97	3.67
Sulfur	K-series	0.88	0.77	0.39	0.19
	Total:	113.47	100.00	100.00	

Figure SI 12. EDS of **NP 8**.

UV-Vis

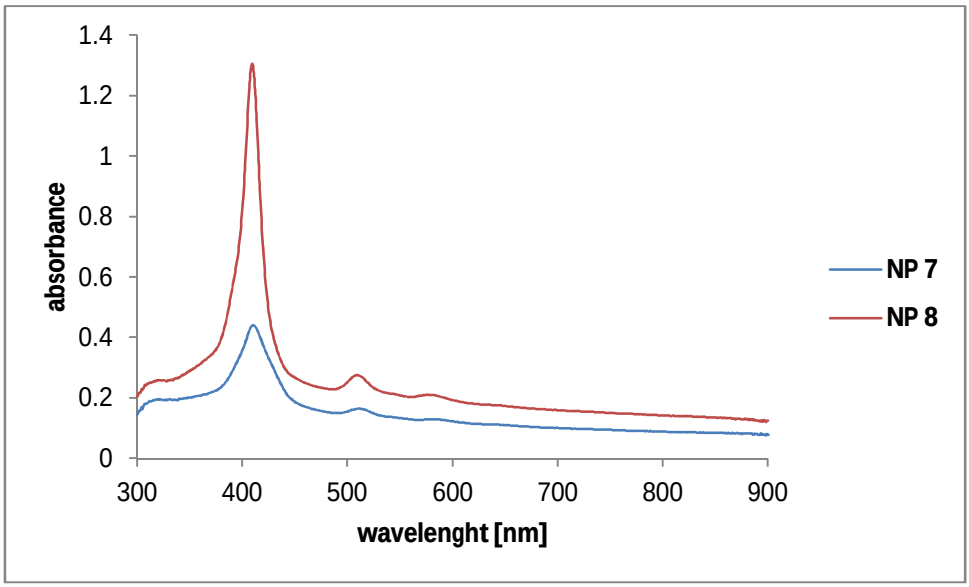

Figure SI 13. UV-Vis spectra of **NP 7** and **NP 8**. UV-Vis absorption spectra were collected after dispersion of 0.535 mg of **NP 7** in 3mL of distilled water and 0.510 mg of **NP 8** in 3 mL of distilled water.

FT-IR

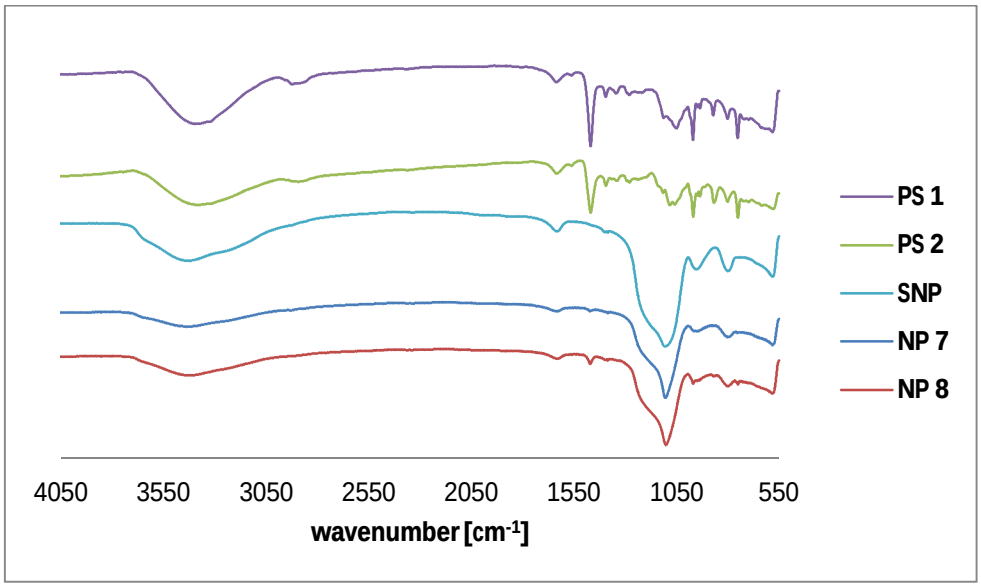

Figure SI 14. FT-IR spectra of **PS 1**, **PS 2**, **NP 7**, **NP 8** and **SNP**. FT-IR spectra were recorded in KBr pellets.

In vitro assays

Cells culture

Human bladder cancer cell lines UM-UC-3 and HT-1376 derived from high-grade transitional cell carcinoma were obtained from the American Type Culture Collection (ATCC®, Manassas, VA, USA). Cells were cultured in Roswell Park Memorial Institute (RPMI)-1640 medium (Sigma) supplemented with 2 $g.L^{-1}$ sodium bicarbonate (Sigma), 2 mM L-glutamine (Sigma), 10% (v/v) of heat-inactivated Fetal Bovine Serum (FBS; Life Technologies, Carlsbad, CA, USA) and antibiotic/antimicotic containing 100 units.mL-1 penicillin, 100 µg.mL-1 streptomycin and 0.25 µg.mL-1 amphotericin B (Sigma). UM-UC-3 and HT-1376 cells were seeded at a density of 1.5 x 104 in 96-well culture plates (Orange Scientific, Braine-l'Alleud, Belgium). 24 hours after plating, cells were overnight incubated with different concentrations of NPs (0-0.010 mg/mL in medium) in the dark.

Cellular uptake of NPs

After incubation with NPs in the dark, UM-UC-3 and HT-1376 cells were washed with PBS buffer and mechanically scrapped in 1% (m/v) sodium dodecyl sulfate (SDS; Sigma) in PBS buffer at pH 7.0. NPs intracellular concentration was determined by spectrofluorimetry using a microplate reader (Synergy HT, Biotek, Winooski, VT, USA) with the excitation filter (set at 360±40 nm) and emission filter (645±40 nm). Results were normalized for protein concentration (determined by bicinchoninic acid reagent; Pierce, Rockford, IL, USA).

Microscopic evaluation

UM-UC-3 and HT-1376 bladder cancer cells were left to grown on coated glass coverslips with poly-L-lysine (Sigma). After 24 h cells were incubated with 0.010 mg/mL of NPs overnight, at 37 ºC. Then, cells were fixed with 4% paraformaldehyde (PFA; Merck, Darmstadt, Germany) for 10 min at RT. In the end, the samples were rinsed in PBS, and mounted in VectaSHIELD mounting medium containing 4´,6-diamidino-2-phenylindole (DAPI; Vector Laboratories, CA, Burlingame) for visualization under a confocal microscope (LSM 510, Carl Zeiss, Gottingen, Germany). For DAPI detection, specimen was excited at 405 nm and light emitted was collected between 430-500 nm.

PDT treatments on cells

Photodynamic irradiation was carried out in fresh culture medium, in the absence of NPs, covering UM-UC-3 and HT-1376 cell monolayers with RPMI medium and exposing them to white light delivered by the illumination system LC-122 LumaCare at 12 mW/cm^{-2} for 40 min. As a control, sham-irradiated cells were used. These cells were kept in the dark for the same durations and under the same conditions as the irradiated cells. In all trials, triplicate wells were settled under each experimental condition, and each experiment was repeated at least three times.

MTT assay

MTT assay was used to determine cell metabolic activity after NPs incubation in the dark, irradiation, or both after 24 h. This colorimetric assay is measuring the ability of bladder cancer cells to reduce yellow 3-[4,5-dimethylthiazol-2-yl]-2,5-diphenyl-tetrazolium bromide (MTT, Sigma), to a purple formazan on a microplate reader (Synergy HT). The results are expressed in percentage of control (i.e. optical density of formazan from cells not exposed to NPs).

Redox quenching studies

Photodynamic treatment was performed with cell monolayers covered with culture medium containing 50 nM of redox quenchers (sodium azide, L-histidine and L-cysteine from Sigma) just after NPs uptake. 24 h after PDT, the effect of quenchers on cell viability was evaluated using MTT viability assay.

PSs release form NPs in the biological media

In 2 mL eppendorf, 0.5 mg of **NP 7** (bearing 0.145 µmol of **PS 1**) or 0.5 mg of **NP 8** (bearing 0.108 µmol of **PS 2**) were dispersed in 1 mL of PBS buffer or RPMI medium. The dispersion was placed in laboratory incubator shaker (IKA KS4000) and kept at 37 °C without agitation for 4 h and 18 h. After 4 h and 18 h, 0.250 mL of the mixture was mixed with 1.250 mL of EtOH and nanoparticles were centrifuged (13300 RPM, RT, 1 min). Then, 1 mL of supernatant was mixed with 2 mL of EtOH and UV-Vis was measured. The

release of PS form NPs was calculated as follows: *release of PS form NPs = mol of release PS from NPs / mol of PS in NPs.*

Compering the behavior of nanoparticles after 4 h and 18 h incubations, slow release of PS form the silica matrix was observed. Higher release in case of **NP 8** was noted then in **NP 7**. However, during singlet oxygen study nanoparticles were stable under conditions used in the study (**Figure SI 4** and **Figure SI 5**).

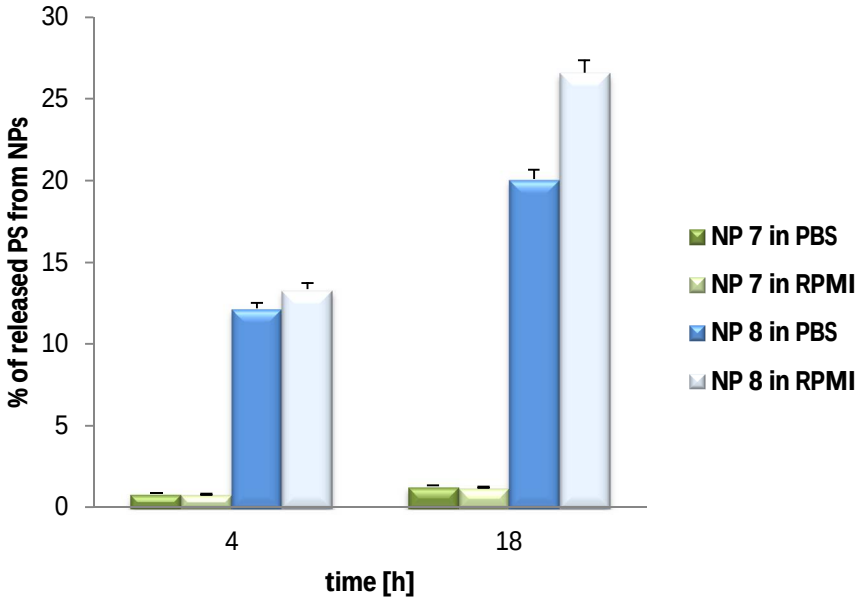

Figure SI 15. PSs release form **NP 7** and **NP 8** in the biological media. Each point represents the mean of at least three independent experiments, and has a standard deviation lower than 3%.

Dark toxicity studies of PSs and NPs

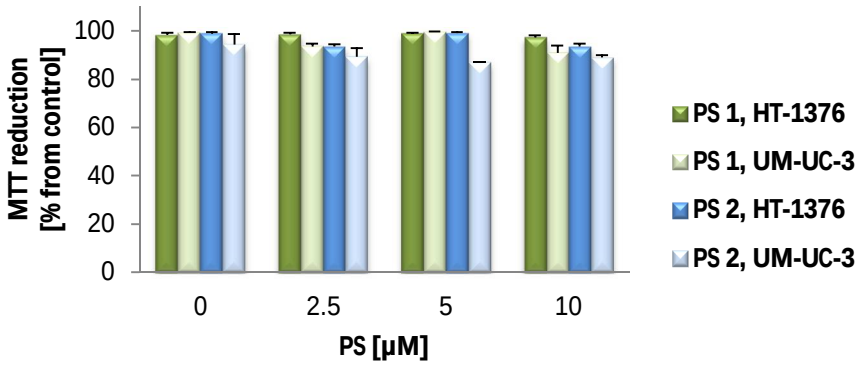

Figure SI 16. Non-dark toxicity of **PS 1** and **PS 2** (0-10 μM in PBS) determined 24 h after treatment using the MTT assay. The percentage of cytotoxicity was calculated relatively to control cells (cells incubated with PBS). Data are means ± s.e.m. of at least three independent experiments performed in triplicates.

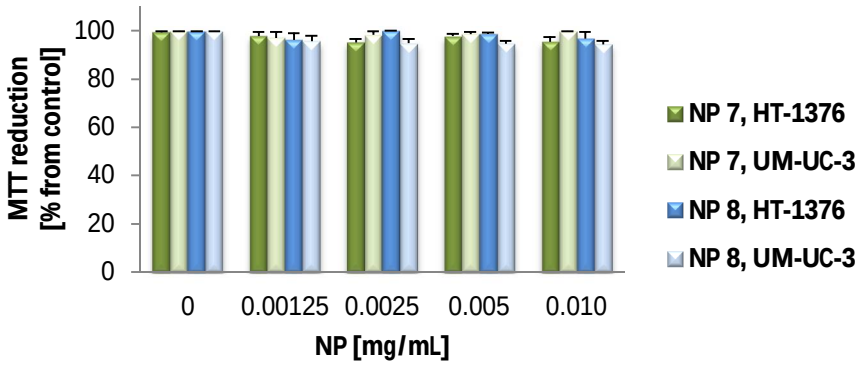

Figure SI 17. Non-dark toxicity of **NP 7** (0-0.010 mg/mL, 0-2.89 μM in medium) and **NP 8** (0-0.010 mg/mL, 0-2.15 μM in medium) determined 24 h after treatment using the MTT assay. The percentage of cytotoxicity was calculated relatively to control cells (cells incubated with RPMI medium). Data are means ± s.e.m. of at least three independent experiments performed in triplicates.

CHAPTER 3: Nanoparticle-based systems as efficient vehicles to transport and deliver photosensitizers into tumor tissues during photodynamic therapy *in vitro*

Wioleta Borzęcka,[1,2,3] Patrícia M. R. Pereira,[1,4] Rosa Fernandes,[4,5] Tito Trindade,[2] Tomás Torres,[3,6] and João Tomé[1,7]

[1]QOPNA and [2]CICECO, Department of Chemistry, University of Aveiro, 3810-193 Aveiro, Portugal; [3]Department of Organic Chemistry, Autonoma University of Madrid, 28049 Madrid, Spain; [4]Laboratory of Pharmacology and Experimental Therapeutics, Institute for Biomedical Imaging and Life Sciences (IBILI), Faculty of Medicine, University of Coimbra, Azinhaga de Santa Comba, Coimbra, Portugal; [5]CNC.IBILI, University of Coimbra, 3000 Coimbra, Portugal; [6]IMDEA-Nanociencia, Campus de Cantoblanco, c/Faraday 9, 28049 Madrid, Spain; [7]Centro de Química Estrutural, Departamento de Engenharia Química, Instituto Superior Técnico, Universidade de Lisboa, 1049-001 Lisboa, Portugal

Keywords: Porphyrins, Photosensitizers, Nanosilicas, PDT, Cancer

Abstract: In recent years, mesoporous silica nanoparticles (MSNPs) have attracted tremendous attention in many biomedical applications. One of the fields where smart functional nanosystems have found great application is cancer treatment. Here, we present nanoparticle-based systems which have been explored as efficient vehicles to transport and deliver photosensitizers (PSs) into tumor tissues during photodynamic therapy (PDT). Herein we report the preparation, characterization and *in vitro* studies of distinct shaped MSNPs grafted with *S*-glycoside porphyrins (Pors). The ensuing nanomaterials were fully characterized and their properties as new third generation PSs for PDT against two bladder cancer cell lines, HT-1376 and UM-UC-3 were examined.

Introduction

In the early 1990s it was discovered a new family of molecular sieves, often called M41S.[72] In 2001, J. Perez-Pariente *et al.*[177] presented for the first time MCM-41 as a drug delivery system by using such materials as hosts and ibuprofen molecules as guests. They reported that ibuprofen molecules occupied partially the MCM-41 mesopores and could diffuse out of them when the loaded samples were placed in a simulated body fluid. This led to new studies on the use of silica nanoparticles (SNPs) as drug delivery systems[178,179] and since then mesoporous silica materials have been explored and used in biomedical applications.

MSNPs in particular have attracted great attention for PDT owing to their biocompatibility, large surface area per volume ratio, controllable size formation, hydrophilic surface and ability for surface functionalization.[42] The possibility of using these systems for tumor targeting through adequate surface modification is a key to successful cancer treatment. Currently there are nanoparticle-based drug delivery systems which were approved by FDA and others are still under clinical trials.[153-155]

Despite the fact that researchers established different therapies to treat cancer, for example surgery, chemotherapy, radiotherapy and PDT, cancer is still one of the leading cause of death in developing countries.[180] Nevertheless, PDT has been a very promising and used therapy for certain cancer treatments. PDT combines three components: drug, light and oxygen. By its own these components do not have any toxic effects on the biological systems. They become strongly cytotoxic to the target cells when reactive oxygen species (ROS) are produced such as singlet oxygen ($^1O_2$), hydroxyl ($^{\bullet}HO$), peroxyl ($^{\bullet}ROO$) and superoxide anion ($^{\bullet}O^{2-}$) radicals. This production occurs only when the drug (PS) is in contact with molecular oxygen and exposed to light within a wavelength region. In these conditions, there is production of radicals *via* a Type I reaction or, more likely, it takes place the production of $^1O_2$ *via* Type II reaction, which is the major cytotoxic agent involved in PDT .[132-135]

The lifetime of $^1O_2$ in biological media is very short (10-320 nanoseconds). Hence, the photodynamic action in cancer PDT occurs exclusively close to the intracellular location of the PS. The lifetime of $^1O_2$ limits its diffusion to more or less 10 to 55 nm in cells[158]

making PDT a selective treatment with less secondary effects than conventional therapies. There are three mechanisms in PDT for killing cancer cells: i) ROS directly kill tumor cells; ii) damage of the tumor-associated vascular system leading to tumor infarction; iii) activation of an immune response against tumor cells. Finally, these three mechanisms can influence each other.[34]

PDT was approved 20 years ago by the Food and Drug Admnistration (FDA) as a clinical protocol for cancer treatment. Still the method has limitations as a general protocol to treat any type of cancer. In this context, nanoparticles (NPs) have emerged as promising vehicles for use in PDT giving the possibility to successfully improve cancer treatment.[38,136,137] The application of PSs nanoformulations in PDT can enhance the treatment by increasing the biocompatibility of hydrophobic PSs', their blood circulation and selective accumulation in tumor tissues due to enhanced permeability and retention effect (EPR).[39,40,151]

According to the time of development and specific characteristics of PSs, they have been divided in three generations. Most of them are based on a tetrapyrrole structure (Pors,[10,138,139] chlorins,[140-143] bacteriochlorins,[144-146] and phthalocyanines[147-150]). For PDT, an ideal PS should be a photostable and water-soluble chemically pure compound. Ideally the PS should not exhibit dark toxicity and it should absorb light in the red or deep red wavelengths in order to efficiently penetrate tissues. Lastly, PS agent should accumulate in the target tissues and rapidly clear from surrounding normal tissues and organs to maximize therapy selectivity.[158-161,181]

In the design of new PSs for cancer treatment, Pors conjugated to MSNPs surface or encapsulated in the silica matrix, appear as a promising third generation PSs. The combination of Pors and MSNPs can improve the photophysical properties of Pors. Recent studies have demonstrated that by grafting Pors inside or over the surfaces of MSNPs could limit the formation of Pors aggregates, low water compatibility and pre-mature release of Pors. This method could enhance selectivity for targeted tissues and consequently increase the PDT efficiency.[93,156,182-186]

Among the variety of examples, Ximing *et al.*[94] prepared an interesting family of Por and MSNPs with excellent optical properties and good stability in aqueous solution grafting

Por-bridged silsesquioxane into MSNPs. Additionally, Hocine *et al.*[187] incorporated water-soluble Pors into MSNPs *via* covalent linkages and then decorated the ensuing hybrids with mannose moieties aiming at better cancer cells recognition. In a final step PDT was performed on MDA-MB-231 breast cancer cells with great success. Vivero-Escoto *et al.* employed one of the most studied Por, protoporphyrin IX (PpIX), attached through a redox-responsive linker to the surface of MSNPs.[99] These non-cytotoxic drug delivery platforms were able to release PS in reducing conditions present in cancer cells by breaking the disulfide bond between NP and PS. Thus, PpIX in monomeric form was released and upon light exposure there was HeLa cells destruction due to the photogenerated $^1O_2$. On the other hand, Durand *et al.*[103] combined two-photon imaging and PDT by preparing mannose-functionalized porous silica-coated magnetic nanoparticles with covalently attached Por. After performing PDT on MDA-MB-231 breast cancer cells, it was clear that mannose functionalization improved both imaging and PDT due to the presence of mannose receptors on breast cancer cells. The same group[118] reported cancer therapy improvements by exploiting the synergic anticancer effect of two active molecules (Por and camptothecin) within a single nanocarrier. They combined targeting, drug delivery and PDT by preparing galactose functionalized MSNPs that have been loaded with camptothecin and possessing Por at the walls. This enhanced anticancer activity of the nanocarriers by improvement of cancer cell death on three cancer cell lines, colorectal (HCT-116), pancreatic (Capan-1) and breast cancer (MDA-MB-231). One more example how to improve PDT is to combine it with another cancer therapy to get a double action of both treatments. Recently, Koichiro Hayashi *et al.* [128] joined PDT with photothermal therapy (PTT) by using a single light source with photostable iodinated silica/Por hybrid NPs with heavy-atom effect. They demonstrated that these NPs could be used in PDT/PTT combination therapy against multiple myeloma, which is resistant to conventional chemotherapy.

In our research we focused on third generation PSs. Therefore MSNPs bearing *S*-glycoside porphyrins were prepared. As a model PS 5,10,15,20-tetrakis(pentafluorophenyl)porphyrin ($TPPF_{20}$, **PS0**, **Figure 1**) was chosen. The results with this PS were promising which encouraged us to prepare NPs with ability for cancer cells targeting. Hence, further systems have been investigated that include 5,10,15,20-tetrakis(4-1'-thio-glucosyl-2,3,5,6-tetrafluorophenyl) porphyrin (Glu-Por, **PS1**, **Figure 1**) and 5,10,15,20-Tetrakis(4-1'-thio-

galactosyl-2,3,5,6-tetrafluorophenyl) porphyrin (Gal-Por, **PS2**, **Figure 1**). These two PSs bear glucose and galactose moieties which are crucial for tumor targeting. Since galectin[148,188] and glucose[148,189,190] proteins are expressed in high levels in cancer cells it is important to design PSs with glycol-molecules to obtain successful cancer treatment by precise tumor targeting. Thus, **PS1** and **PS2** were grafted on the surface of MSNPs. As a model cancer cells HT-1376 and UM-UC-3 bladder cancer cells, derived from transitional cell carcinoma were chosen because both have affinity for galactose and glucose molecules. Both carbohydrates express the glyco-binding proteins in different levels: glucose transporter (GLUT1) and galactose-binding protein (galectin-1).[148] Moreover, in order to compare the silica particles' shape-dependent behavior in HT-1376 and UM-UC-3 cancer cell lines, sphere-shaped MSNPs and rod-shaped mesoporous silica nanorods (MSNRs) were prepared in this research. Finally, the *in vitro* photodynamic efficacy of the new nanomaterials was undertaken with HT-1376 and UM-UC-3 bladder cancer cells.

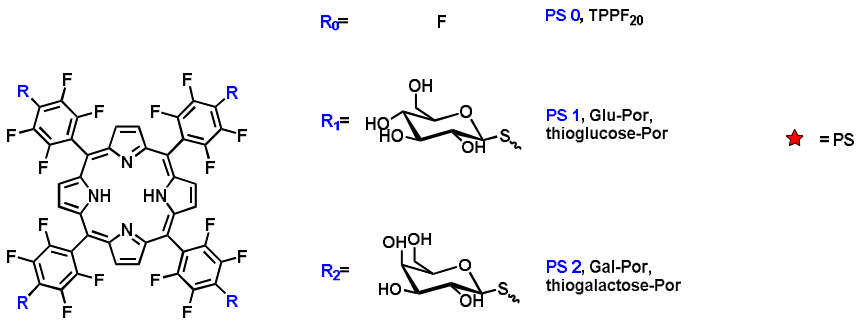

Figure 1. Structures of **PS0**, **PS1** and **PS2**.

Results and discussion

Preparation and characterization of MSNPs and MSNRs

In this work **PS0**, **PS1** and **PS2** were used as PSs (**Figure 1**). Firstly, we studied MSNPs grafted with commercially available **PS0**. After satisfactory outcome with these NPs, **PS1** and **PS2** were synthesized according to literature procedures described elsewhere.[162-166] There are a number of reports highlighting the potential of glycosylated Pors in PDT cancer treatment.[162-166] Poor solubility and aggregation of PSs molecules in biological media drastically reduce the efficiency of $^1O_2$ photogeneration. Thus, to enhance their

stability in aqueous media, the PSs were covalently attached to mesoporous silica matrix and deliver to cancer cells as nanovehicles.

In the beginning of the study, as a model nanomaterial **MSNP-PS0** were prepared (**Figure 2**). Subsequently, after satisfying evaluation of the $^1O_2$ generation properties of these NPs and *in vitro* studies into two human bladder cancer cell lines, HT-1376 and UM-UC-3, it was decided to prepare NPs with better cancer cells recognition. Thus, nanomaterials bearing PS with sugar moieties (**MSNP-PS1**, **MSNP-PS2**, **MSNR-PS1**, **MSNR-PS2**) were prepared (**Figure 2**) and fully characterized.

MSNPs and MSNRs were prepared under alkaline conditions in which tetraethoxysilane (TEOS) was used as the silica precursor and cetyltrimethylammonium bromide (CTAB) was used as the structure directing agent (**Figure 2**).[191]

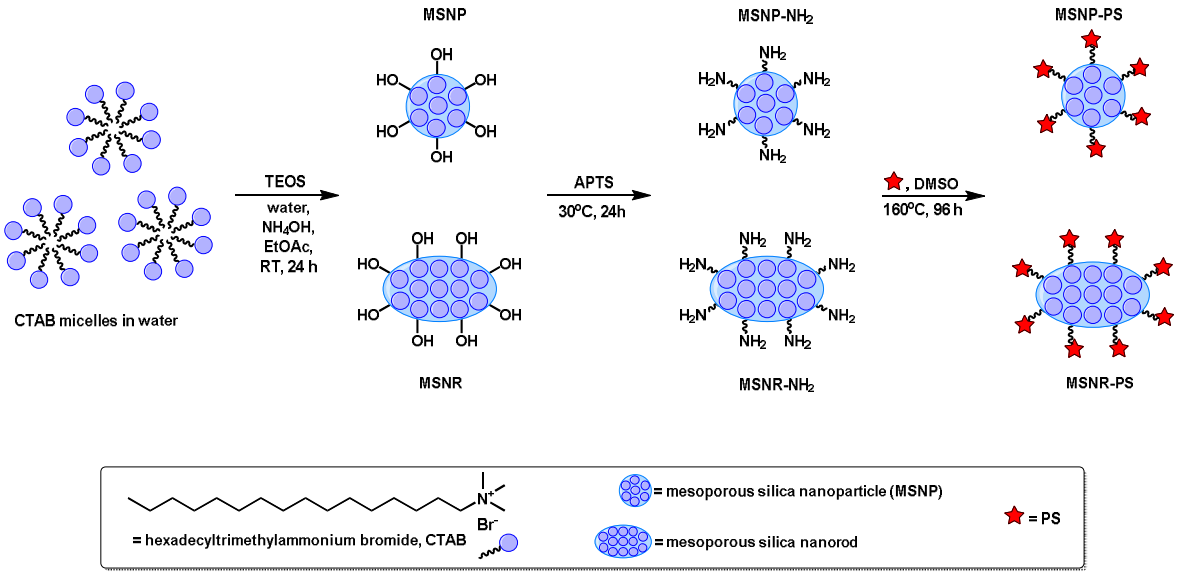

Figure 2. Schematic preparation of nanomaterials grafted with PSs.

In the first step, different amounts of CTAB (100 mg for **MSNP-100**, 200 mg for **MSNP-200**, 400 mg for **MSNP-400**, 500 mg for **MSNP-500**, **Figure 2**, **Table 1**) were dissolved in water. In this reaction CTAB serves as an organic template for the formation of mesoporous silica spheres. After adding ethyl acetate, NH_4OH, and TEOS, the solution was stirred for 5 min at RT. After that time, additional water was added and pH decreased which slower the hydrolysis of TEOS and accelerates the silica condensation. To remove the surfactant templates acid extraction was used and NPs were air-dried.

The average size of the NPs was estimated by transmission electron microscopy (TEM)) after dispersing the sample in water and drying at ambient temperature. (**Figure 3, Table 1**).

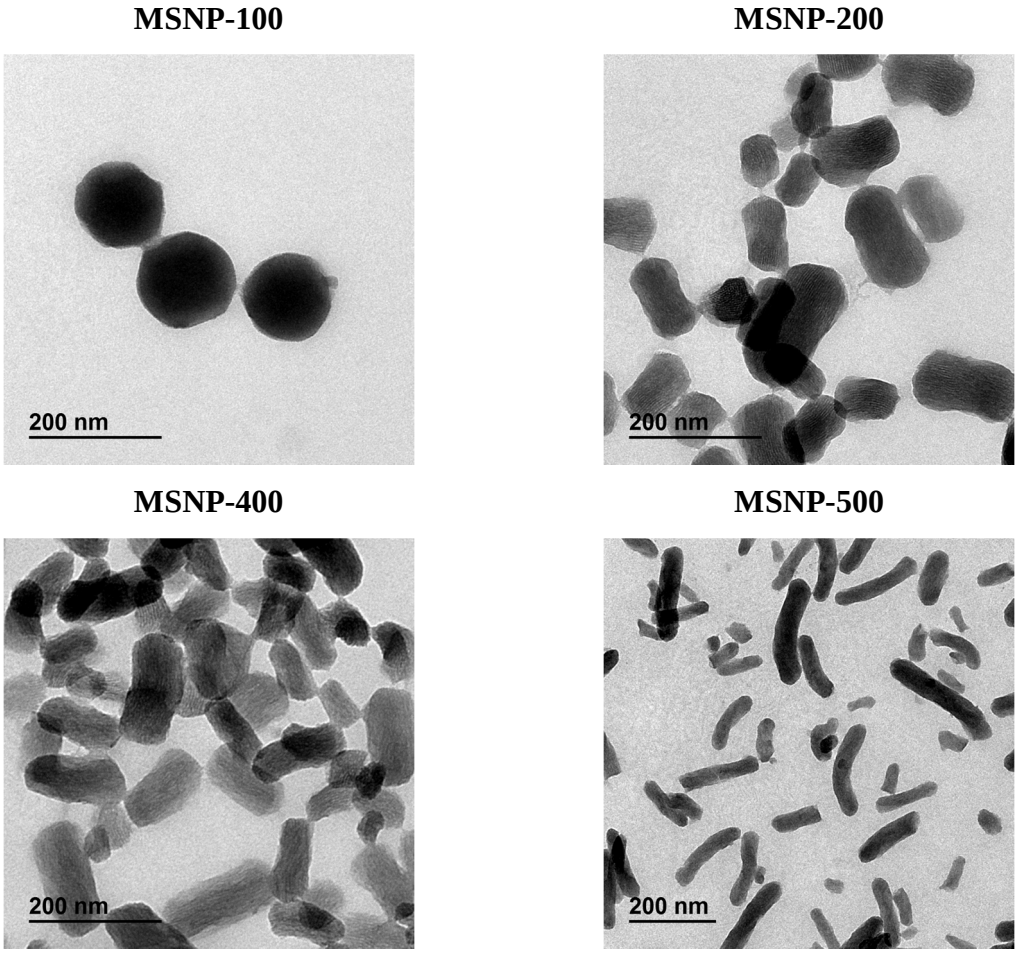

Figure 3. TEM images of **MSNP-100**, **MSNP-200**, **MSNP-400** and **MSNP-500**.

Nanomaterials' core	CTAB [mg]	Nanomaterials'		Aspect ratio (length:width)
		length [nm]	width [nm]	
MSNP-100*	100	117 ± 16	117 ± 16	1
MSNR-200	200	125 ± 32	65 ± 11	1.9
MSNR-400	400	134 ± 25	57 ± 12	2.4
MSNR-500*	500	175 ± 39	36 ± 7	4.9

Table 1. Size of NPs estimated form TEM. Information on mean size and standard deviation was calculated from measuring more than 100 NPs in random fields of TEM grids.*NPs used as cores for further experiments.

The above table (**Table 1**) indicates that the shape of the particles depends on the CTAB concentration in the method of synthesis employed. The higher the concentration of CTAB

in the reaction mixture the higher is the aspect ratio of the particles, which is in agreement with reports found in the literature.[192-194] Moreover, with the growing concentration of CTAB, particles become longer and narrower. To compare shape-dependent behavior in HT-1376 and UM-UC-3 cancer cell lines, sphere-shaped **MSNP-100** (117 ± 16 nm) and rod-shaped **MSNR-500** (175 ± 39 nm x 36 ± 7 nm) were chosen and named, respectively as **MSNP** and **MSNR**. **Figure 4** shows the TEM images of samples **MSNP** and **MSNR**.

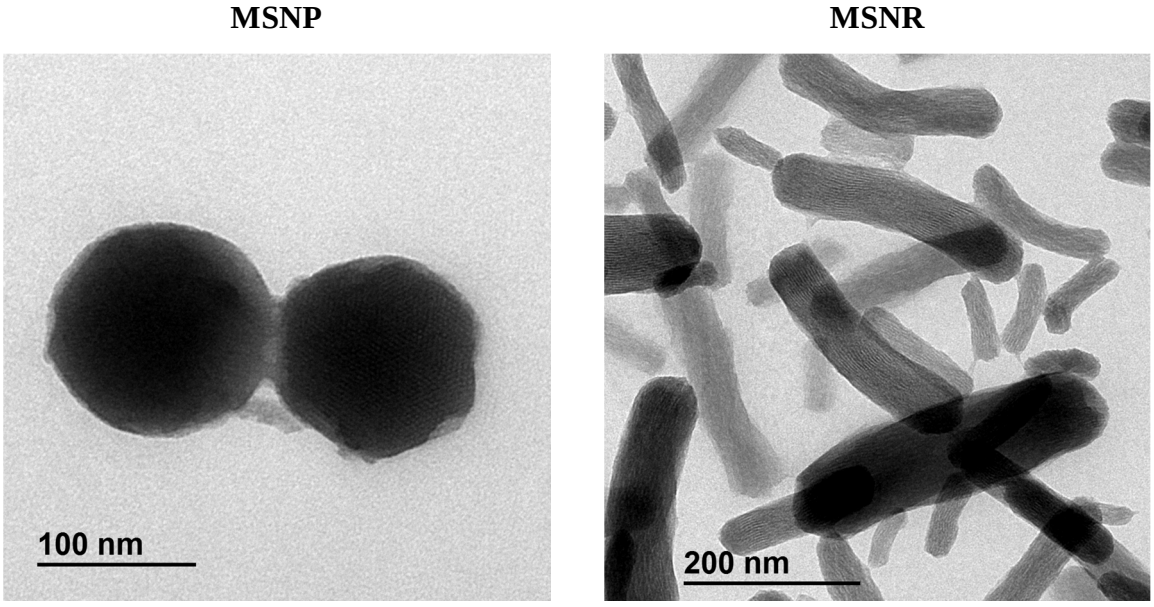

Figure 4. TEM images showing mesoporous silica particles of distinct shape

The PSs molecules were grafted on the surfaces of MSNPs and MSNRs using (3-aminopropyl)triethoxysilane (APTS) as a linker. Firstly, MSNPs and MSNRs were functionalized with APTS by dispersing the NPs in water and then adding a solution of APTS in ethanol to produce mesoporous silicas with amine terminal groups at the surfaces (**MSNPs-NH_2** and **MSNRs-NH_2**). In the last step of the preparation, the grafting of Por: **PS0**, **PS1**, and **PS2** on the surface of **MSNPs-NH_2** and **MSNRs-NH_2** was carried out in DMSO at 160 °C, following a method reported in the literature but with minor modifications.[65] The final hybrid materials were washed with DMSO and EtOH until the typical Soret and Q bands of Pors were not observed in the rinsed solvent. The amount of Por covalntly attached to NPs was calculated using UV-Vis spectrophotometry by subtracting the unreacted Por (from the rinse solvent) from Por taken into rection mixture. The highest amount of PS in the mesoporous silica samples was observed for **MSNP-PS0** (26.4 nmol/mg, **Table 2**), which could be explained by the fact that **PS0** is not bearing any

sugar molecules. Thus, **PS0** has free access to all peripheral fluorine atoms which allows easier conjugation with nanomaterials compare to **PS1** and **PS2**.

Nanomaterial's core	PS	Final hybrid	Concentration of PS on the surface of NP [nmol of PS/mg of NP]
MSNP	PS 0	**MSNP-PS0**	26.4
MSNP	PS 1	**MSNP-PS1**	25.0
MSNP	PS 2	**MSNP-PS2**	19.8
MSNR	PS 1	**MSNR-PS1**	22.9
MSNR	PS 2	**MSNR-PS2**	22.6

Table 2. Concentration of PS on the surface of NP.

The UV-Vis absorption spectra of all PSs and their nanoformulations were collected after dissolving and dispersing the samples in DMSO, respectively (**Figures SI 3-5**). Pors presented Soret bands at 417 nm (**PS0**), 421 nm (**PS1**), 421 nm (**PS1**). Furthermore, all NPs showed the typical spectra of a free base Por, with Soret bands at 436 nm (**MSNP-PS0**), 431 nm (**MSNP-PS1**), 436 nm (**MSNR-PS1**), 435 nm (**MSNP-PS2**), 438 nm (**MSNR-PS2**).

The FT-IR was used to evaluate the functionalization of MSNPs and MSNRs with APTS (**Figure SI 6**) and further covalent bonding with Pors (**Figure SI 7-9**). The aminated NPs exhibited the presence of the N−H bending band at ~1600 cm^{-1} and broad bands in the 2800 to 3800 cm^{-1} region, corresponding to stretching vibrations of primary amines, which indicated that the amino groups were bound onto the NPs surface.[195-197] After covalent functionalization with Pors, a new band appeared at ~1590 cm^{-1} corresponding to the C=C vibrational modes of Pors. The band at ~1700 cm^{-1} could be attributed to the bending vibration of the C=N of the Por ring. Hence, the FT-IR spectra provided evidence that Pors molecules have been covalently attached to the surface of MSNPs and MSNRs.

Singlet oxygen generation study

The ability of the functionalized nanomaterials to generate $^1O_2$ was determined by an indirect chemical method in which 1,3-diphenylisobenzofuran (DPBF) acts as $^1O_2$ quencher. DPBF has an absorption maximum at 415 nm and forms a colorless endoperoxide product when it reacts with singlet oxygen (**Figure SI 1**). In this method the

ability of PSs or NPs to generate $^1O_2$ is measured by following the DPBF absorption decay at its maximum absorption (415 nm).

In this study, all solutions or suspensions for analysis were prepared in DMSO and stirred under irradiation for defined time intervals, at room temperature. Probes were exposed to light of a 300 W halogen lamp. Incident light was filtered through orange filter to take out light below 530 nm. 5,10,15,20-tetrakis-phenyl-21,23-H-porphyrin (TPP) was used as a reference compound. Under these conditions all MSNPs and MSNRs tested were photostable (**Table SI 1**).

The $^1O_2$ generation was determined for all nanoformulations (**MSNP-PS0**, **MSNP-PS1**, **MSNR-PS1**, **MSNP-PS2**, **MSNR-PS2**) and the corresponding PSs (**PS0**, **PS1** and **PS2**) (**Figure 5**). The free **PS0**, **PS1** and **PS2** were tested at concentrations of 0.5 µM and new nanomaterials were tested at concentrations of PS: 0.5 µM and 2.5 µM (**Figure 5**). Free **PS 1** and **PS 2** oxidized DPBF in the same way. **PS0** oxidized DPBF slightly less than PSs bearing sugar moieties.

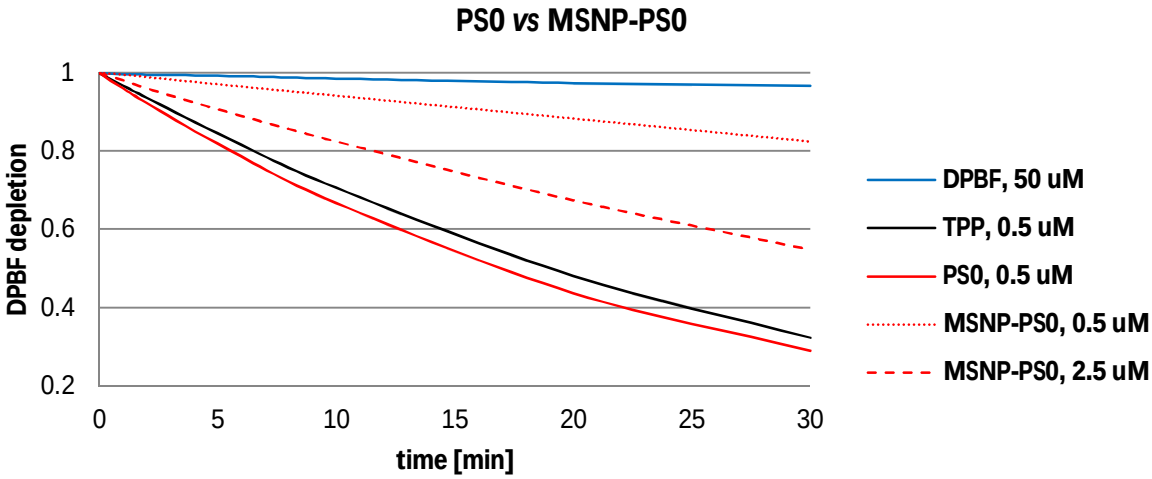

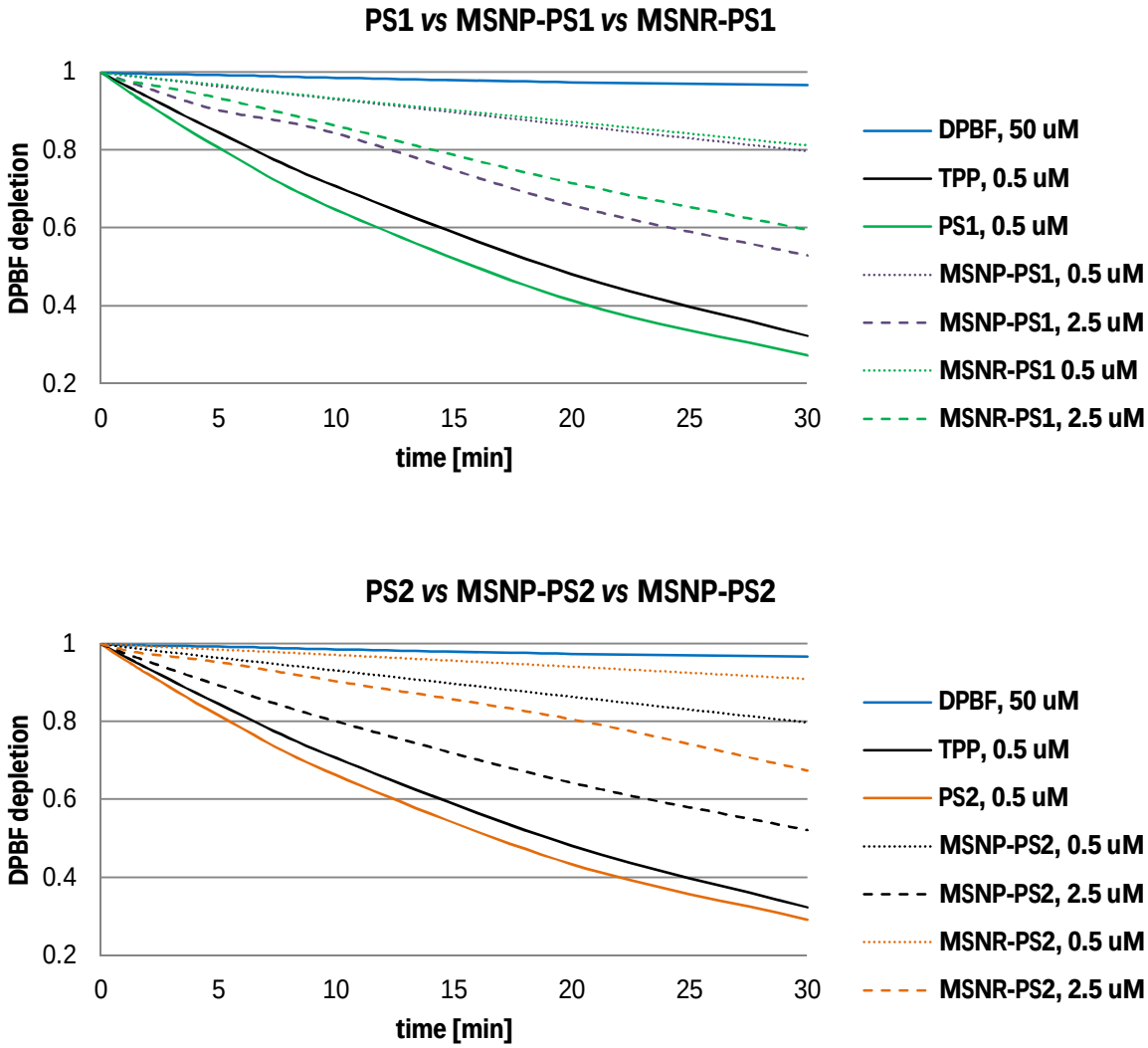

Figure 5. $^1O_2$ generation by **PS0**, **PS1**, **PS2** and its corresponding NPs (**MSNP-PS0, MSNP-PS1, MSNP-PS2** and **MSNR-PS1, MSNR-PS2**) were each point represents the mean of at least three independent experiments, and has a standard deviation lower than 3 %. Concentrations indicated for all nanomaterials refer to the equivalent concentration of non-immobilized porphyrins.

From the $^1O_2$ generation study we can observe that free **PS0**, **PS1** and **PS2** oxidized DPBF almost in the same way (**Figure 5**, **Figure 6**).

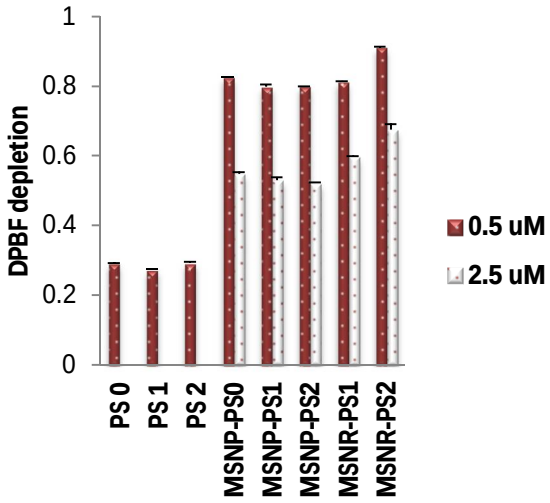

Figure 6. DPBF absorbance depletion in the presence of **PS0**, **PS1**, **PS2** and its corresponding NPs (**MSNP-PS0, MSNP-PS1, MSNP-PS2** and **MSNR-PS1, MSNR-PS2**) at different concentrations (0.5 and 2.5 μM) after 30 min of irradiation. Concentrations indicated for all nanomaterials refer to the equivalent concentration of non-immobilized Pors. Data are the mean value of at least three independent experiments.

DPBF kinetic decay was similar in all sphere-shaped particles (**MSNP-PS0, MSNP-PS1, MSNP-PS2**). After 30 min of irradiation these nanoformulations were able to reduce about 50 % of DPBF with 2.5 μM of PS concentration. All sphere-shaped particles produced more $^1O_2$ than rod-shaped particles (**Figure 6**). Which means that MSNPs should be more efficient than MSNRs in terms of cancer treatment in PDT. This could be due to the fact that in case of smaller NPs (NPs with smaller aspect ratio) oxygen can penetrate better their pores and $^1O_2$ has shorter way to go out from nanoformulation than in bigger NPs. Thus, MSNPs are more effective in $^1O_2$ production than MSNRs while corresponding free Pors (**PS1** and **PS2**) are producing the same amount of $^1O_2$ under the equal experimental conditions.

In vitro studies

In vitro studies were carried out into two human bladder cancer cell lines, HT-1376 and UM-UC-3. These cell lines are suitable *in vitro* cancer models for the evaluation of new glyco-porphyrinoids, since they express the glyco-binding proteins (glucose transporter, GLUT1 and galactose-binding protein, galectin-1) in different levels.[148] Previous studies

have proved that these two proteins have a key role on the uptake and finally on the phototoxicity of a galactodendritic phthalocyanine.[148] HT-1376 cancer cells express GLUT1 in higher levels when compared with UM-UC-3 and the former expresses galectin-1 in higher levels when compared with HT-1376.[148]

Cellular uptake of PSs and its nanoformulations

Preliminary uptake studies were performed using free PS (**PS0**, **PS1**, **PS2**). Bladder cancer cells were incubated in dark conditions with increasing concentrations of PS (0, 2.5, 5, 10 μM prepared in PBS, maximum 0.5% DMSO v/v) for 4 h. Fluorescence spectroscopy studies demonstrated that **PS1** accumulation was higher in HT-1376 than in UM-UC-3 cancer cells (**Figure 7**). On the other hand, the uptake of **PS0** and **PS2** was higher in UM-UC-3 than in HT-1376 cancer cells. Accumulation of **PS0** was much lower in both cancer cells than accumulation of PS bearing sugar groups. This can be explained by the fact that these cells express the glyco-binding proteins and **PS0** is free Por without any sugar units. Thus, the uptake of **PS1** and **PS2** should be higher as compared with **PS0**. In the case of **PS1** and **PS2**, the uptake was dependent on the concentration of the PS and cell line. Among the studied PSs, the highest uptake was observed for **PS1**. 10 μM of gluco-**PS1** was almost two times better accumulated in both cancer cell lines as compared to galacto-**PS2**. This could be caused by the fact that both HT-1376 and UM-UC-3 cancer cells have higher levels of glucose receptors when compared with galactose receptors. Thus, the presence of sugar moieties is important during the uptake of PSs by both cancer cells.

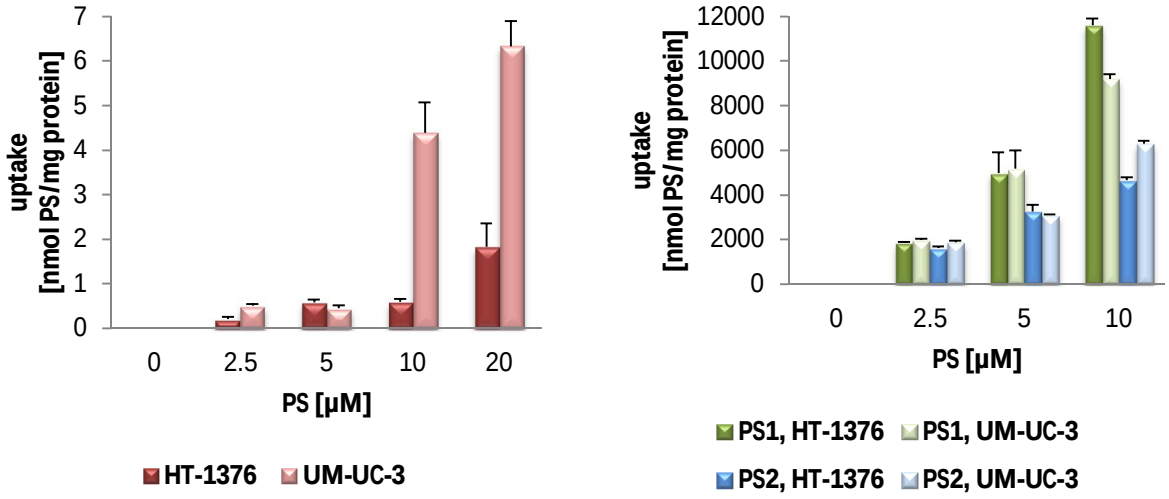

Figure 7. Intracellular uptake of **PS0**, **PS1**, **PS2** (0-10 μM in PBS) by UM-UC-3 and HT-1376 bladder cancer cells. Cells were incubated with **PS** for 4 h and uptake was determined by fluorescence spectroscopy. Data are means ± s.e.m. of at least three independent experiments performed in triplicates.

Next, the uptake of **MSNP-PS0, MSNP-PS1, MSNP-PS2**, **MSNR-PS1** and **MSNR-PS2** was evaluated by fluorescence spectroscopy (**Figure 8**) after incubating UM-UC-3 and HT-1376 bladder cancer cells in dark condition with different concentrations of new NPs (0-20 μM of PS).

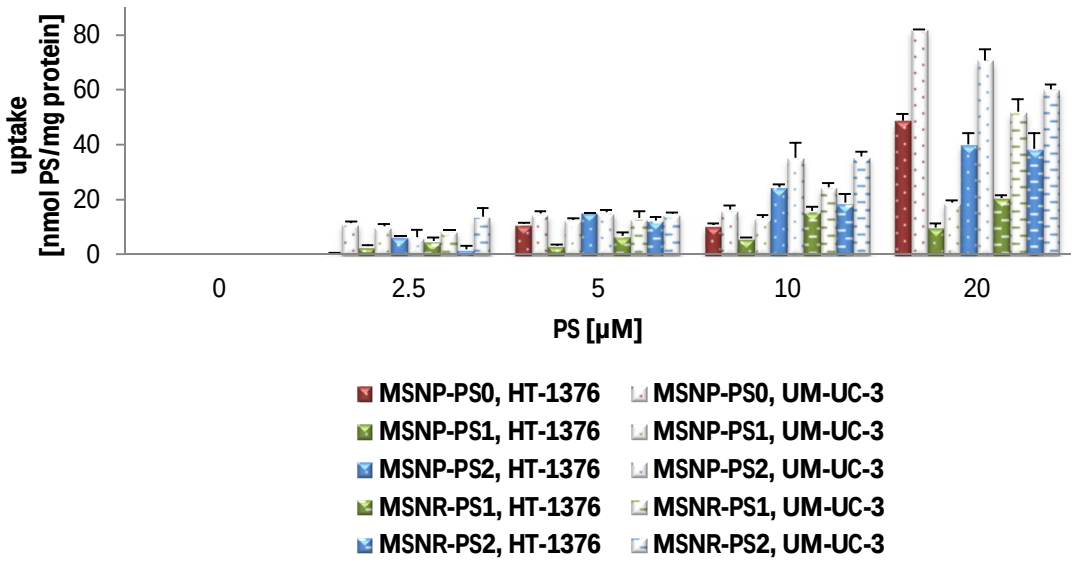

Figure 8. Intracellular overnight uptake of **MSNP-PS0**, **MSNP-PS1**, **MSNR-PS1**, **MSNP-PS2** and **MSNR-PS2** (0-20 μM of PS in RPMI medium) by UM-UC-3 and HT-1376

bladder cancer cells. Data are means ± s.e.m. of at least three independent experiments performed in triplicates.

Uptake studies were performed by incubating cancer cells with PS nanoformulations overnight. When the cells were incubated overnight with medium containing NPs solutions there was uptake dependent on the concentration of the NPs but not on the cell line (which was observed with free PSs). Interestingly, the uptake of **MSNP-PS1** was almost three times lower when compared with the uptake of **MSNR-PS1**. On the other hand, the uptake of **MSNP-PS2** was negligible higher than **MSNR-P2**. This could be explained by different concentrations of PS on the surface of NPs (**Table 3**).

NP name	Concentration of PS on the surface of NP [nmol of PS/mg of NP]	Uptake in HT-1376 [nmol PS/mg protein]*	Uptake in UM-UC-3 [nmol PS/mg protein]*
MSNP-PS1	25.0	9.8	18.7
MSNR-PS1	22.9	20.5	51.8
MSNR-PS2	22.6	38.3	60.1
MSNP-PS2	19.8	39.9	70.6

Table 3. Comparison between concentration of PS on the surface of NPs and its uptake behavior (*the uptake is presented for 20 μM of PS into each experiment). Concentrations indicated for all nanomaterials refer to the equivalent concentration of non-immobilized porphyrins.

The comparison between the amount of PS on the surface of NPs and the corresponding cell uptake value shows that there is an inverse trend relating this data, i.e. as the amount of PS per mg of NP increases there is a decrease on the cell uptake (**Table 3**, **Figure 9**). In the present uptake studies, although the same amount of PS was used the nanoformulations had different amounts of PS on their surfaces, thus different amounts of NPs were used in the experiments. When the concentration of PS on the NPs' surface was higher, the smaller was the amount of NPs (in mg) taken into experiment resulting in a smaller uptake. In conclusion, the uptake depends not only on the concentration of PS on the surface of NPs but also on the amount of NPs (in mg or numbers of NPs).

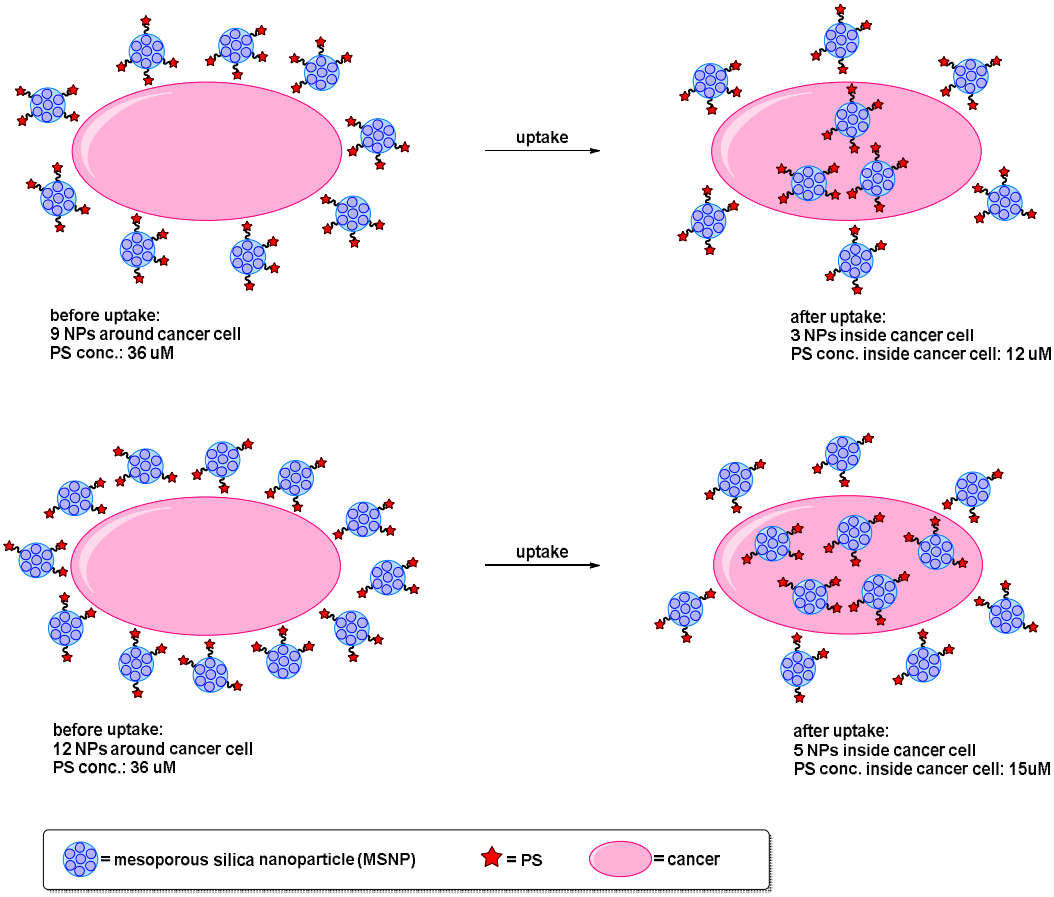

Figure 9. Schematic representation of suggested uptake process in cancer cells which is in inverse proportion to the concentration of PS on the surface of NP per mg of NP. The same mechanism is proposed for MSNPs and MSNRs.

Furthermore, it was observed that the uptake of all new nanoformulations was higher in UM-UC-3 cancer cells (with high level of galectin-1) when compared with HT-1376 cells (with high level of GLUT1 protein). This could be a result of better delivery process of MSNPs and MSNRs in UM-UC-3 than in HT-1376 cells. Interestingly, **MSNP-PS0** was the only sample that accumulated better in both cancer cell lines than the corresponding non-immobilized Por (**Figures 7**, **8**). The uptake of these sphere-shaped particles was ten times better in cancer cells when compared to free **PS0**. **MSNP-PS0** (117 ± 16 nm) had the tendency to accumulate in tumor tissue much more than smaller molecules of **PS0**. This selective accumulation in tumor tissues could be related with EPR effect in which certain size particles accumulate in tumor tissue much better than in normal tissues.[39,40,151]

Dark toxicity and phototoxicity

The dark toxicity of **PS0**, **PS1**, **PS2** and its corresponding nanoformulations (**MSNP-PS0, MSNP-PS1, MSNP-PS2** and **MSNR-PS1, MSNR-PS2**) was evaluated using the well-known MTT assay (**Figures SI 10**, **11**) in UM-UC-3 and HT-1376 bladder cancer cells. This colorimetric assay uses the ability of living bladder cancer cells to reduce yellow 3-[4,5-dimethylthiazol-2-yl]-2,5-diphenyl-tetrazolium bromide (MTT), to a purple formazan. Thus, it is a straightforward tool to determine the cell metabolic activity. After overnight incubation of cancer cells (in dark) with NPs (0-20 µM of PS in RPMI medium) or 4 h incubation with PSs (0-10 µM in PBS buffer), none of the PSs or new NPs induced dark toxicity in cancer cells. This outcome is crucial in the PDT concept, since the ideal therapeutic drug should not show cytotoxicity until photoactivation.

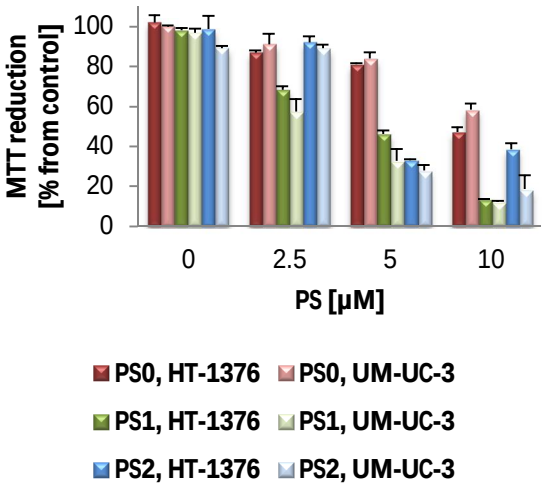

Figure 10. Phototoxicity of **PS0**, **PS1**, **PS2** (0-10 µM) determined 24 h after PDT treatment using the MTT assay. The percentage of cytotoxicity was calculated relatively to control cells (cells incubated with PBS and then irradiated). Data are means ± s.e.m. of at least three independent experiments performed in triplicates.

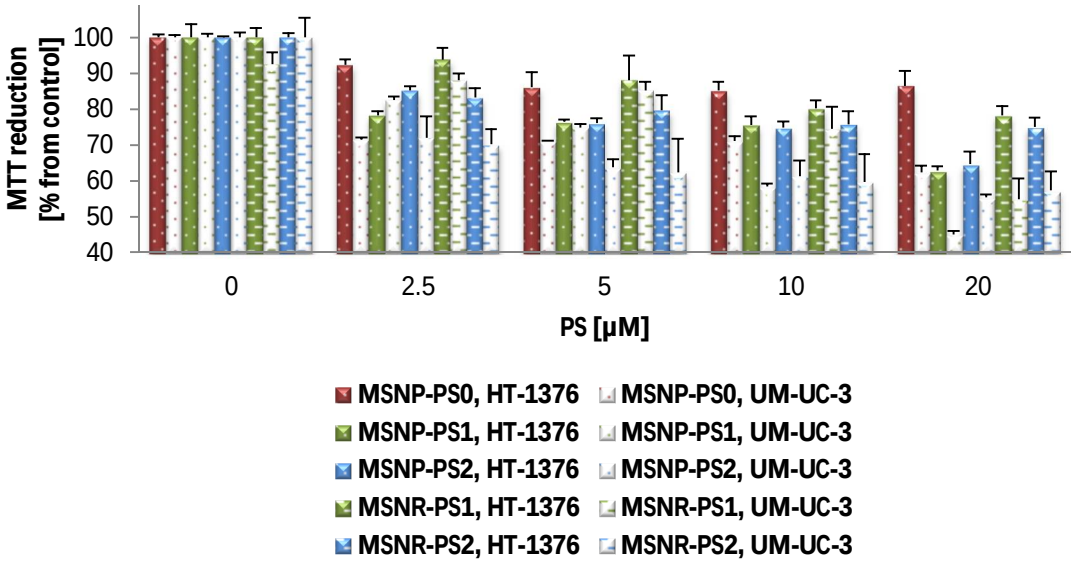

Figure 11. Phototoxicity of **MSNP-PS0, MSNP-PS1, MSNP-PS2** and **MSNR-PS1, MSNR-PS2** (0-20 μM of PS) determined 24 h after PDT treatment using the MTT assay. The percentage of cytotoxicity was calculated relatively to control cells (cells incubated with medium and then irradiated). Data are means ± s.e.m. of at least three independent experiments performed in triplicates.

Following the confirmation of the uptake and non-dark toxicity of PSs and their new nanoformulations in UM-UC-3 and HT-1376 bladder cancer cells, their toxicity after light irradiation was evaluated using the MTT assay (**Figures 10**, **11**). In this study UM-UC-3 and HT-1376 bladder cancer cells were incubated with PSs (0-10 μM in PBS buffer) for 4 h or with NPs (0-20 μM of PS in RPMI medium) overnight, and then irradiated with an optical fiber emitting white light for 40 min (12 mW/cm^2). No cytotoxicity was observed in the untreated (cells incubated in the absence of NP) sham irradiated cells.

When the cells were incubated for 4 h in PBS containing PSs (0-10 μM in PBS buffer) there was phototoxicity dependent on the concentration of the PSs (**Figure 10**). **PS1** and **PS2**, led to higher phototoxicity in both cancer cells than the **PS0** sample. This could be explained by the fact that these two PSs with sugar units presented much better uptake properties in HT-1376 and UM-UC-3 cancer cells compared to **PS0**. **PS1** and **PS2** presented slightly higher phototoxicity in UM-UC-3 cancer cells than in HT-1376 cancer cells.

After UM-UC-3 and HT-1376 bladder cancer cells were incubated overnight in medium with NPs (0-20 μM of PS) there was phototoxicity dependent on the concentration of the PSs (**Figure 11**). Although all new NPs induced photoxicity in UM-UC-3 and HT-1376 bladder cancer cells in a concentration-dependent manner, the overall phototoxicity was higher with PSs than with NP formulations.

In general, the phototoxicity was higher with **MSNPs** than with **MSNRs** (**Table 4**). All NPs presented higher phototoxicity in UM-UC-3 cancer cells than in HT-1376 cancer cells. Which could be the result of better uptake observed in these cell lines (**Figure 8**). Although the best uptake was observed for **MSNP-PS2** in both, UM-UC-3 and HT-1376 bladder cancer cells, in case of photoxicity, **MSNP-PS1** with the lowest uptake results presented the highest photoxicity in the same cancer cells lines (**Table 4**).

NP name	Concentration of PS on the surface of NP [nmol of PS/mg of NP]	Uptake in		Phototoxicity in	
		HT-1376 [nmol PS/mg protein]*	UM-UC-3 [nmol PS/mg protein]*	HT-1376 [%]**	UM-UC-3 [%]**
MSNP-PS1	25.0	9.8	18.7	62.8	44.9
MSNR-PS1	22.9	20.5	51.8	78.1	54.8
MSNR-PS2	22.6	38.3	60.1	74.9	57.2
MSNP-PS2	19.8	39.9	70.6	64.5	55.2

Table 4. Relation between concentration of PS on the surface of NPs and its uptake behavior with phototoxicity results (*the uptake is presented for 20 μM of PS into each experiment, **the phototoxicity is presented after 30 min of light irriadiation).

There is a clear relation between the uptake behavior and phototoxicity results. For all nanovehicles, the higher uptake was observed in UM-UC-3 than in HT-1376 cancer cells. The same behavior was spotted during phototoxicity studies. The phototoxicity was higher in UM-UC-3 than in HT-1376 cancer cells.

To improve the phototoxicity of all new nanovehicles, second light irradiation treatment could increase *in vitro* photodynamic efficacy as it was already demonstrated in the literature.[174] In the period between single and repeated irradiation NPs could accumulate in cancer cells which could enhance phototoxicity in both cancer cell lines.

Conclusions

In summary, sphere-shaped mesoporous silica particles and rod-shaped mesoporous silica particles grafted with *S*-glycoside Pors were successfully prepared and characterized. All novel nanomaterials were able to produce $^1O_2$ hence *in vitro* studies with two human bladder cancer cell lines, HT-1376 and UM-UC-3, were performed.

When HT-1376 and UM-UC-3 cells were incubated overnight with medium containing NPs solutions there was an uptake dependent on the concentration of the NPs but not on the cell line which was observed with free PSs. Furthermore, it was noted that the uptake of all new nanoformulations was higher in UM-UC-3 cancer cells (with high level of galectin-1) when compared with HT-1376 cells (with high level of GLUT1 protein). From these results, it can be concluded that the cells uptake depends not only on the concentration of PS on the surface of NPs but also on the amount of NPs employed (in mg or numbers of NPs). Comparing the concentration of PS on the surface of NPs with uptake studies, the uptake is in inverse proportion to concentration of PS per mg of NP. Although **MSNP-PS0** presented the lowest phototoxicity among all tested NPs samples, these NPs were the only which accumulated better in both cancer cell lines than the corresponding non-immobilized porphyrin (**PS0**). The uptake of these sphere-shaped particles was ten times better in cancer cells when compared to free **PS0**.

None of the PSs or new NPs induced dark toxicity in cancer cells. Despite the fact that all new NPs induced photoxicity in UM-UC-3 and HT-1376 bladder cancer cells in a concentration-dependent manner, the overall phototoxicity was higher with free PSs than with NPs. In general the phototoxicity was higher with MSNPs than with MSNRs. For all nanovehicles higher uptake was observed in UM-UC-3 than in HT-1376 cancer cells. The same behavior was noted during phototoxicity studies. The phototoxicity was higher in UM-UC-3 than in HT-1376 cancer cells.

The resulting new nanocarriers were fully described and their properties as new third generation PSs for PDT against two bladder cancer cell lines, HT-1376 and UMUC-3 were proved. The final results showed that our new nano-systems could be successfully use in PDT of bladder cancer which is the fourth most commonly diagnosed cancer[180] with the

high rate of recurrence. Further advances towards improving therapeutic efficacy of PDT treatment by these NPs are under research.

Acknowledgements

Thanks are due to FCT/MEC for the financial support to QOPNA (FCT UID/QUI/00062/2013), CICECO-Aveiro Institute of Materials (FCT UID/CTM/50011/2013), IBILI (FCT UID/NEU/04539/2013) and CQE (FCT UID/QUI/0100/2013) research units, through national funds and where applicable cofinanced by the FEDER, within the PT2020 Partnership Agreement. The work was also supported by the Spanish MINECO (CTQ-2014-52869-P), Comunidad de Madrid (FOTOCARBON, S2013/MIT-2841) and Portuguese COMPETE (POCI-01-0145-FEDER-007440). We further wish to thank the Seventh Framework Programme (FP7-People-2012-ITN) for funding the SO2S project (grant agreement number: 316975).

Supplementary Information

Nanoparticle-based systems as efficient vehicles to transport and deliver photosensitizers into tumor tissues during photodynamic therapy *in vitro*

Experimental section

General methods

Absorption spectra were recorded using a JASCO V-660 UV-Visible Spectrophotometer. FT-IR spectra were recorded in KBr pellets using GRASEBY SPECAC or with Cary 630 FT-IR Spectrometer. The irradiation system used to determine the production of $^1O_2$ was the Newport irradiation system, consisting on a 300 W halogen lamp, FSQ-OG530 color glass filter for wavelengths <530 nm and magnetic stirrer. The irradiation system used to determine the phototoxicity during biological experiments was a Lumacare system, model LC-122, consisting on a 250 W halogen lamp coupled to an optical fiber (with a cutoff filter for wavelengths <540 nm). The radiation power was measured with a potentiometer bright Spectra Physics, model 407A and the sensor of the same brand, model 407A-2. Transmission electron microscopy (TEM) images were obtained using a JEOL JEM1010 transmission electron microscope operating at an acceleration voltage of 100 kV.

All reagents were obtained from commercial sources and were used without further purification steps. Reverse phase column chromatography was carried out on Waters Sep-Pak C18 35 cm^3 cartridges. Analytical thin layer chromatography (TLC) was carried out on pre-coated silica gel sheets (Merck, 60, 0.2 mm).

Synthesis of NPs

Synthesis of MSNPs and MSNRs

MSNPs and **MSNRs** were prepared after slight modification of the method presented in the literature.[191] In a first step, CTAB (100 mg for **MSNP-100**, 200 mg for **MSNP-200**, 400 mg for **MSNP-400**, 500 mg for **MSNP-500**,) was dissolved in water (100 mL) in Erlenmeyer flask equipped with magnetic bar. Next, to the above solution ethyl acetate (0.88 mL) and NH_4OH (30%, 2.7 mL) were subsequently added. In the end, TEOS (500 µL) was added and the solution was stirred for 5 min at RT. After that, 100 mL of water

was added to slower the hydrolysis of TEOS and accelerates the silica condensation. After 24 h of stirring at RT, NPs were filtered and washed with EtOH. To remove the surfactant templates, nanoparticles were redispersed in 100 mL of ethanol/acetic acid (glacial) mixture (95/5, v/v) and the mixture was stirred for 30 minutes. In the end, nanoparticles were washed with EtOH and air-dried.

MSNPs' and MSNRs' functionalization with APTS

To the suspension of 30 mg of **MSNPs** or **MSNRs** in 2.5 mL H_2O, 158 µL of APTS in 750 µL of EtOH was added. After adjusting the pH to 7 by adding 0.2 M HCl (2.25 mL) the reaction was stirred at RT for 24 h. **MSNPs-NH_2** and **MSNRs-NH_2** were washed with EtOH and air-dried.

Grafting of PS on the surface of MSNPs-NH_2 and MSNRs-NH_2

The grafting of porphyrins **PS0**, **PS1**, and **PS2** on the nanomaterials **MSNPs-NH_2** and **MSNRs-NH_2** was carried out in DMSO at 160 °C according to the literature, with minor modifications.[65] 35 mg of **MSNPs-NH_2** or **MSNPs-NH_2** were resuspended in DMSO (1 mL). A solution of **PS** (2.38 µmol) in DMSO (4 mL) was added to that suspension and the resulting mixture was magnetically stirred for 96 h at 160 °C. After that time, a red hybrid materials were obtained. The resulting hybrid materials were washed with DMSO and EtOH until no Soret and Q bands were observed in the rinse solvent and air-dried. The amount of unreacted porphyrin was calculated by UV-Vis spectrophotometry.

Singlet oxygen generation study

Singlet oxygen ($^1O_2$) was determined by a chemical method using 1,3-diphenylisobenzofuran (DPBF). DPBF has an absorption maximum at 415 nm, thus it is possible to follow the ability of the NPs to generate $^1O_2$ by measuring the DPBF absorption decay, at this wavelength.

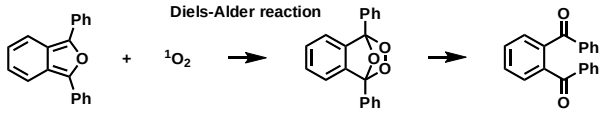

Figure SI 1. Reaction occurring during singlet oxygen generation study. The yellow-colored DPBF reacts with $^1O_2$ in [4+2] cycloaddition reaction, being oxidized to the colorless o-benzoylbenzene.

The solutions were irradiated at RT under magnetic stirring and light from a 300 W halogen lamp with a cutoff filter for wavelengths <530 nm (**Figure SI 2**). 5,10,15,20-tetrakis-phenyl-21,23-H-porphyrin (**TPP**) was used as a reference compound.

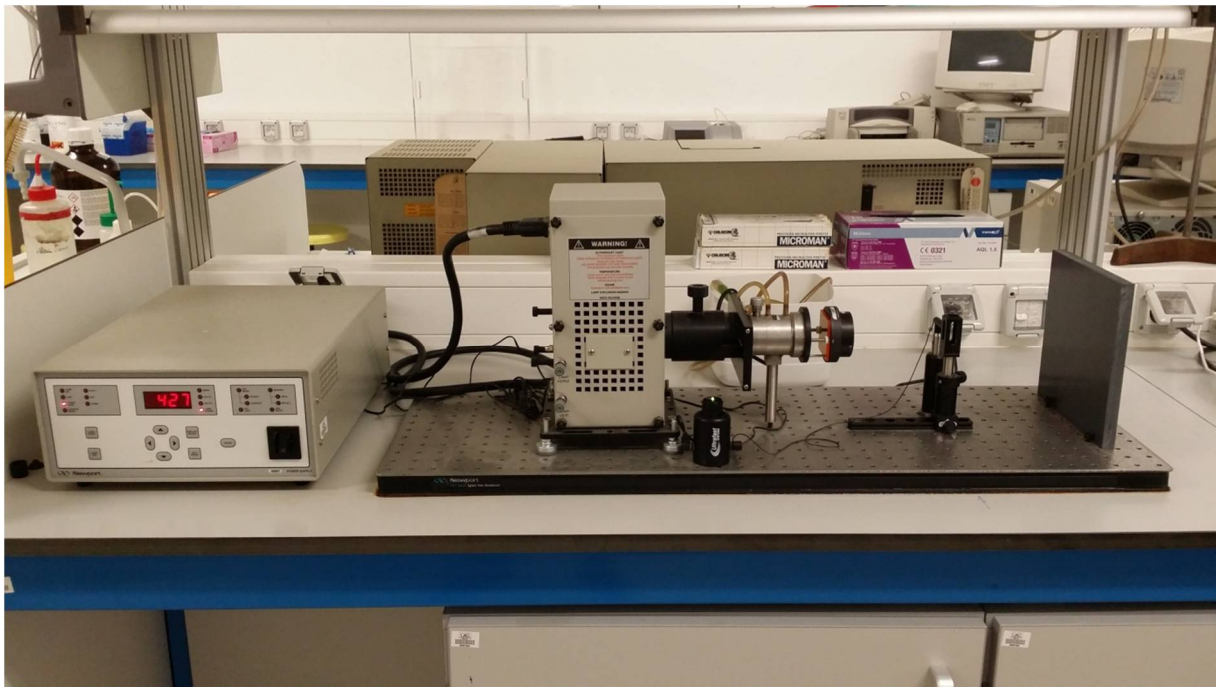

Figure SI 2. Equipment used for singlet oxygen generation study.

TPP (0.5 μM), **PS0** (0.5 μM), **PS1** (0.5 μM), **PS2** (0.5 μM), **MSNP-PS0** (0.5 μM, 2.5 μM of PS), **MSNP-PS1** (0.5 μM, 2.5 μM of PS), **MSNR-PS1** (2.5 μM of PS), **MSNP-PS2** (0.5 μM, 2.5 μM of PS) or **MSNR-PS2** (2.5 μM of PS) were placed into 3 mL cuvette which contained DMSO. Then DPBF (50 μM) in DMSO was added (total volume in cuvette 3 mL). The final solutions were irradiated at RT and under gentle magnetic stirring and light from a 300 W halogen lamp (with a cut off filter for wavelengths <530 nm). The breakdown of DPBF was monitored by measuring the decrease in absorbance at 415 nm at pre-established irradiation intervals. The results were expressed by plotting the DPBF

depletion against the irradiation time. The depletion of DPBF was calculated as follows: *DPBF depletion* = Abs_1/Abs_0. Abs_0 and Abs_1 are the absorbance values at 415 nm before and after irradiation, respectively.

Photostability of NPs during singlet oxygen generation study

Photostability studies were carried out in the same conditions of irradiation of the singlet oxygen studies but without DPBF. The results are presented in ratio calculated by the ratio of residual absorbance at 415 nm (**DPBF**), 418 nm (**TPP**), 417 nm (**PS0**), 421 nm (**PS1**), 421 nm (**PS1**), 436 nm (**MSNP-PS0**), 431 nm (**MSNP-PS1**), 436 nm (**MSNR-PS1**), 435 nm (**MSNP-PS2**), 438 nm (**MSNR-PS2**) at different periods of time and absorbance before irradiation. Each point represents the mean of at least three independent experiments, and has a standard deviation lower than 2%. Nanoparticles were stable during singlet oxygen study.

Compounds/NPs	**Irradiation time (min)**						
	0	**1**	**2**	**5**	**10**	**20**	**30**
DPBF	1	0.99	0.99	0.99	0.98	0.97	0.97
TPP	1	0.99	0.99	0.99	0.99	0.99	0.99
PS0	1	0.99	0.99	0.99	0.99	0.99	0.99
PS1	1	0.99	0.99	0.98	0.98	0.98	0.98
PS2	1	0.99	0.99	0.99	0.99	0.99	0.98
MSNP-PS0	1	0.99	0.98	0.97	0.95	0.93	0.92
MSNP-PS1	1	0.99	0.98	0.96	0.93	0.91	0.89
MSNP-PS2	1	0.99	0.99	0.98	0.97	0.95	0.94
MSNR-PS1	1	0.99	0.98	0.97	0.96	0.94	0.93
MSNR-PS2	1	0.99	0.98	0.97	0.97	0.97	0.94

Table SI 1. Photostability of NPs during singlet oxygen study.

Characterization of NPs

UV-Vis spectra of PSs, MSNPs and MSNRs

UV-Vis absorption spectra were collected after dispersion of **MSNPs** and **MSNRs** in DMSO or after dissolving **PS0**, **PS1** and **PS2** in DMSO. Concentrations indicated for all nanomaterials refer to the equivalent concentration of non-immobilized porphyrins.

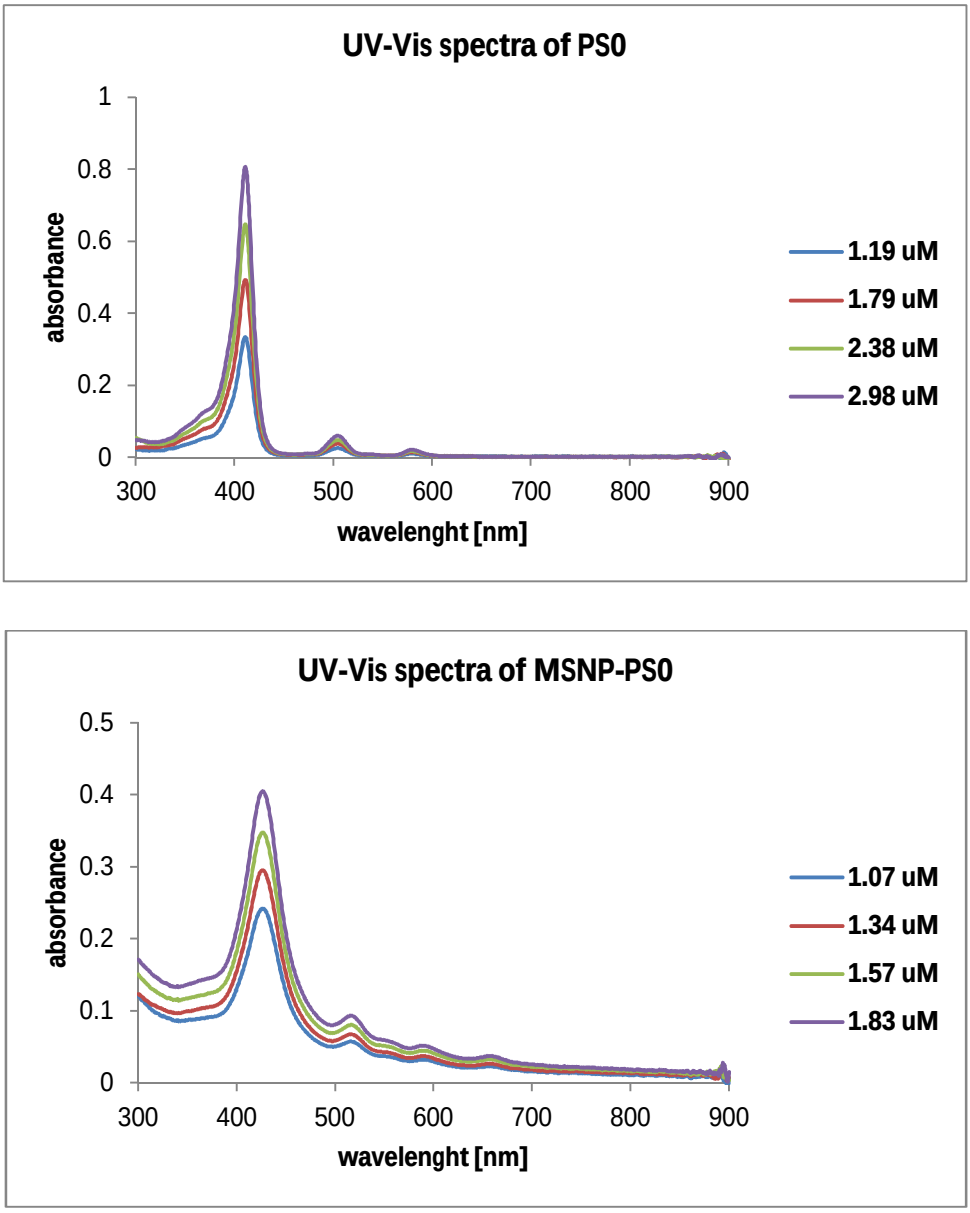

Figure SI 3. UV-Vis spectra of **PS0** and corresponding **MSNP-PS0**.

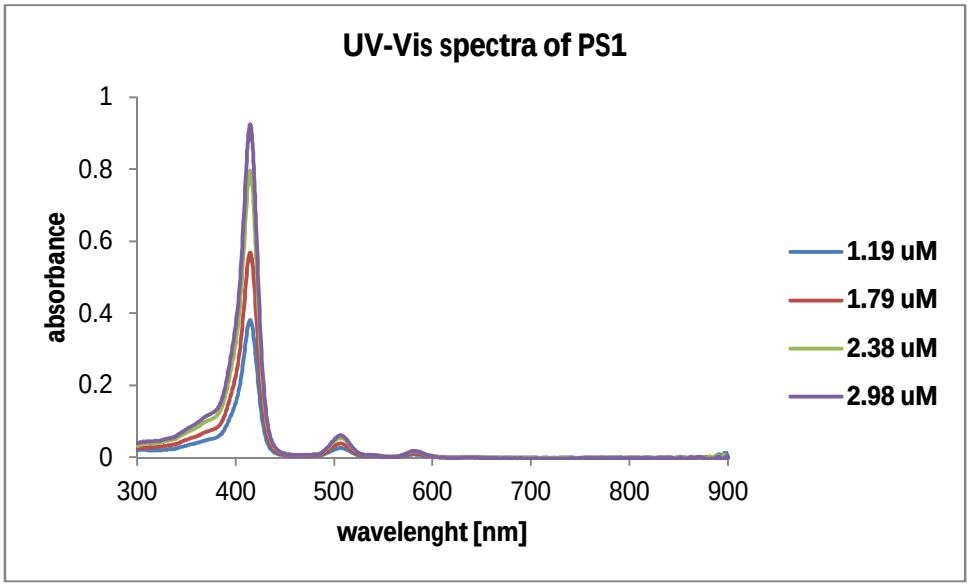
UV-Vis spectra of PS1
absorbance
1
0.8
0.6
0.4
0.2
0
300
400
500
600
700
800
900
wavelenght [nm]
1.19 uM
1.79 uM
2.38 uM
2.98 uM

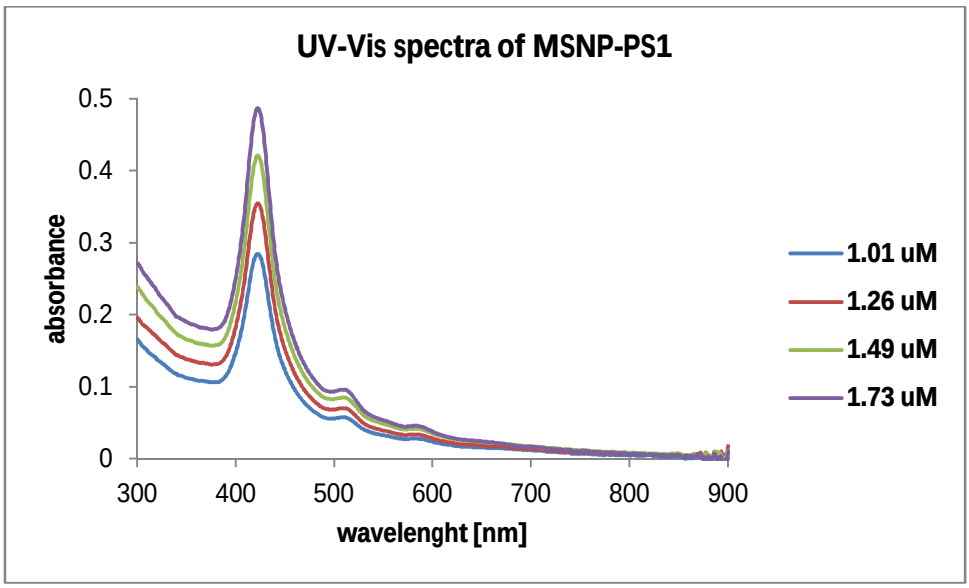
UV-Vis spectra of MSNP-PS1
absorbance
0.5
0.4
0.3
0.2
0.1
0
300
400
500
600
700
800
900
wavelenght [nm]
1.01 uM
1.26 uM
1.49 uM
1.73 uM

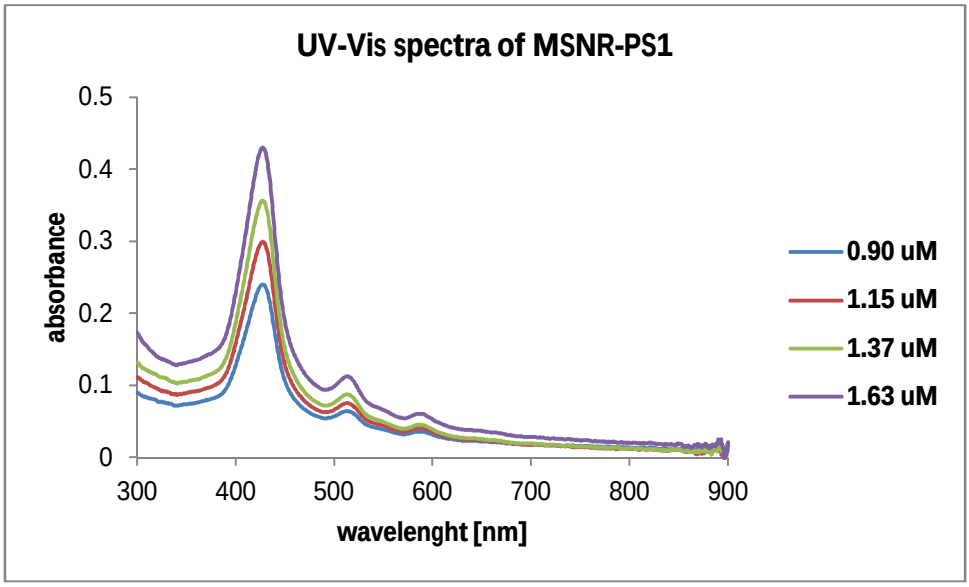

Figure SI 4. UV-Vis spectra of **PS1** and corresponding **MSNP-PS1**, **MSNR-PS1**.

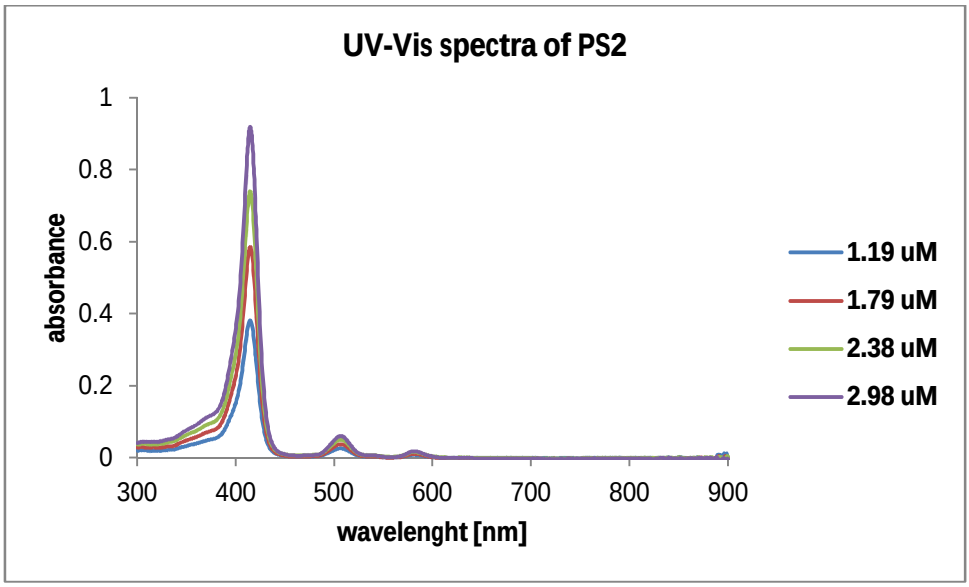

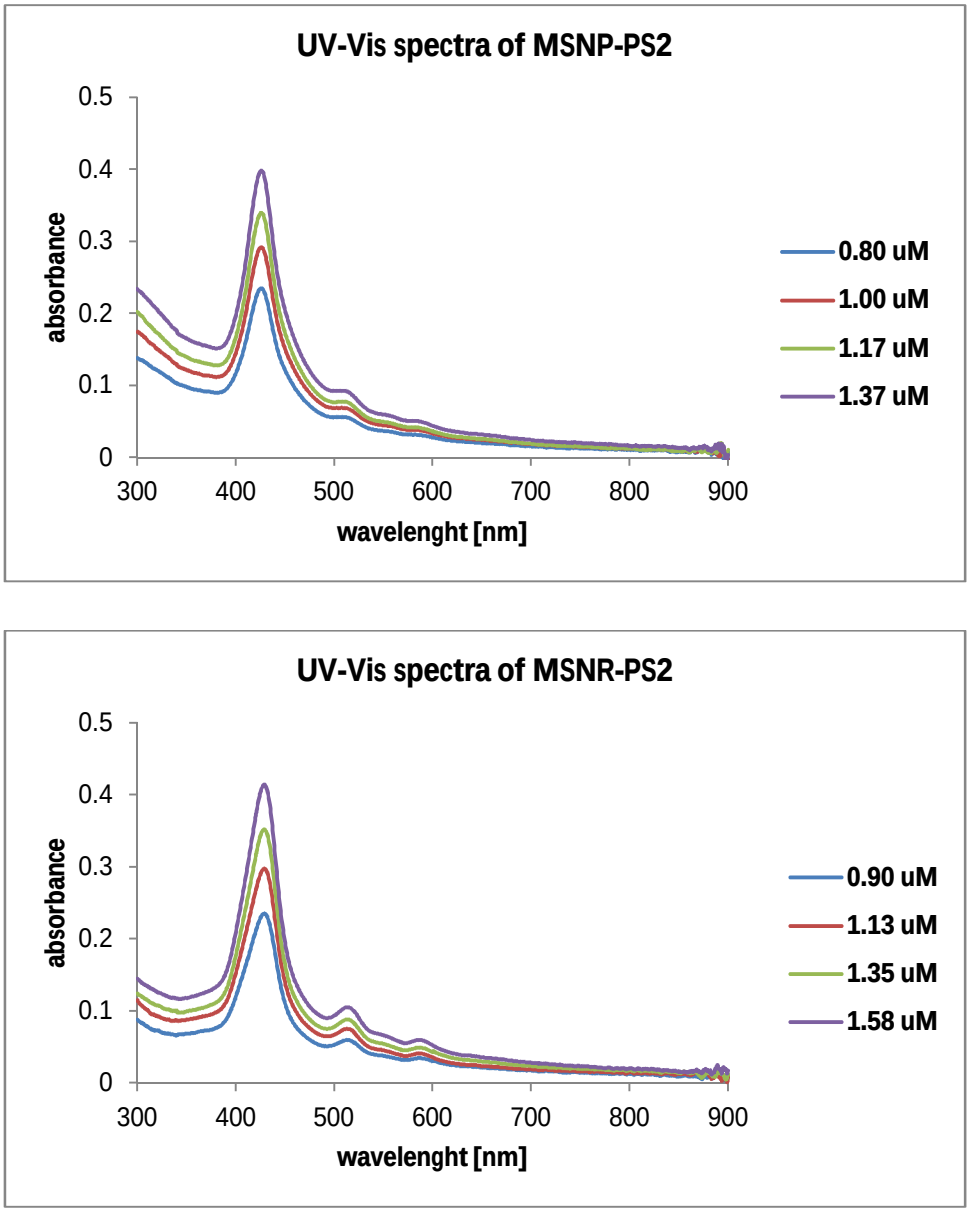

Figure SI 5. UV-Vis spectra of **PS2** and corresponding **MSNP-PS2**, **MSNR-PS2**.

FT-IR spectra of PSs, MSNPs and MSNRs

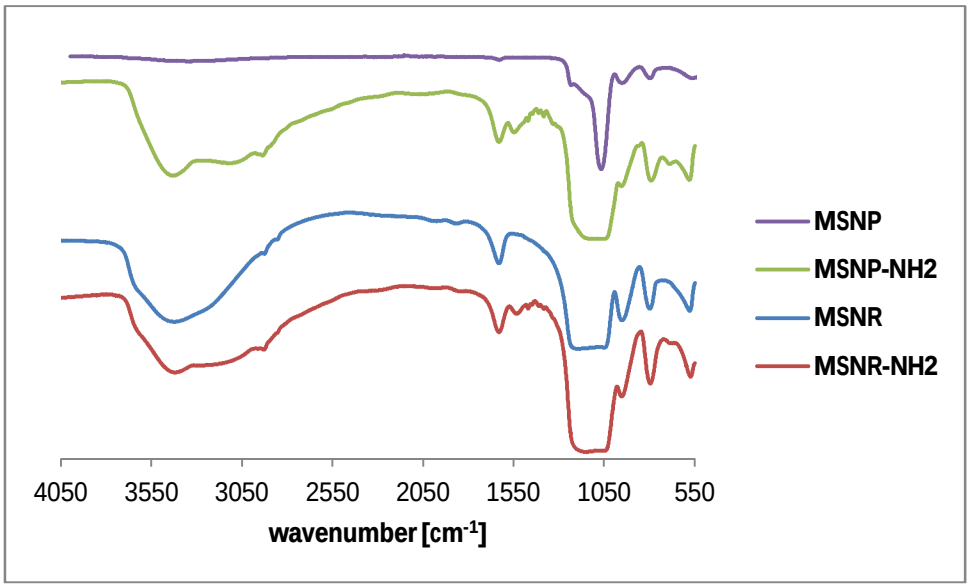

Figure SI 6. FT-IR spectra of **MSNP**, **MSNP-NH$_2$**, **MSNR** and **MSNR-NH$_2$**.

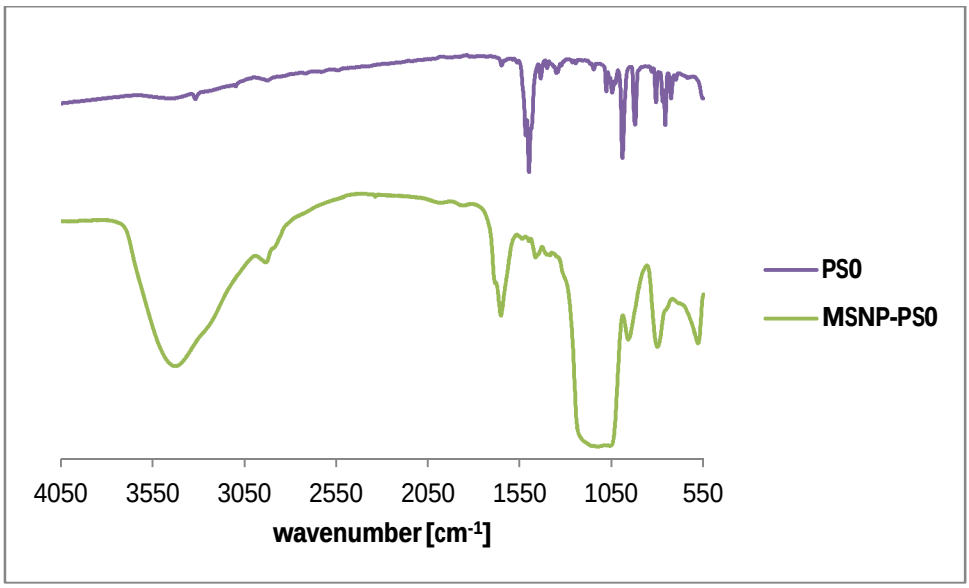

Figure SI 7. FT-IR spectra of **PS0** and corresponding **MSNP-PS0**.

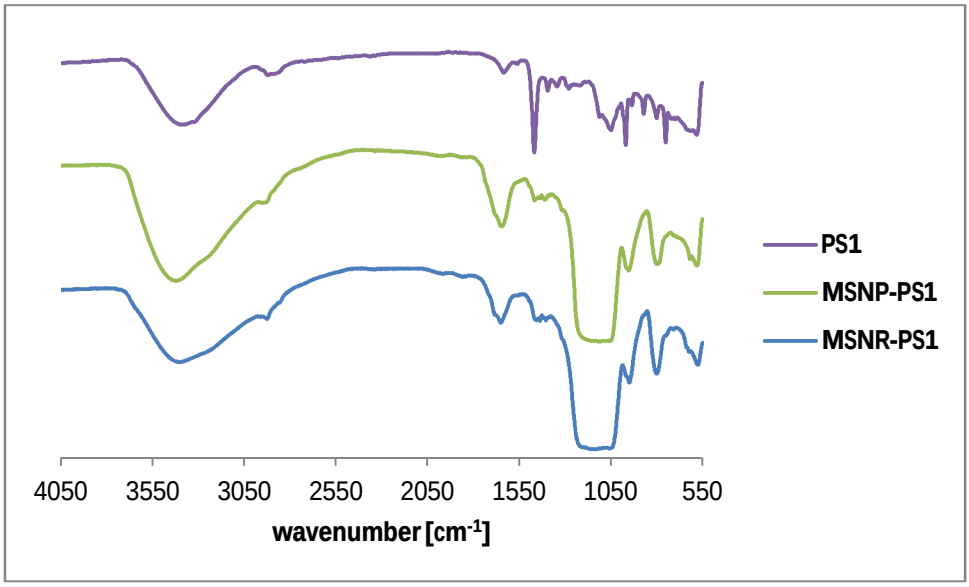

Figure SI 8. FT-IR spectra of **PS1** and corresponding **MSNP-PS1**, **MSNR-PS1**.

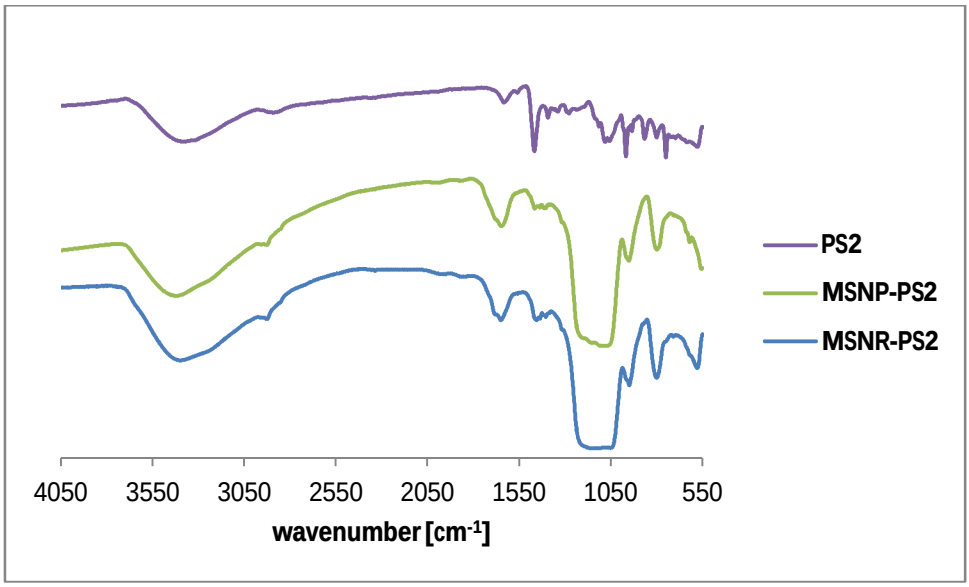

Figure SI 9. FT-IR spectra of **PS2** and corresponding **MSNP-PS2**, **MSNR-PS2**.

In vitro assays

Cells culture

Human bladder cancer cell lines UM-UC-3 and HT-1376 derived from high-grade transitional cell carcinoma were obtained from the American Type Culture Collection (ATCC®, Manassas, VA, USA). Cells were cultured in Roswell Park Memorial Institute

(RPMI)-1640 medium (Sigma) supplemented with 2 $g.L^{-1}$ sodium bicarbonate (Sigma), 2 mM L-glutamine (Sigma), 10% (v/v) of heat-inactivated Fetal Bovine Serum (FBS; Life Technologies, Carlsbad, CA, USA) and antibiotic/antimicotic containing 100 units.mL-1 penicillin, 100 µg.mL-1 streptomycin and 0.25 µg.mL-1 amphotericin B (Sigma). UM-UC-3 and HT-1376 cells were seeded at a density of 1.5 x 104 in 96-well culture plates (Orange Scientific, Braine-l'Alleud, Belgium). 24 hours after plating, cells were overnight incubated with different concentrations of NPs (0-20 µM of PS in RPMI medium) in the dark.

Cellular uptake of NPs

After incubation with NPs in the dark, UM-UC-3 and HT-1376 cells were washed with PBS buffer and mechanically scrapped in 1% (m/v) sodium dodecyl sulfate (SDS; Sigma) in PBS buffer at pH 7.0. NPs intracellular concentration was determined by spectrofluorimetry using a microplate reader (Synergy HT, Biotek, Winooski, VT, USA) with the excitation filter (set at 360±40 nm) and emission filter (645±40 nm). Results were normalized for protein concentration (determined by bicinchoninic acid reagent; Pierce, Rockford, IL, USA).

PDT treatments on cells

Photodynamic irradiation was carried out in fresh culture medium, in the absence of NPs, covering UM-UC-3 and HT-1376 cell monolayers with RPMI medium and exposing them to white light delivered by the illumination system LC-122 LumaCare at 12 mW/cm^{-2} for 40 min. As a control, sham-irradiated cells were used. These cells were kept in the dark for the same durations and under the same conditions as the irradiated cells. In all trials, triplicate wells were settled under each experimental condition, and each experiment was repeated at least three times.

MTT assay

MTT assay was used to determine cell metabolic activity after NPs incubation in the dark, irradiation, or both after 24 h. This colorimetric assay is measuring the ability of bladder cancer cells to reduce yellow 3-[4,5-dimethylthiazol-2-yl]-2,5-diphenyl-tetrazolium bromide (MTT, Sigma), to a purple formazan on a microplate reader (Synergy HT). The

results are expressed in percentage of control (i.e. optical density of formazan from cells not exposed to NPs).

Dark toxicity studies of PSs, MSNPs and MSNRs

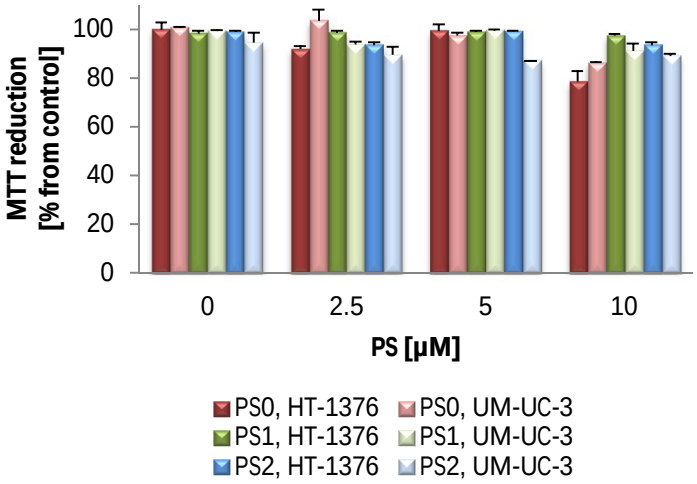

Figure SI 10. Non-dark toxicity of **PS 1, PS2** and **PS3** (0-10 μM) determined 24 h after treatment using the MTT assay. The percentage of cytotoxicity was calculated relatively to control cells (cells incubated with PBS). Data are means ± s.e.m. of at least three independent experiments performed in triplicates.

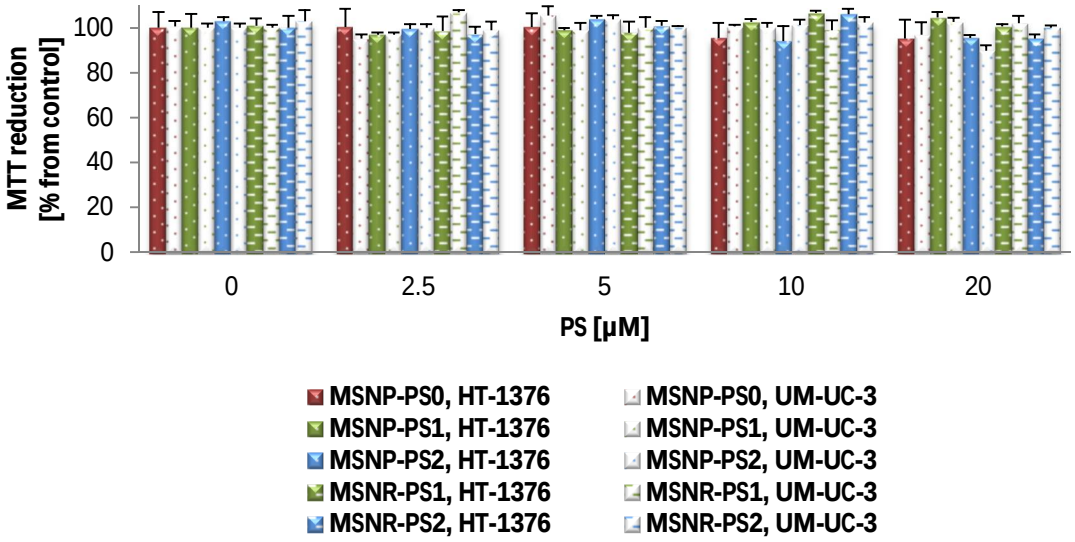

Figure SI 11. Non-dark toxicity of **MSNP-PS0, MSNP-PS1, MSNP-PS2** and **MSNR-PS1, MSNR-PS2** (0-20 µM of PS) determined 24 h after treatment using the MTT assay. The percentage of cytotoxicity was calculated relatively to control cells (cells incubated with medium). Data are means ± s.e.m. of at least three independent experiments performed in triplicates.

CHAPTER 4: Silica nanoformulations of phosphonated-phthalocyanines as novel anticancer agents for photodynamic therapy

Wioleta Borzęcka,[1,2,3] Patrícia M. R. Pereira,[1,4] Nutalapati Venkatramaiah,[1,2] Rosa Fernandes, [*4,5] Tito Trindade,[2] Tomás Torres,[3,6] and João Tomé[1,7]

[1]QOPNA and [2]CICECO, Department of Chemistry, University of Aveiro, 3810-193 Aveiro, Portugal; [3]Department of Organic Chemistry, Autonoma University of Madrid, 28049 Madrid, Spain; [4]Laboratory of Pharmacology and Experimental Therapeutics, Institute for Biomedical Imaging and Life Sciences (IBILI), Faculty of Medicine, University of Coimbra, Azinhaga de Santa Coimba, Coimbra, Portugal; [5]CNC.IBILI, University of Coimbra, 3000 Coimbra, Portugal; [6]IMDEA-Nanociencia, Campus de Cantoblanco, c/Faraday 9, 28049 Madrid, Spain; [7]Centro de Química Estrutural, Departamento de Engenharia Química, Instituto Superior Técnico, Universidade de Lisboa, 1049-001 Lisboa, Portugal

Keywords: Phosphonate-phthalocyanines, Photosensitizers, Silica Nanoparticles, PDT

Abstract: This research reports the combination of amorphous silica nanoparticles (SNPs) with phosphonated phthalocyanines (Pcs) which presents very interesting properties for photodynamic therapy (PDT). NPs were synthetized after slight modification of the reverse microemulsion method. The new materials presented high ability to generate singlet oxygen ($^1O_2$) after light irradiation. Thus, the *in vitro* photodynamic properties of phosphonate-Pc SNPs were determined using human bladder cancer epithelial cell line UM-UC-3. Obtained results could be very promising for cancer treatment in PDT.

Introduction

Silica materials are ‘‘generally recognized as safe’’ (GRAS) by the US Food and Drug Administration (FDA).[198] Together with facile silica nanoparticles’ preparation and broad range of their potential future applications, these new nanomaterials play an important role in current cancer research.

Cancer is one of the biggest health problem for humans. On nanomedicine, one of the therapies that has explored this concept is cancer PDT, an alternative method to the conventional cancer treatment options, including chemotherapy, radiotherapy and surgery.[199-202] This technique combines three components: drug, visible or near-infrared light and oxygen. None of them are toxic for the biological systems by its own. Only when the drug, called photosensitizer (PS) or photosensitizing agent, is in contact with molecular oxygen and exposed to proper light, can produce reactive oxygen species (ROS), which are strongly cytotoxic to the target cancer cells[132-135].

Based on the time of development and specific characteristics of PSs, they have been divided in three generations. The first generation PSs are the hematoporphyrins (Hp) to which belongs the first FDA approved PDT sensitizer, Photofrin® (porfimer sodium).[35] These first generation PSs are complex mixture of oligomers and their intensity of light absorption at the maximum wavelength is quite low. Second generation photosensitizers have lower skin phototoxicity, higher absorption in the red region of the visible spectrum and higher purity compare to their first generation precursors. They refers to porphyrins, chlorins, pheophorbides, bacteriopheophorbides, texaphyrins and phthalocyanines. A third generation PSs arose to improve selectivity, bioavailability and therapeutic properties of the previously mentioned PSs. They are first and second generation PSs conjugated to biomolecules, like proteins, peptides and also nanocarriers.[203]

Although this straightforward therapy was approved 20 years ago as a clinical protocol for cancer treatment,[204] there are still several limitations to use it as a general protocol to treat all cancer types. In the context of these limitations, nanoparticles (NPs) have recently emerged as promising vehicles for PDT.[38,136,137] Among others NPs, a number of applications of SNPs take advantage of their properties as protecting shells for sensitive compounds and magnetic cores.[152]

Pcs are synthetic porphyrin analogues, consisting of four isoindole units linked together through nitrogen atoms.[205] Very often Psc are hydrophobic species and undergo self-aggregation in aqueous solutions, which drastically reduces their photosensitizing efficiency. Nevertheless, Pcs can be conjugated to SNPs surface or encapsulated in the silica matrix, improving their photophysical properties, as recently described by Lei Ren *et al.*[106] They proved that the preparation of zinc Pc-loaded mesoporous silica nanoparticles (ZnPc-MSNPs) can help to maintain ZnPc molecules as a monomers and enhance PDT effect. ZnPc in monomeric state has higher production of $^1O_2$ thus acts as a better PS than in aggregate state.[106] After intravenous injection of these NPs in tumor-bearing mice followed by light exposure, these nanoplatforms exhibited great PDT efficacy. On the other hand, to avoid aggregation of ZnPc in aqueous environments, Zhao *et al.* [107] loaded ZnPc into the nanochannels of adamantane-functionalized MSNPs. To examine the PDT efficiency of this new nanomaterial, the MTT cell viability assay on HeLa cancer cell lines was performed. Comparing new NPs with free ZnPc in solution, more effective apoptosis effect by the hybrid after light irradiation was observed. These ZnPc loaded NPs exhibited stability in aqueous solution and low cytotoxicity in the dark. Additionally, the preparation of amorphous SNPs of mono-PEGylated ZnPc and its *in vitro* photodynamic activity was described by Dennis K. P. Ng *et al.*[109] The photodynamic activity of these systems toward HepG2 human hepatocarcinoma cells was studied with great success. These NPs were promising PDT agents, because of their uniform size, stability in aqueous media, high $^1O_2$ generation efficiency and high cellular uptake.

Nanovehicles could combine not only therapeutic effect but also other features crucial for cancer treatment. Hence, Ren *et al.* [110] combined distance-dependent metal-enhanced fluorescence (MEF) and metal-enhanced $^1O_2$ generation phenomenon by attaching tetra-substituted carboxyl phthalocyaninatealuminum(II) (AlC_4Pc) to silica-coated gold nanorods (AuNRs) core-shell nanoparticles. It was observed that the fluorescence intensity and $^1O_2$ generation varied with the thickness difference of silica shell. Thus, amorphous silica shell could serve as a spacer layer between the AuNRs and AlC_4Pc to get an optimum fluorescence enhancement effect. Moreover, thanks to silica matrix Zheng *et al.*[113] were able to fuse tree features: magnetic resonance imaging and fluorescence imaging, cell targeting and PDT. The core of the NPs was made from a single Fe_3O_4 NP encapsulated in fluorescent dyes co-doped nonporous silica. This core was covered by

ordered mesoporous silica containing PSs. Folic acid was used as fluorescence imaging agent which was covalently incorporated into the silica core. As PS, AlC_4Pc was chosen and it was covalently linked to mesoporous silica to avoid the degradation of PS in biological environments, and overcome their premature release. Again, these NPs presented much higher $^1O_2$ production than the same amount of free AlC_4Pc in solution which suggested that these nanovehicles act as nanoreactors to facilitate the photo-oxidation reaction. Juan L. Vivero-Escoto *et al.*[126] took the advantage of encapsulating and attaching drugs on SNPs surface which occurred with the development of multi drug delivery systems for combination chemotherapy and PDT by loading MSNPs with cisplatin and aluminum chloride Pc (AlClPc). The combination of both AlClPc and cisplatin compounds in the same MSNPs produced higher cytotoxic effect against human cervical cancer HeLa cells in comparison to the control MSNPs loaded with AlClPc and MSNPs loaded with cisplatin. This is another good example of SNPs which simultaneously carry PS and anticancer drug for combination PDT and chemotherapy to treat cancer. With this procedure they were able to enhance cancer therapy in the synergic anticancer effect of two active molecules in the same nanocarrier.

Encouraged by all examples of improving photophysical properties of Pcs by integrating PS with SNPs, we decided to combine amorphous SNPs with phosphonate-Pcs, previously described by some of us as novel anticancer agents for PDT.[206] Herein, Pc was encapsulated into SNPs or covalently attached to the surface of SNPs. As it was mentioned before one of the drawbacks of Pcs is their tendency to form aggregates in biological media. This aggregation phenomenon decreases the ROS production and thus phototoxicity. Encapsulation of Pc into SNPs or covalently attaching on the surface of SNPs could increase the specificity and the target release/accumulation of the PS. [39,40,151]

Results and discussion

Preparation of Pc

Phosphonate Pc was synthetized according to the procedure described by Venkatramaiah, N. *et al.*[206] in the literature. The synthetic route is presented below (**Figure 1**).

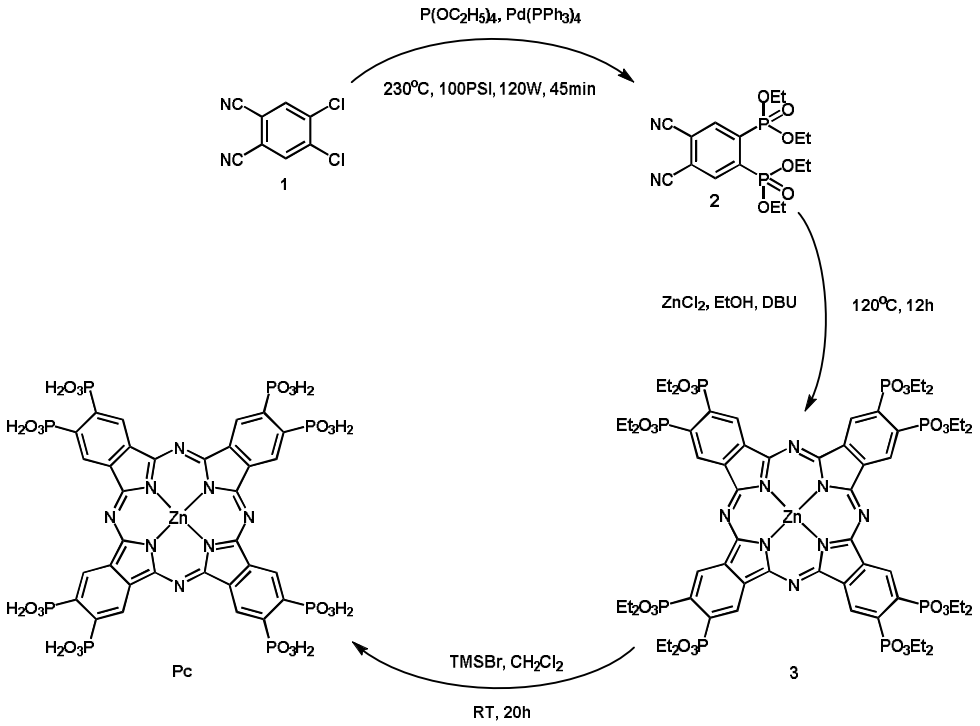

Figure 1. Synthetic route for the preparation of phosphonate-functionalized Pc (**Pc**).

First, 4,5-dichlorophthalonitrile (**1**) and triethylphosphite reacted under microwave conditions at 230 °C for 45 min in a palladium-catalyzed cross coupling reaction, yielding tetraethyl(4,5-dicyano-1,2-phenylene)bisphosphonate (**2**). Then, cyclotetramerization of **2** took place in a sealed glass tube under a nitrogen atmosphere with $ZnCl_2$, DBU and EtOH at 120 °C for 12 h. In the end, final green-coloured **Pc** was obtained after the hydrolysis of the protected octaphosphonate groups of Pc **3**, using for that trimethylsilyl bromide (TMSBr) in dry CH_2Cl_2 at room temperature.

Preparation and characterization of SNPs

SNPs (**NP-0, Figure 2**) were synthetized after slight modification of the reverse microemulsion method described by Aurélien Auger *et al.*[207] First, a quaternary microemulsion was prepared by mixing Triton X-100, 1-octanol and cyclohexane at RT. Then, water, NH_4OH and TEOS were added. The mixture was stirred for 24 h at RT and after that time ethanol was added to disrupt the inverse micelles. NPs were collected by centrifugation and washed with water and ethanol.

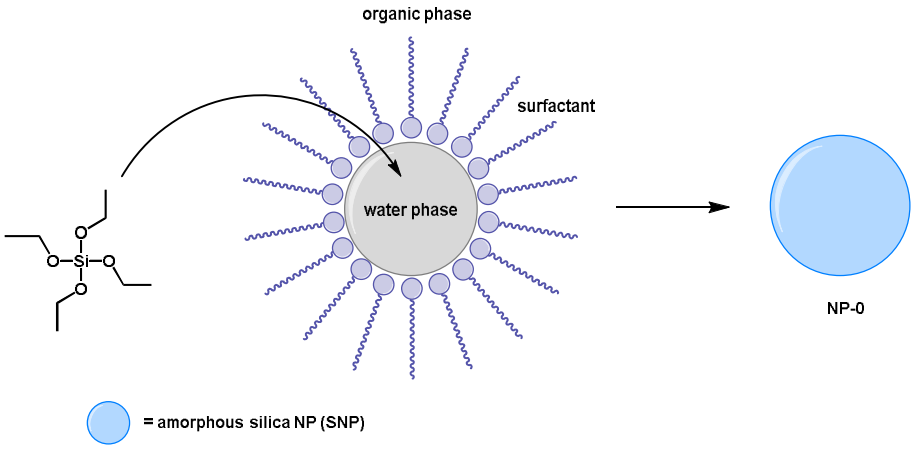

Figure 2. Schematic illustration of the preparation of SNPs (**NP-0**).

Next, **Pc** was encapsulated into SNPs (**NP-1** and **NP-2**, **Figure 3**) using the same method except that **Pc** was present in the reaction mixture. In case of **NP-1**, to the mixture of Triton X-100, 1-octanol and cyclohexane, the solution of **Pc** in water was added. In the end, NH_4OH and TEOS were added. On the other hand, **NP-2** were synthetized after slight modification of the above approach. The mixture of Triton X-100, 1-octanol and cyclohexane was first prepared in the same way and then the solution of **Pc** in the mixture of water and NH_4OH was added. In the last step, TEOS was added. The water/NH_4OH mixture promoted a better solubility of the **Pc** in the reaction mixture, enhancing the concentration of PS into final NPs.

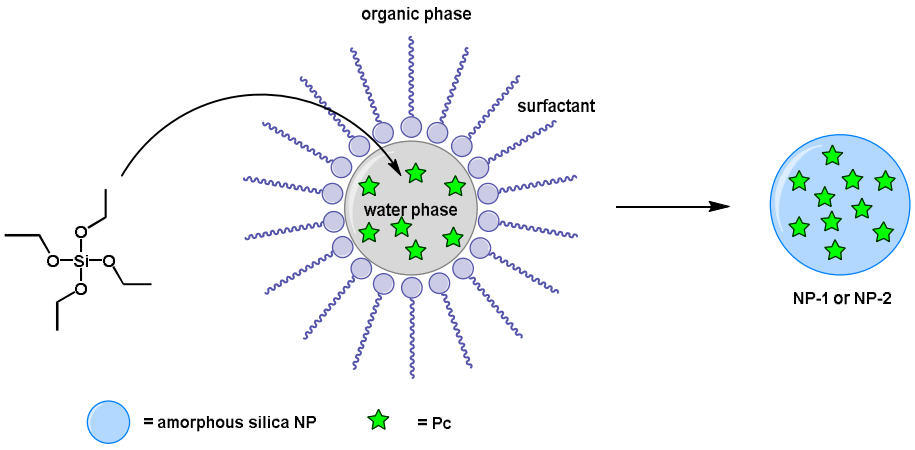

Figure 3. Schematic illustration of the preparation of **NP-1** and **NP-2**.

In the last case, phosphonate-Pc was covalently attached to the surface of SNPs (**NP-3**, **Figure 4**). These NPs were synthetized by combining solution of **Pc** in DMSO with **NP-0**

dispersed in 1,2,4-trichlorobenzene. The mixture was stirred for 24 h at 200 °C under nitrogen atmosphere and then NPs were collected by centrifugation and carefully washed. Having the covalent bond between **NP-0** and **Pc** could avoid premature leakage of PS in biological environment.

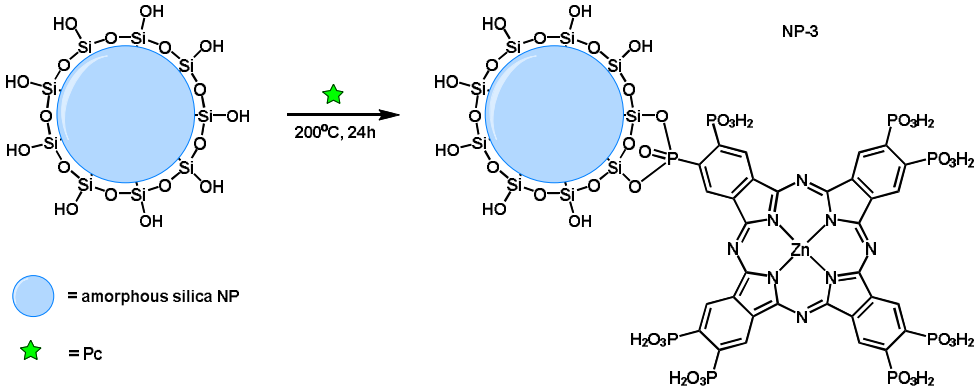

Figure 4. Schematic illustration of the hybrid **Pc**-SNP **NP-3**.

The average size of all NPs was measured by transmission electron microscopy (TEM) after drying the sample and dynamic light scattering (DLS) as a dispersion in water (**Figures SI 2-10**). The difference in particle sizes measured by TEM (**NP-0**, 35.14 ± 2.22 nm; **NP-1**, 35.67 ± 3.27 nm; **NP-2**, 36.92 ± 3.71 nm; 36.00 ± 1.88 nm) and DLS (**NP-0**, 56.65 nm; **NP-1**, 55.36 nm; **NP-2**, 55.23 nm; **NP-3**, 88.63 nm) presented the frequent difference between the size measured by TEM and the mean hydrodynamic diameter by DLS. Presented NPs are regular in terms of the size and shape and have uniform size distribution. Moreover, these NPs have very good size for passive targeting to tumor tissues.[170]

The UV-Vis absorption spectra of **NP-0**, **NP-1**, **NP-2** and **NP-3** were collected after dispersing, 0.150 mg of each NPs in 3 mL of EtOH (**Figure SI 11**). It is clear that **NP-1**, **NP-2** and **NP-3** show the typical broad bands of a free Pc. FT-IR spectra of **Pc** and all new NPs were also recorded (**Figure SI 12**) and proved the presence of PS in the SNPs.

The amount of encapsulated **Pc** inside SNPs or covalently attached to the SNPs was calculated by UV-Vis spectrophotometry. The final NPs were washed with the appropriate solvent until no typical Soret and Q bands were observed in the rinse solvent. **NP-1** (0.0874 µmol **Pc**/mg) and **NP-2** (0.0812 µmol **Pc**/mg) have almost the same concentration

of PS per mg of final material. The lower concentration of PS was observed for **NP-3** (0.0683 μmol **Pc**/mg).

Singlet oxygen generation study

In PDT treatment, when the PS is in contact with molecular oxygen and exposed to proper light it can produce ROS that are strongly cytotoxic to the cancer cells. Thus, after NPs' preparation and their full characterization an indirect chemical method was used to determined $^1O_2$ generation. As a quencher diphenylisobenzofuran (DPBF) with absorption maximum at 415 nm was employed. By measuring the DPBF absorption decay at this wavelength it was possible to follow the ability of the NPs to generate $^1O_2$. In $^1O_2$ study, the solutions contained **Pc 1** (0.5 μM), **NP-1** (0.5 mg, 14.57 μM of **Pc**), **NP-2** (0.5 mg, 13.53 μM of **Pc**) or **NP-3** (0.5 mg, 11.38 μM of **Pc**) were compared (**Figure 5**).

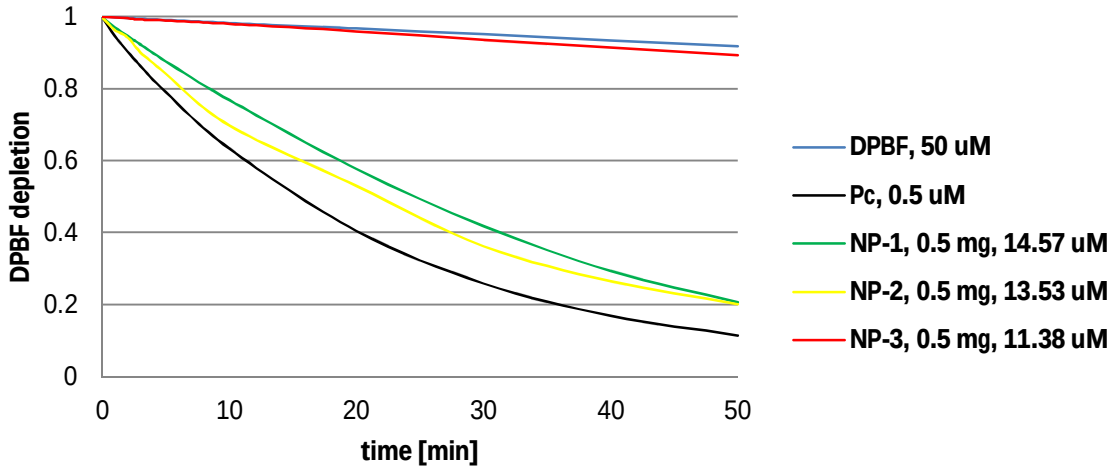

Figure 5. Photo-oxidation of DPBF (50 μM) in DMF:H_2O (9:1, by volume) with or without NPs (**NP-1**: 0.5 mg, 14.57 μM of **Pc**; **NP-2**: 0.5 mg, 13.53 μM of **Pc**, or **NP-3**: 0.5 mg, 11.38 μM of **Pc**) and **Pc** (0.5 μM), after irradiation with red light (620–750 nm) at a fluence rate of 10 mW/cm^2 for different periods of time (0-50 min). The DPBF absorbance was recorded at 415 nm. Each point represents the mean of at least three independent experiments, and has a standard deviation lower than 3%.

From the above graph it is clearly visible that both NPs, **NP-1** and **NP-2** are producing almost the same amount of singlet oxygen. **NP-3** are generating very small amount of $^1O_2$. This may be explained by the fact that these NPs have the tendency to aggregate in the

water-based solution what was observed during DLS measurement. The difference in **NP-3** sizes measured by TEM (36.00 ± 1.88 nm) and DLS (88.63 nm) showed not only the common difference between the mean hydrodynamic diameter and the size measured by TEM but also the predisposition to form small aggregates. These aggregates could make difficulties for oxygen and $^1O_2$ to travel freely in the experimental environment.

It is also very important to point out the different morphologies of the NPs used in the $^1O_2$ tests. **NP-1** and **NP-2** do not have any covalent bonds between SNPs and **Pc** thus PS could be released during experiments. On the contrary, **Pc** is permanently attached to SNPs through covalent bond in **NP-3**.

It was crucial to check the release of **Pc** from all phosphonate-Pc SNPs (**Figure 6**). The conditions of experiment were the same as for $^1O_2$ generation study, but under dark. The **Pc** release was determined by following the absorbance spectra after gentle stirring at ambient temperature. The results were displayed as follows: *Pc release [%] = Absorbance at given time (Abs_t)/ initial Absorbance (Abs_0).*

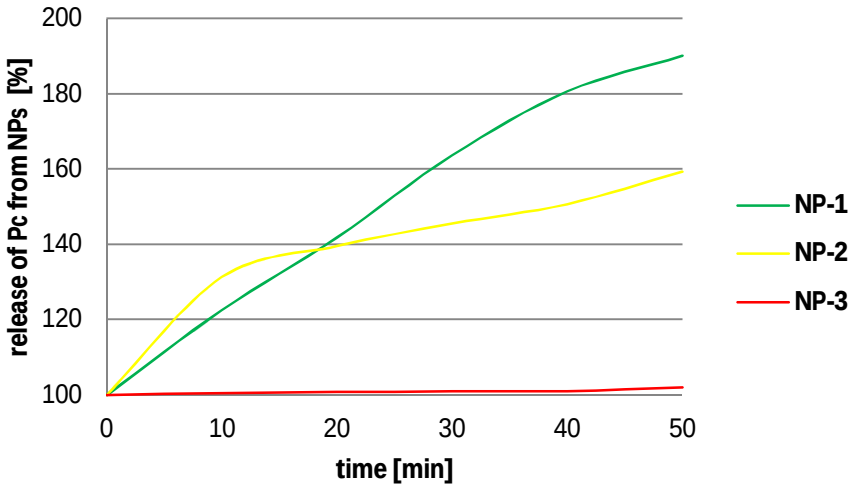

Figure 6. Release of **Pc** from NPs in DMF:H_2O (9:1, by volume) after gentle stirring in the dark at ambient temperature for different periods of time (0-50 min). The results are presented in percentage calculated by the ratio of residual absorbance 680 nm (Abs of **Pc**) at different periods of time and initial absorbance. Each point represents the mean of at least three independent experiments, and has a standard deviation lower than 3%.

Figure 6 shows that **Pc** was slowly released from **NP-1** and **NP-2** but not from **NP-3**. This could explain the high production of $^1O_2$ by **NP-1** and **NP-2**. It is important to remember that small production of $^1O_2$ by **NP-3** is not only due to the absence of Pc release but most probably because of NPs' aggregates were formed during experiment. The high ability of these new hybrid NPs to generate $^1O_2$ after light irradiation lead us to determine their photocytotoxicity in human bladder cancer cells.

In vitro studies

In vitro studies were carried out into UM-UC-3 cancer cell line. Previous studies have demonstrated that this **Pc**, containing phosphonic acid groups, exhibit dual anticancer functionality, inhibiting the urokinase plasminogen activator and efficiently generating $^1O_2$ inducing (photo)toxicity on human bladder cancer epithelial cells UM-UC-3.[206]

Cellular uptake of PS and its nanoformulations

Preliminary uptake studies were performed with **NP-1**, **NP-2**, **NP-3** (**Figure 7**) and free **Pc**. Bladder cancer cells were incubated in darkness with increasing concentrations of PS (0-25 µM) for 2 h and with NPs (**NP-1**: 0-0.01 mg/mL, 0-0.874 µM of **Pc**; **NP-2**: 0-0.01 mg/mL, 0-0.812 µM of **Pc**; **NP-3**: 0-0.01 mg/mL, 0-0.683µM of **Pc**) prepared in RPMI medium, maximum 0.5% DMSO v/v) overnight.

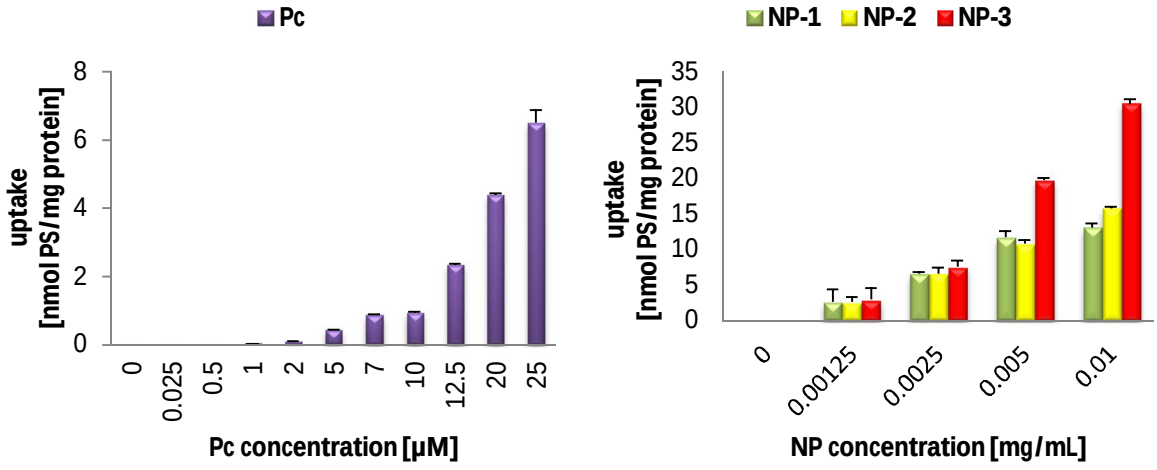

Figure 7. Intracellular 2 h uptake of free **Pc** (0-25 µM),[206] and overnight uptake of **NP-1**, (0-0.01 mg/mL, 0-0.874 µM of **Pc** in RPMI medium), **NP-2** (0-0.01 mg/mL, 0-0.812 µM of **Pc** in RPMI medium), **NP-3** (0-0.01 mg/mL, 0-0.683µM of **Pc** in RPMI medium) by

UM-UC-3 bladder cancer cells. Data are means ± s.e.m. of at least three independent experiments performed in triplicates.

When the cells were incubated overnight with RPMI medium containing NPs solutions there was uptake dependent on the concentration of the NPs. In all cases NPs presented higher uptake than free **Pc**. This could be due to the tendency of particles of certain size to accumulate in tumor tissue much more than they do in normal tissue which is called enhanced permeability and retention effect. Although **NP-1** (0.0874 µmol **Pc**/mg) and **NP-2** (0.0812 µmol **Pc**/mg) have almost the same concentration of PS per mg of final material, **NP-2** presented higher uptake than **NP-1**. Interestingly, the lowest concentration of PS in **NP-3** (0.0683µmol **Pc**/mg) not interfered with the highest uptake of **NP-3** among all new materials tested. The uptake of **NP-3** was about two times highest than **NP-1** and **NP-2**. In **NP-3**, **Pc** is permanently attached to the SNPs through covalent bonds and is located on the surface of NPs. Presence of **Pc** on the surface of SNPs could enhance cellular uptake of **NP-3**. It was already proven that presence of phosphonic acid groups in the periphery of Pc (**Pc**, **Figure 1**) rather than protected groups in octaphosphonate Pc (**3**, **Figure 1**) could increase its accumulation inside bladder cancer cells with consequently higher phototoxicity.[206]

Dark toxicity and phototoxicity

The dark toxicity of **Pc**, **NP-0**, **NP-1**, **NP-2** or **NP-3** in UM-UC-3 bladder cancer cells was evaluated using the well-known MTT assay (**Figure SI 13**). MTT assay is a colorimetric assay which use the ability of living bladder cancer cells to reduce yellow 3-[4,5-dimethylthiazol-2-yl]-2,5-diphenyl-tetrazolium bromide (MTT), to a purple formazan. After overnight incubation of cancer cells (in dark) with NPs (**NP-1**: 0-0.01 mg/mL, 0-0.874 µM of **Pc**; **NP-2**: 0-0.01 mg/mL, 0-0.812 µM of **Pc**; **NP-3**: 0-0.01 mg/mL, 0-0.683µM of **Pc**) in RPMI medium or 2 h incubation with PS (0-25 µM in PBS buffer), none of the PS or new NPs induced dark toxicity in cancer cells (**Figure SI 13**). Non-dark toxicity is crucial in the PDT concept in which the therapeutic drug has to have no toxicity until it is activated by light.

After confirming the uptake and non-dark toxicity of **Pc** and their new NP formulations in UM-UC-3 bladder cancer cells, their toxicity after light irradiation was evaluated using the

MTT assay (**Figure 8**). UM-UC-3 bladder cancer cells were incubated for 2 h with **Pc** (0-25 µM in PBS buffer) or overnight with NPs (0-20 µM in RPMI medium) and then irradiated with an optical fiber emitting white light for 40 min (12 mW/cm^2). No cytotoxicity was observed in the untreated (cells incubated in the absence of NP) sham irradiated cells.

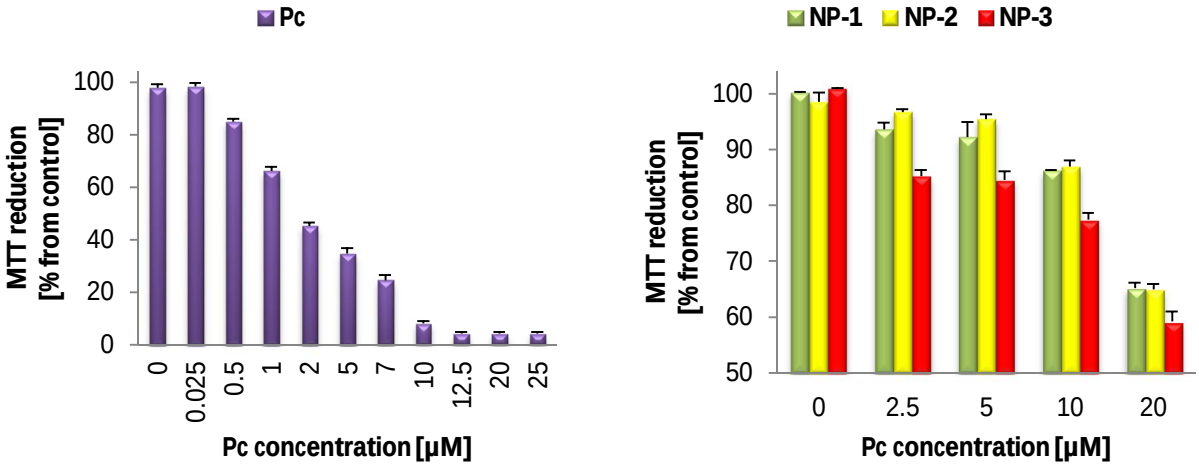

Figure 8. Phototoxicity of **Pc** (0-25 µM)[206] and **NP-1**, **NP-2**, **NP-3** (0-20 µM of **Pc**) determined 24 h after PDT treatment using the MTT assay. The percentage of cytotoxicity was calculated relatively to control cells (cells incubated with RPMI medium and then irradiated). Data are means ± s.e.m. of at least three independent experiments performed in triplicates.

Phototoxicity of **Pc** determined after PDT treatment was higher compared with corresponding NP formulations. **NP-0** do not present any phototoxicity against cancer cells (**Figure SI 14**). Other NPs induced photoxicity in UM-UC-3 bladder cancer cells in a concentration-dependent manner. MTT assay showed that after PDT treatment phototoxicity of **NP-1** and **NP-2** was almost the same. Remembering outcome from singlet oxygen generation studies (**Figure 5**) and cellular uptake studies (**Figure 7**), this result was not surprising. Maybe in UM-UC-3 bladder cancer cells resistant to therapy, a second light irradiation treatment could enhanced *in vitro* photodynamic efficacy as it was described before.[174] In the period between single and repeated irradiation NPs could accumulate in cancer cells which could enhanced phototoxicity in UM-UC-3 cancer cells.

Remarkable, **NP-3** led to a significantly higher phototoxicity on UM-UC-3 cells compared to **NP-1** and **NP-2**. Although in $^1O_2$ generation studies these NPs produced very poor amount of $^1O_2$, in biological condition they appeared as the most efficient among all tested NPs. The reason of this result could be because the uptake of these NPs was higher due to the presence of **Pc** on the surface of NPs compare to the **NP-1** and **NP-2** (**Figure 7**). Also during $^1O_2$ generation studies the NPs were dispersed into the mixture of DMF:H_2O (9:1, by volume). This could cause the aggregation of **NP-3** because of the presence of **Pc** on the surface of SNPs. In UM-UC-3 cells the environment was different and it could enhance the NPs internalization into the target organelles.

Conclusions

In summary, novel NPs encapsulating **Pc** (**NP-1**, **NP-2**) or covalently appended **Pc** (**NP-3**) were prepared and evaluated as photoactive nanoformulations in cancer PDT. These NPs had uniform size distribution and were regular in terms of size and shape with a very good size for passive targeting to tumor tissues. $^1O_2$ generation studies showed that **NP-1** and **NP-2** are producing almost the same amount of $^1O_2$ whereas **NP-3** were generating poor amount of $^1O_2$. *In vitro* studies were carried out in UM-UC-3 cancer cell line. After incubation of cancer cells (in dark) with NPs or PS, none of the PS or new NPs induced dark toxicity in UM-UC-3 cancer cells. The uptake of **NP-3** in these cells was about two times higher than **NP-1** and **NP-2**. In **NP-3**, the cellular uptake could be enhance by presence of **Pc** on the surface of NPs. In the last experiment **NP-3** led to a significantly higher phototoxicity on UM-UC-3 cells compared to **NP-1** and **NP-2**. Even though these new nanocarriers had lower pototoxicity efficiency compered to non-immobilized **Pc**, they offer an alternative route to enhance PDT by their surface modification to get even higher selectivity/recognition and uptake by cancer cells. The discussed studies showed that these NPs could be used as efficient nanoplatform agents for cancer PDT. Further advances towards *in vitro* and *in vivo* protocols to increase therapeutic efficacy of PDT treatments are strongly encouraged.

Acknowledgements

Thanks are due to FCT/MEC for the financial support to QOPNA (FCT UID/QUI/00062/2013), CICECO-Aveiro Institute of Materials (FCT UID/CTM/50011/2013), IBILI (FCT UID/NEU/04539/2013) and CQE (FCT UID/QUI/0100/2013) research units, through national funds and where applicable cofinanced by the

FEDER, within the PT2020 Partnership Agreement. The work was also supported by the Spanish MINECO (CTQ-2014-52869-P), Comunidad de Madrid (FOTOCARBON, S2013/MIT-2841) and Portuguese COMPETE (POCI-01-0145-FEDER-007440). We further wish to thank the Seventh Framework Programme (FP7-People-2012-ITN) for funding the SO2S project (grant agreement number: 316975).

Supplementary Information

Silica nanoformulations of phosphonated-phthalocyanines as novel anticancer agents for photodynamic therapy

Experimental section

General methods

Absorption spectra were recorded using a Shimadzu UV-2501-PC. FT-IR spectra were recorded in KBr pellets using Spectrophotometer Bruker IFS 66V. The irradiation system used to determine the production of $^1O_2$ and the phototoxicity during *in vitro* experiments was a Lumacare source, model LC-122, consisting on a 250 W halogen lamp coupled to an optical fiber (with a cutoff filter for wavelengths <540 nm). The fluence rate was measured with an energy meter (Coherent Field MaxII-Top) combined with a Coherent Power Sens PS19Q energy sensor. The Dynamic light scattering (DLS) measurements were taken by Zetasizer Nano ZS from Malvern Instruments. Transmission electron microscopy (TEM) images were obtained using a Hitachi H-9000 transmission electron microscope operating at an acceleration voltage of 300 kV and JEOL 2200FS transmission electronmicroscope operating at an acceleration voltage of 200 kV.

All reagents were obtained from commercial sources and were used without further purification steps. Analytical thin layer chromatography (TLC) was carried out on pre-coated silica gel sheets (Merck, 60, 0.2 mm).

Synthesis of Pc

Pc was synthetized according to procedure described by Venkatramaiah, N. *et al.*[206]

Preparation of NPs

Preparation of NP-0

NPs were synthetized after slight modification of the reverse microemulsion method described by Aurélien Auger *et al.*[207] First, a quaternary microemulsion was prepared by

mixing Triton X-100 (4.2 mL), 1-octanol (4.0 mL) and cyclohexane (18.8 mL) at RT. Then, water (1.2 mL), NH_4OH (25%, 0.240 mL) and TEOS (0.250 mL) were added. The mixture was stirred for 24 h at RT and after that time ethanol (100 mL) was added to disrupted the inverse micelles. NPs were collected by centrifugation and washed with water and ethanol.

Preparation of NP-1

NPs were synthetized after slight modification of the reverse microemulsion method described by Auger A. *et al.*[207] First, a quaternary microemulsion was prepared by mixing Triton X-100 (2.1 mL), 1-octanol (2.0 mL) and cyclohexane (9.4 mL) at RT. Then, the solution of **Pc** (5.6 mg) in water (0.600 mL) was added. In the end, NH_4OH (25%, 0.120 mL) and TEOS (0.125 mL) were added. The mixture was stirred for 24 h at RT and after that time ethanol (100 mL) was added to disrupted the inverse micelles. NPs were collected by centrifugation and washed with water and ethanol.

Preparation of NP-2

NPs were synthetized after slight modification of the reverse microemulsion method described by Auger A. *et al.*[207] First, a quaternary microemulsion was prepared by mixing Triton X-100 (2.1 mL), 1-octanol (2.0 mL) and cyclohexane (9.4 mL) at RT. Then, the solution of **Pc** (5.6 mg) in water (0.600 mL) and NH_4OH (25%, 0.120 mL) was added. In the last step TEOS (0.125 mL) was added. The mixture was stirred for 24 h at RT and after that time ethanol (100 mL) was added to disrupted the inverse micelles. NPs were collected by centrifugation and washed with water and ethanol.

Preparation of NP-3

NPs were synthetized by combining solution of **Pc** (1 mg) in DMSO (0.500 mL) with SNPs (**NP-0**, 10 mg) dispersed in 1,2,4-trichlorobenzene (1.2 mL). The mixture was stirred for 24 h at 200 °C under nitrogen atmosphere. After that time NPs were collected by centrifugation and washed with DMSO, water and ethanol.

Singlet oxygen generation study

Singlet oxygen ($^1O_2$) was determined by a chemical method using 1,3-diphenylisobenzofuran (DPBF). DPBF has an absorption maximum at 415 nm, thus it is possible to follow the ability of the NPs to generate $^1O_2$ by measuring the DPBF absorption decay, at this wavelength. The solutions were irradiated at RT and under magnetic stirring, with optical fiber (with a cutoff filter for wavelengths <540 nm) at a fluence rate of 10 mW/cm^2.

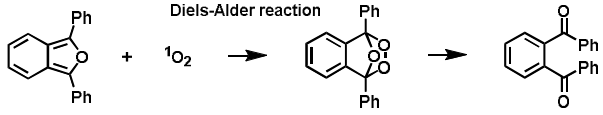

Figure SI 1. Reaction of DPBF with $^1O_2$.

Pc (0.5 μM), **NP-1** (0.5 mg, 14.57 μM of **Pc**), **NP-2** (0.5 mg, 13.53 μM of **Pc**) or **NP-3** (0.5 mg, 11.38 μM of **Pc**) were placed into 3 mL cuvette which contained solution of DMF:H_2O (9:1, by volume). Then, DPBF (50 μM) in solution of DMF:H_2O was added (total volume in cuvette 3 mL). The final solutions were irradiated at RT and under gentle magnetic stirring, with optical fiber (with a cut off filter for wavelengths <540 nm) at a fluence rate of 10 mW/cm^2 for different periods of time (0-50 min). The breakdown of DPBF was monitored by measuring the decrease in absorbance at 415 nm at pre-established irradiation intervals. The results were expressed by plotting the DPBF depletion against the irradiation time. The depletion of DPBF was calculated as follows:

DPBF depletion = Absorbance at given time of irradiation (Abs_t)/ Absorbance before irradiation (Abs_0)

Release of Pc from NPs

The release of the phosphonate phthalocyanine **Pc** from NPs was determined by following its absorbance spectra after gentle stirring in the dark at ambient temperature. In all experiments, 0.5 mg of NPs (**NP-1**, **NP-2**, **NP-3**) were dispersed in 3 mL of DMF:H_2O (9:1, by volume). The dispersions were placed into cuvettes and were stirred in the dark room during 50 min. The results were calculated as follows:

Photostability [%] = Absorbance at given time (Abs_t)/ initial Absorbance (Abs_0)

Characterization of NPs

Size of NPs form TEM and DLS

NP name	Average size of NPs calculated in ImageJ form TEM images [nm]*	Average size of NPs from DLS measurement [nm]
NP-0	35.14 ± 2.22	56.65
NP-1	35.67 ± 3.27	55.36
NP-2	36.92 ± 3.71	55.23
NP-3	36.00 ± 1.88	88.63

Figure SI 2. Size of NPs form TEM and DLS. *****Information on mean size and standard deviation was calculated from measuring more than 100 nanoparticles in random fields of TEM grids.

TEM

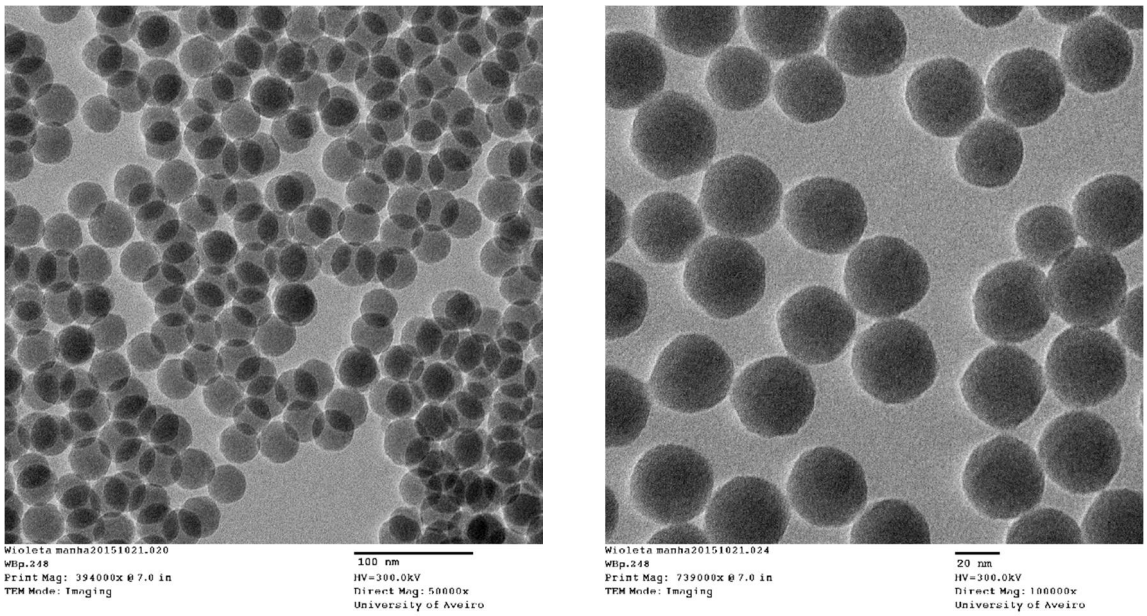

Figure SI 3. TEM images of **NP-0**.

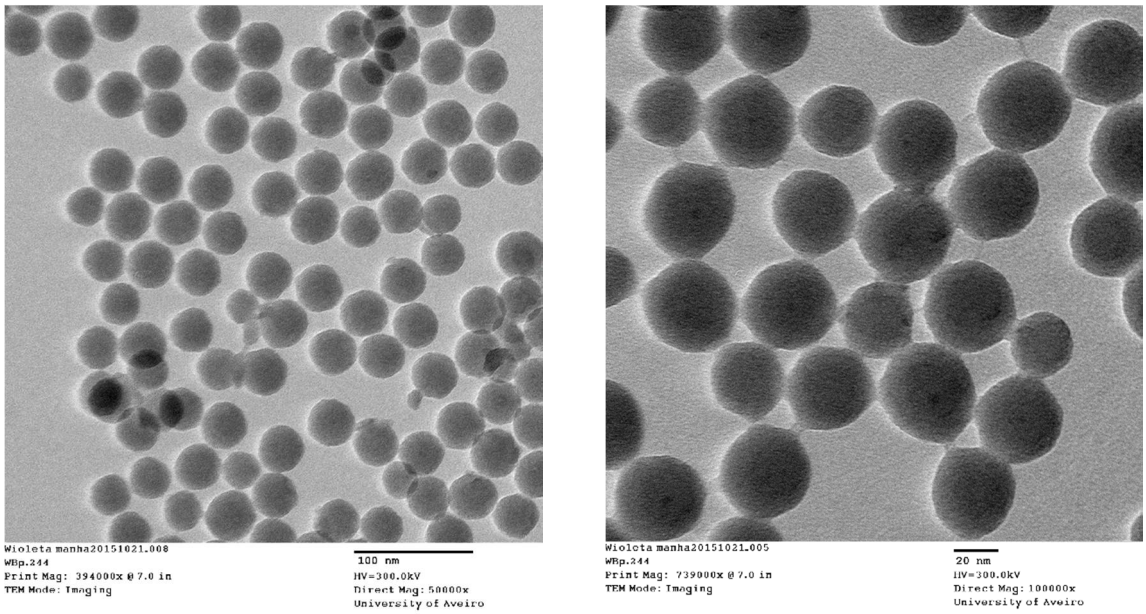

Figure SI 4. TEM images of **NP-1**.

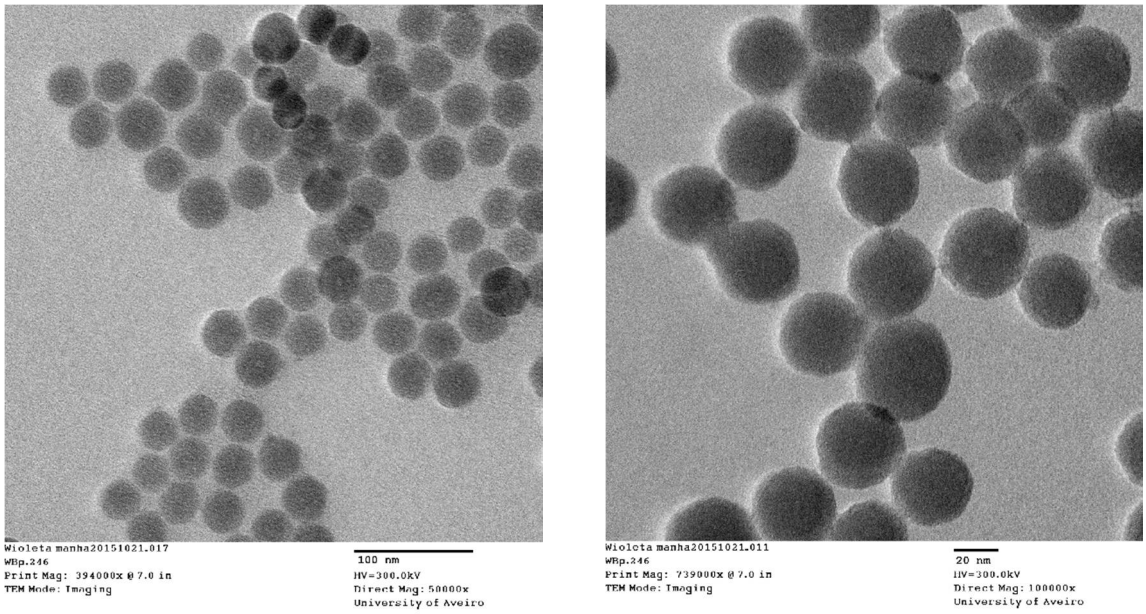

Figure SI 5. TEM images of **NP-2**.

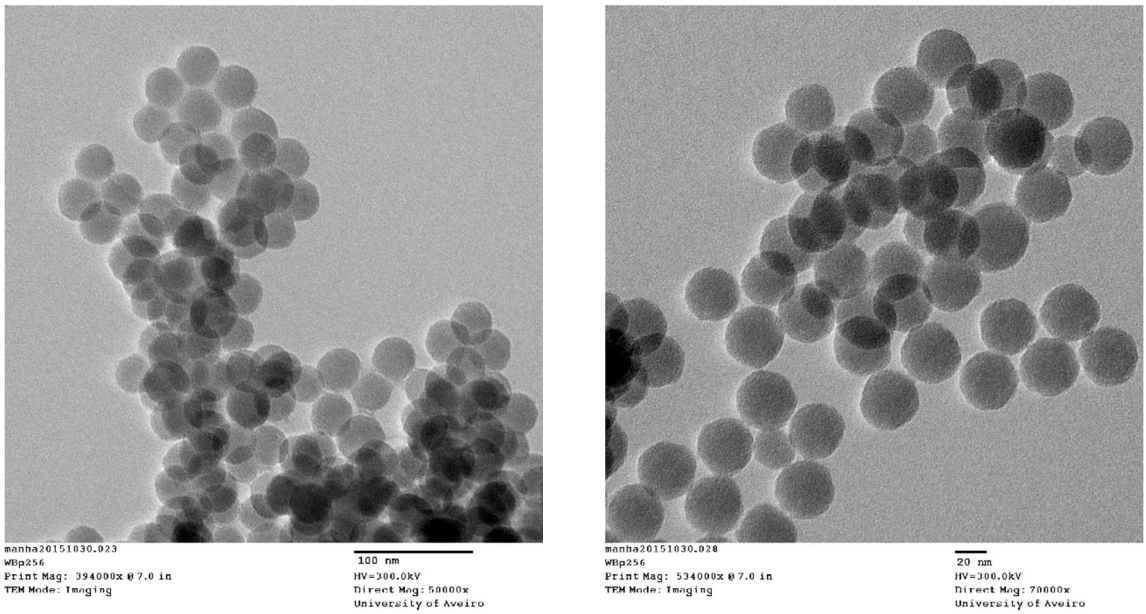

Figure SI 6. TEM images of **NP-3**.

DLS

			Size (d.n...	% Number:	St Dev (d.n...
Z-Average (d.nm):	137.6	Peak 1:	56.65	100.0	17.01
PdI:	0.460	Peak 2:	0.000	0.0	0.000
Intercept:	0.944	Peak 3:	0.000	0.0	0.000
Result quality	Good				

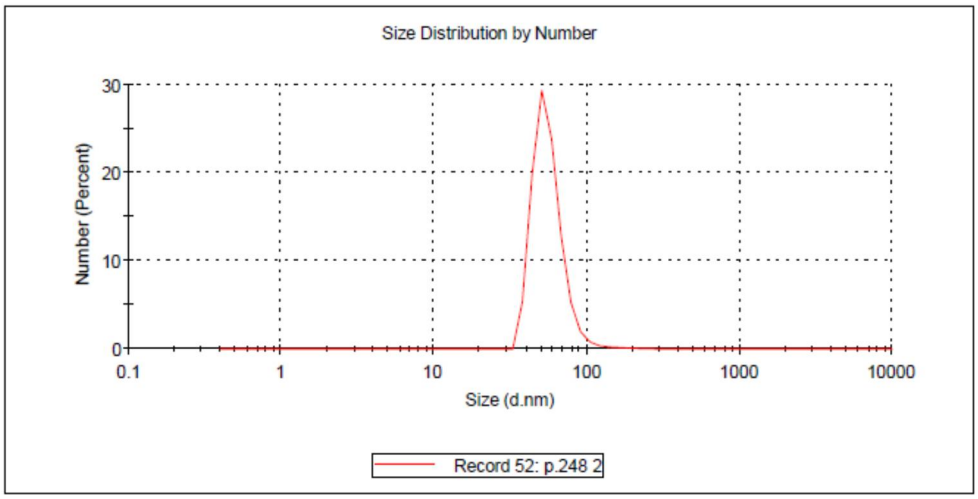

Figure SI 7. DLS size distribution of **NP-0** in water.

		Size (d.n...	% Number:	St Dev (d.n...
Z-Average (d.nm): 183.5	Peak 1:	55.36	100.0	19.07
PdI: 0.418	Peak 2:	0.000	0.0	0.000
Intercept: 0.879	Peak 3:	0.000	0.0	0.000

Result quality Good

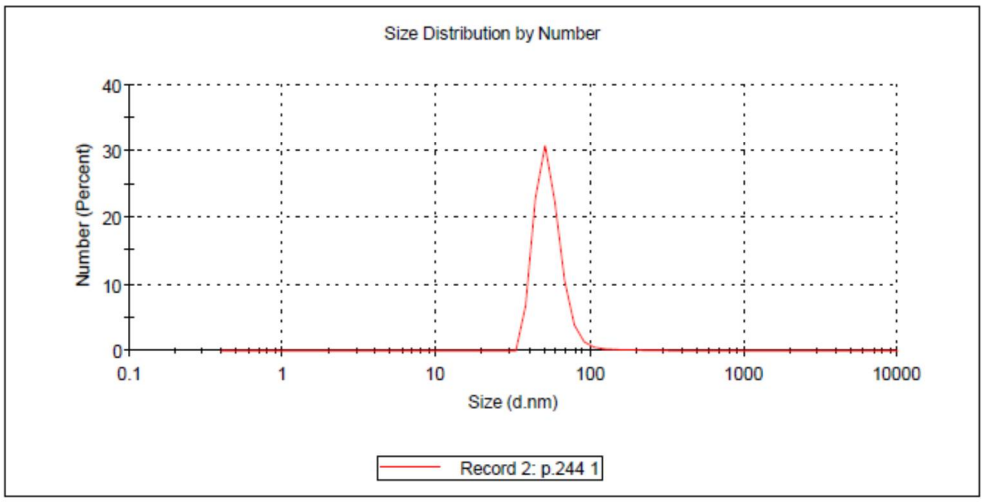

Figure SI 8. DLS size distribution of **NP-1** in water.

		Size (d.n...	% Number:	St Dev (d.n...
Z-Average (d.nm): 160.2	Peak 1:	55.23	100.0	17.15
PdI: 0.389	Peak 2:	757.2	0.0	214.4
Intercept: 0.942	Peak 3:	0.000	0.0	0.000

Result quality Good

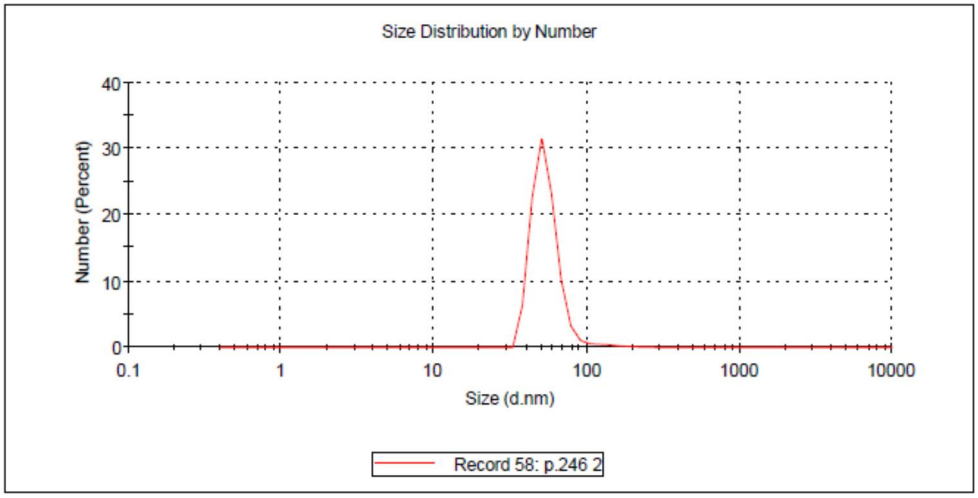

Figure SI 9. DLS size distribution of **NP-2** in water.

		Size (d.n...	% Number:	St Dev (d.n...
Z-Average (d.nm): 153.6	Peak 1:	88.63	99.2	20.23
PdI: 0.437	Peak 2:	305.9	0.8	65.51
Intercept: 0.958	Peak 3:	0.000	0.0	0.000
Result quality Good				

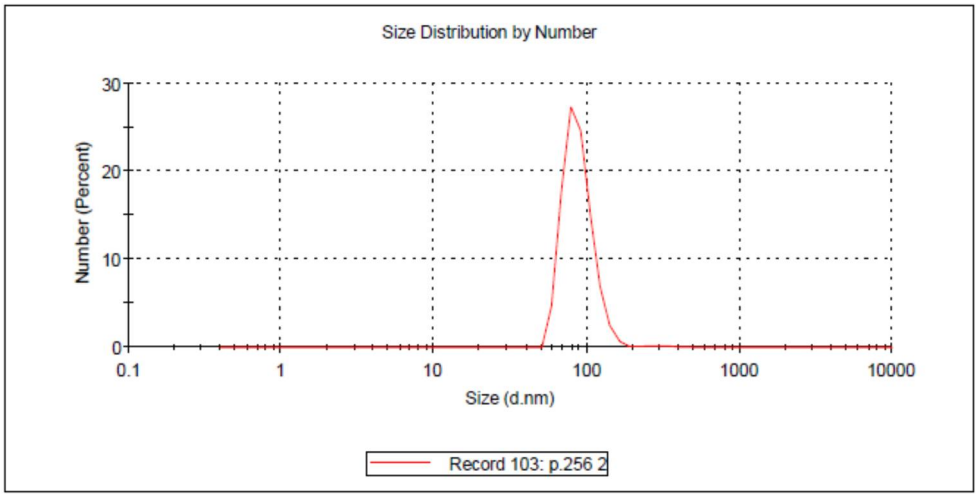

Figure SI 10. DLS size distribution of **NP-3** in water.

UV-Vis

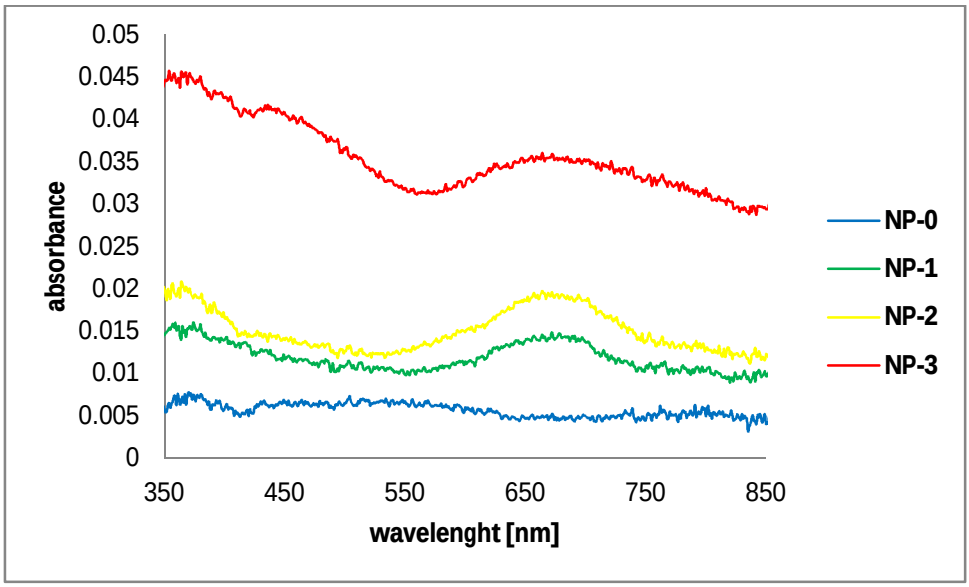

Figure SI 11. UV-Vis absorption spectra of all new NPs in EtOH. UV-Vis absorption spectra were collected after dispersion of 0.150 mg of NPs in 3 mL of EtOH.

FT-IR

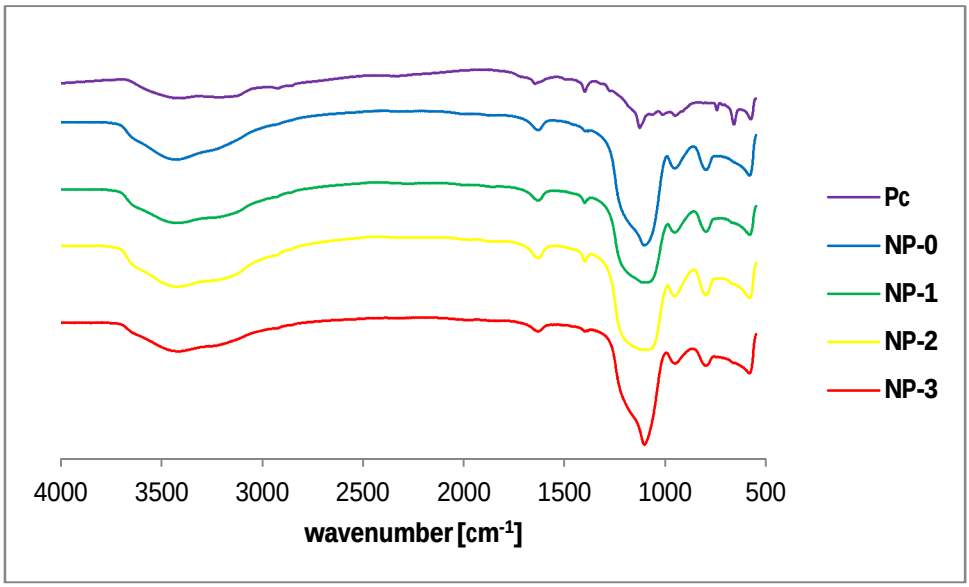

Figure SI 12. FT-IR spectra of **Pc** and all new NPs.

In vitro assays

Cells culture

Human bladder cancer cell line UM-UC-3 derived from high-grade transitional cell carcinoma was obtained from the American Type Culture Collection (ATCC®, Manassas, VA, USA). Cells were cultured in Roswell Park Memorial Institute (RPMI)-1640 medium (Sigma) supplemented with 2 $g.L^{-1}$ sodium bicarbonate (Sigma), 2 mM L-glutamine (Sigma), 10% (v/v) of heat-inactivated Fetal Bovine Serum (FBS; Life Technologies, Carlsbad, CA, USA) and antibiotic/antimicotic containing 100 units.mL-1 penicillin, 100 µg.mL-1 streptomycin and 0.25 µg.mL-1 amphotericin B (Sigma). UM-UC-3 cells were seeded at a density of 1.5 x 104 in 96-well culture plates (Orange Scientific, Braine-l'Alleud, Belgium). 24 hours after plating, cells were overnight incubated with different concentrations of NPs (0-0.010 mg/mL or 0-20 µM) in the dark.

Cellular uptake of NPs

After incubation with NPs in the dark, UM-UC-3 cells were washed with PBS buffer and mechanically scrapped in 1% (m/v) sodium dodecyl sulfate (SDS; Sigma) in PBS buffer at pH 7.0. NPs intracellular concentration was determined by spectrofluorimetry using a

Typhoon FLA 9000 imager (GE Healthcare) with a 100-µm spot resolution and 300 V. The excitation and emission wavelengths were set at 635 nm (red LD laser) and LPR (665LP). The results were normalized for protein concentration (determined by bicinchoninic acid reagent; Pierce, Rockford, IL, USA).

PDT treatments on cells

Photodynamic irradiation was carried out in fresh culture medium, in the absence of NPs, covering UM-UC-3 cell monolayers with RPMI medium and exposing them to red light delivered by the illumination system LC-122 LumaCare at 12 mW/cm^{-2} for 40 min. As a control, sham-irradiated cells were used. These cells were kept in the dark for the same durations and under the same conditions as the irradiated cells. In all trials, triplicate wells were settled under each experimental condition, and each experiment was repeated at least three times.

MTT assay

MTT assay was used to determine cell metabolic activity after NPs incubation in the dark, irradiation, or both after 24 h treatments. This colorimetric assay is measuring the ability of bladder cancer cells to reduce yellow 3-[4,5-dimethylthiazol-2-yl]-2,5-diphenyl-tetrazolium bromide (MTT, Sigma), to a purple formazan on a microplate reader (Synergy HT). The results are expressed in percentage of control (i.e. optical density of formazan from cells not exposed to NPs).

Dark toxicity studies of Pc, NP-0, NP-1, NP-2 and NP-3

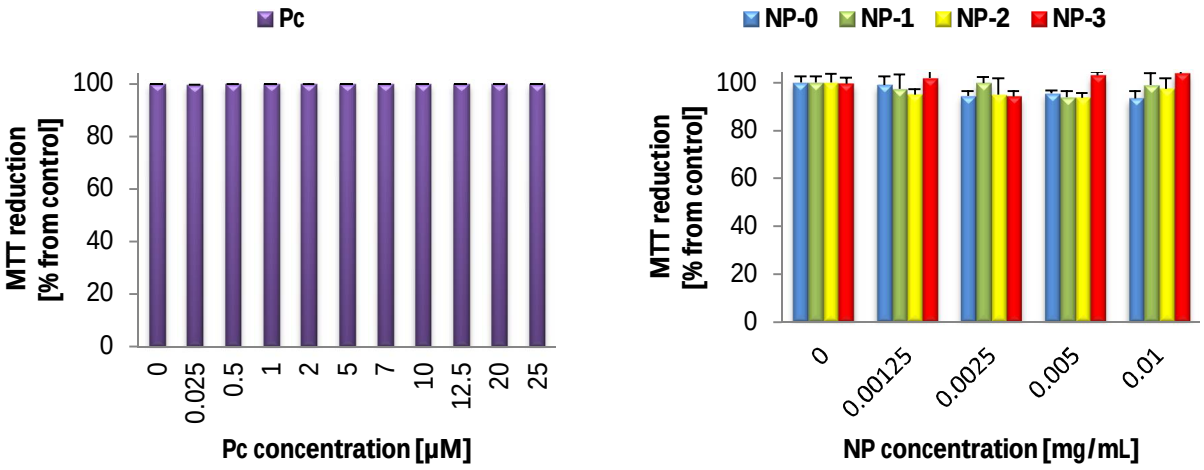

Figure SI 13. Non-dark toxicity of **Pc** (0-25 µM)[206] and **NP-0** (0-0.01 mg/mL, 0 µM of **Pc**), **NP-1** (0-0.01 mg/mL, 0-0.874 µM of **Pc**), **NP-2** (0-0.01 mg/mL, 0-0.812 µM of **Pc**), **NP-3** (0-0.01 mg/mL, 0-0.683µM of **Pc**) determined 24 h after treatment using the MTT assay. The percentage of cytotoxicity was calculated relatively to control cells (cells incubated with RPMI medium). Data are means ± s.e.m. of at least three independent experiments performed in triplicates.

Phototoxicity studies of NP-0

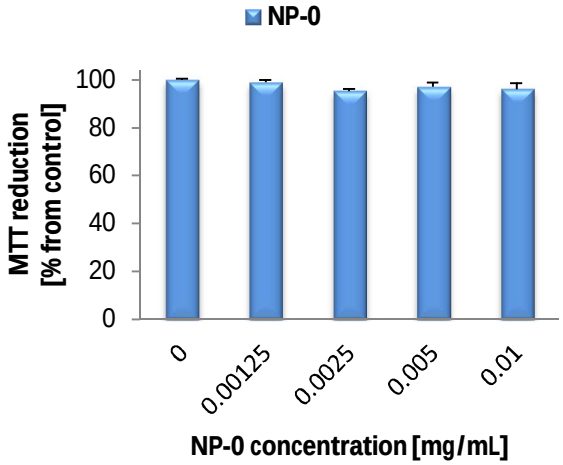

Figure SI 14. Phototoxicity of **NP-0** (0-0.01 mg/mL) determined 24 h after PDT treatment using the MTT assay. The percentage of cytotoxicity was calculated relatively to control

cells (cells incubated with medium and then irradiated). Data are means ± s.e.m. of at least three independent experiments performed in triplicates.

References

(1) Siegel, R.; Naishadham, D.; Jemal, A. *CA Cancer J Clin.* **2013**, *63*, 11.

(2) Silva, S.; Pereira, P. M. R.; Silva, P.; Paz, F. A. A.; Faustino, M. A. F.; Cavaleiro, J. A. S.; Tome, J. P. C. *Chem. Commun.* **2012**, *48*, 3608.

(3) Lourenco, L. M.; Pereira, P. M.; Maciel, E.; Valega, M.; Domingues, F. M.; Domingues, M. R.; Neves, M. G.; Cavaleiro, J. A.; Fernandes, R.; Tome, J. P. *Chem. Commun.* **2014**, *50*, 8363.

(4) Nyst, H. J.; Tan, I. B.; Stewart, F. A.; Balm, A. J. M. *Photodiagn. Photodyn. Ther.* **2009**, *6*, 3.

(5) Wolf, P.; Rieger, E.; Kerl, H. *J. Am. Acad. Dermatol.* **1993**, *28*, 17.

(6) Bonnett, R. *Chem. Soc. Rev.* **1995**, *24*, 19.

(7) Henderson, B. W.; Dougherty, T. J. *Photochem. Photobiol.* **1992**, *55*, 145.

(8) Dolmans, D. E. J. G. J.; Fukumura, D.; Jain, R. K. *Nat. Rev. Cancer* **2003**, *3*, 380.

(9) Macdonald, I. J.; Dougherty, T. J. *J. Porphyrins Phthalocyanines* **2001**, *05*, 105.

(10) Sternberg, E. D.; Dolphin, D.; Brückner, C. *Tetrahedron* **1998**, *54*, 4151.

(11) O'Connor, A. E.; Gallagher, W. M.; Byrne, A. T. *Photochem. Photobiol.* **2009**, *85*, 1053.

(12) Hao, E.; Jensen, T. J.; Vicente, M. G. H. *J. Porphyrins Phthalocyanines* **2009**, *13*, 51.

(13) Pereira, P. M.; Korsak, B.; Sarmento, B.; Schneider, R. J.; Fernandes, R.; Tome, J. P. *Org. Biomol. Chem.* **2015**, *13*, 2518.

(14) Ma, L.; Moan, J.; Berg, K. *Int. J. Cancer* **1994**, *57*, 883.

(15) Kostenich, G. A.; Zhuravkin, I. N.; Zhavrid, E. A. *J. Photochem. Photobiol., B* **1994**, *22*, 211.

(16) Ris, H. B.; Altermatt, H. J.; Inderbitzi, R.; Hess, R.; Nachbur, B.; Stewart, J. C.; Wang, Q.; Lim, C. K.; Bonnett, R.; Berenbaum, M. C. *Br. J. Cancer* **1991**, *64*, 1116.

(17) Montforts, F.-P.; Meier, A.; Haake, G.; Höper, F. *Tetrahedron Lett.* **1991**, *32*, 3481.

(18) Silva, J. N.; Silva, A. M. G.; Tome, J. P.; Ribeiro, A. O.; Domingues, M. R. M.; Cavaleiro, J. A. S.; Silva, A. M. S.; Graca, M.; Neves, M. G. P. M. S.; Tome, A. C.; Serra, O. A.; Bosca, F.; Filipe, P.; Santuse, R.; Morliere, P. *Photochem. Photobiol. Sci.* **2008**, *7*, 834.

(19) Singh, S.; Aggarwal, A.; Thompson, S.; Tome, J. P. C.; Zhu, X. C.; Samaroo, D.; Vinodu, M.; Gao, R. M.; Drain, C. M. *Bioconjugate Chem.* **2010**, *21*, 2136.

(20) Silva, E. F. F.; Serpa, C.; Dąbrowski, J. M.; Monteiro, C. J. P.; Formosinho, S. J.; Stochel, G.; Urbanska, K.; Simões, S.; Pereira, M. M.; Arnaut, L. G. *Chem. Eur. J.* **2010**, *16*, 9273.

(21) Hajri, A.; Wack, S.; Meyer, C.; Smith, M. K.; Leberquier, C.; Kedinger, M.; Aprahamian, M. *Photochem. Photobiol.* **2002**, *75*, 140.

(22) Chen, Y.; Li, G.; Pandey, R. K. *Curr. Org. Synth.* **2004**, *8*, 1105.

(23) Allen, C. M.; Sharman, W. M.; Van Lier, J. E. *J. Porphyrins Phthalocyanines* **2001**, *05*, 161.

(24) Lukyanets, E. A. *J. Porphyrins Phthalocyanines* **1999**, *03*, 424.

(25) Soares, A. R. M.; Neves, M. G. P. M. S.; Tomé, A. C.; Iglesias-de la Cruz, M. C.; Zamarrón, A.; Carrasco, E.; González, S.; Cavaleiro, J. A. S.; Torres, T.; Guldi, D. M.; Juarranz, A. *Chem. Res. Toxicol.* **2012**, *25*, 940.

(26) Pereira, P. M. R.; Silva, S.; Cavaleiro, J. A. S.; Ribeiro, C. A. F.; Tome, J. P. C.; Fernandes, R. *Plos One* **2014**, *9*.

(27) Lourenco, L. M. O.; Neves, M. G. P. M. S.; Cavaleiro, J. A. S.; Tome, J. P. C. *Tetrahedron* **2014**, *70*, 2681.

(28) Clifton, J. I.; Leikin, J. B. *Am. J. Ther.* **2003**, *10*, 289.

(29) Agostinis, P.; Berg, K.; Cengel, K. A.; Foster, T. H.; Girotti, A. W.; Gollnick, S. O.; Hahn, S. M.; Hamblin, M. R.; Juzeniene, A.; Kessel, D.; Korbelik, M.; Moan, J.; Mroz, P.; Nowis, D.; Piette, J.; Wilson, B. C.; Golab, J. *CA Cancer J Clin.* **2011**, *61*, 250.

(30) Allison, R. R.; Sibata, C. H. *Photodiagn. Photodyn. Ther.*, *7*, 61.

(31) Yoon, I.; Li, J. Z.; Shim, Y. K. *Clin. Endosc.* **2013**, *46*, 7.

(32) Castano, A. P.; Demidova, T. N.; Hamblin, M. R. *Photodiagn. Photodyn. Ther.* **2004**, *1*, 279.

(33) Figueira, F.; Pereira, P. M. R.; Silva, S.; Cavaleiro, J. A. S.; Tome, J. P. C. *Curr. Org. Synth.* **2014**, *11*, 110.

(34) Dolmans, D. E. J. G. J.; Fukumura, D.; Rakesh, J. K. *Nature* **2003**, *3*, 380.

(35) Ormond, A.; Freeman, H. *Materials* **2013**, *6*, 817.

(36) Chatterjee, D. K.; Fong, L. S.; Zhang, Y. *Adv. Drug Delivery Rev.* **2008**, *60*, 1627.

(37) Idris, N. M.; Gnanasammandhan, M. K.; Zhang, J.; Ho, P. C.; Mahendran, R.; Zhang, Y. *Nat. Med.* **2012**, *18*, 1580.

(38) Qian, H. S.; Guo, H. C.; Ho, P. C.-L.; Mahendran, R.; Zhang, Y. *Small* **2009**, *5*, 2285.

(39) Couleaud, P.; Morosini, V.; Frochot, C.; Richeter, S.; Raehma, L.; Durand, J.-O. *Nanoscale* **2010**, *2*, 1083.

(40) Kobayashi, H.; Watanabe, R.; Choyke, P. L. *Theranostics* **2014**, *4*, 81.

(41) Maeda, H. *Bioconjugate Chem.* **2010**, *21*, 797.

(42) Tang, L.; Cheng, J. *Nano Today* **2013**, *8*, 290.

(43) Ribeiro, T.; Raja, S.; Rodrigues, A. S.; Fernandes, F.; Farinha, J. P. S.; Baleizao, C. *RSC Adv.* **2013**, *3*, 9171.

(44) Gomes, M. C.; Fernandes, R.; Cunha, A.; Tome, J. P.; Trindade, T. *J. Mater. Chem. B* **2013**, *1*, 5429.

(45) Wolfbeis, O. S. *Chem. Soc. Rev.* **2015**, *44*, 4743.

(46) Granadeiro, C. M.; Ferreira, R. A. S.; Soares-Santos, P. C. R.; Carlos, L. D.; Trindade, T.; Nogueira, H. I. S. *J. Mater. Chem.* **2010**, *20*, 3313.

(47) Iwu, K. O.; Soares-Santos, P. C. R.; Nogueira, H. I. S.; Carlos, L. D.; Trindade, T. *The Journal of Physical Chemistry C* **2009**, *113*, 7567.

(48) Ow, H.; Larson, D. R.; Srivastava, M.; Baird, B. A.; Webb, W. W.; Wiesner, U. *Nano Lett.* **2005**, *5*, 113.

(49) Yang, P.; Gai, S.; Lin, J. *Chem. Soc. Rev.* **2012**, *41*, 3679.

(50) Xie, M.; Shi, H.; Ma, K.; Shen, H.; Li, B.; Shen, S.; Wang, X.; Jin, Y. *J. Colloid Interface Sci.* **2013**, *395*, 306.

(51) Wang, Y.; Zhao, Q.; Han, N.; Bai, L.; Li, J.; Liu, J.; Che, E.; Hu, L.; Zhang, Q.; Jiang, T.; Wang, S. *Nanomed. Nanotechnol. Biol. Med.* **2015**, *11*, 313.

(52) Biju, V. *Chem. Soc. Rev.* **2014**, *43*, 744.

(53) Rejeeth, C.; Nag, T. C.; Kannan, S. *Cancer Nanotechnol.* **2013**, *4*, 127.

(54) Huang, I.-P.; Sun, S.-P.; Cheng, S.-H.; Lee, C.-H.; Wu, C.-Y.; Yang, C.-S.; Lo, L.-W.; Lai, Y.-K. *Mol. Cancer Ther.* **2011**, *10*, 761.

(55) Li, Z.-Y.; Liu, Y.; Wang, X.-Q.; Liu, L.-H.; Hu, J.-J.; Luo, G.-F.; Chen, W.-H.; Rong, L.; Zhang, X.-Z. *ACS Appl. Mater. Interfaces* **2013**, *5*, 7995.

(56) Simon, V.; Devaux, C.; Darmon, A.; Donnet, T.; Thiénot, E.; Germain, M.; Honnorat, J.; Duval, A.; Pottier, A.; Borghi, E.; Levy, L.; Marill, J. *Photochem. Photobiol.* **2010**, *86*, 213.

(57) Cheng, S.-H.; Lee, C.-H.; Yang, C.-S.; Tseng, F.-G.; Mou, C.-Y.; Lo, L.-W. *J. Mater. Chem.* **2009**, *19*, 1252.

(58) Yan, F.; Kopelman, R. *Photochem. Photobiol.* **2003**, *78*, 587.

(59) Wang, T.; Zhang, L.; Su, Z.; Wang, C.; Liao, Y.; Fu, Q. *ACS Appl. Mater. Interfaces* **2011**, *3*, 2479.

(60) Fan, W.; Shen, B.; Bu, W.; Chen, F.; He, Q.; Zhao, K.; Zhang, S.; Zhou, L.; Peng, W.; Xiao, Q.; Ni, D.; Liu, J.; Shi, J. *Biomaterials* **2014**, *35*, 8992.

(61) Yang, Y.; Yu, M.; Song, H.; Wang, Y.; Yu, C. *Nanoscale* **2015**, *7*, 11894.

(62) Botella, P.; Ortega, I.; Quesada, M.; Madrigal, R. F.; Muniesa, C.; Fimia, A.; Fernandez, E.; Corma, A. *Dalton Trans.* **2012**, *41*, 9286.

(63) Hervault, A.; Thanh, N. T. K. *Nanoscale* **2014**, *6*, 11553.

(64) Andhariya, N.; Chudasama, B.; Upadhyay, R. V.; Mehta, R. V. *Int. J. Nanosci.* **2011**, *10*, 1061.

(65) Carvalho, C. M. B.; Alves, E.; Costa, L.; Tomé, J. P. C.; Faustino, M. A. F.; Neves, M. G. P. M. S.; Tomé, A. C.; Cavaleiro, J. A. S.; Almeida, A.; Cunha, Â.; Lin, Z.; Rocha, J. *ACS Nano* **2010**, *4*, 7133.

(66) Martín-Saavedra, F. M.; Ruíz-Hernández, E.; Boré, A.; Arcos, D.; Vallet-Regí, M.; Vilaboa, N. *Acta Biomater.* **2010**, *6*, 4522.

(67) Villanueva, A.; de la Presa, P.; Alonso, J. M.; Rueda, T.; Martínez, A.; Crespo, P.; Morales, M. P.; Gonzalez-Fernandez, M. A.; Valdés, J.; Rivero, G. *The Journal of Physical Chemistry C* **2010**, *114*, 1976.

(68) Gongalsky, M. B.; Kargina, Y. V.; Osminkina, L. A.; Perepukhov, A. M.; Gulyaev, M. V.; Vasiliev, A. N.; Pirogov, Y. A.; Maximychev, A. V.; Timoshenko, V. Y. *Appl. Phys. Lett.* **2015**, *107*, 233702.

(69) Yan, F.; Xu, H.; Anker, J.; Kopelman, R.; Ross, B.; Rehemtulla, A.; Reddy, R. *J. Nanosci. Nanotechnol.* **2004**, *4*, 72.

(70) Iqbal, M. Z.; Ma, X.; Chen, T.; Zhang, L. e.; Ren, W.; Xiang, L.; Wu, A. *J. Mater. Chem. B* **2015**, *3*, 5172.

(71) Schroeder, A.; Heller D., A.; Winslow, M. M.; Dahlman, J. E.; Pratt, G. W.; Langer, R.; Jacks, T.; Anderson, D. G. *Nature* **2012**, *12*, 39.

(72) Kresge, C. T.; Leonowicz, M. E.; Roth, W. J.; Vartuli, J. C.; Beck, J. S. *Nature* **1992**, *359*, 710.

(73) Vallet-Regi, M.; Rámila, A.; del Real, R. P.; Pérez-Pariente, J. *Chem. Mater.* **2001**, *13*, 308.

(74) Slowing, I. I.; Trewyn, B. G.; Giri, S.; Lin, V. S. Y. *Adv. Funct. Mater.* **2007**, *17*, 1225.

(75) Muñoz, B.; Rámila, A.; Pérez-Pariente, J.; Díaz, I.; Vallet-Regí, M. *Chem. Mater.* **2003**, *15*, 500.

(76) Yu, B. O.; Tai, H. C.; Xue, W.; Lee, L. J.; Lee, R. J. *Mol. Membr. Biol.* **2010**, *27*, 286.

(77) Yu, M. K.; Park, J.; Jon, S. *Theranostics* **2012**, *2*, 3.

(78) Conniot, J.; Silva, J. M.; Fernandes, J. G.; Silva, L. C.; Gaspar, R.; Brocchini, S.; Florindo, H. F.; Barata, T. S. *Front. Chem.* **2014**, *2*.

(79) Zhao, X.; Li, H.; Lee, R. J. *Expert Opin. Drug Deliv.* **2008**, *5*, 309.

(80) Low, P. S.; Henne, W. A.; Doorneweerd, D. D. *Acc. Chem. Res.* **2008**, *41*, 120.

(81) Yang, H.; Lou, C.; Xu, M.; Wu, C.; Miyoshi, H.; Liu, Y. *Int. J. Nanomed.* **2011**, *6*, 2023.

(82) Yin, F.; Zhang, B.; Zeng, S.; Lin, G.; Tian, J.; Yang, C.; Wang, K.; Xu, G.; Yong, K.-T. *J. Mater. Chem. B* **2015**, *3*, 6081.

(83) Asefa, T.; Tao, Z. *Chem. Res. Toxicol.* **2012**, *25*, 2265.

(84) Knežević, N. Ž.; Durand, J.-O. *ChemPlusChem* **2015**, *80*, 26

(85) Lu, J.; Liong, M.; Li, Z.; Zink, J. I.; Tamanoi, F. *Small* **2010**, *16*, 1794.

(86) Lu, J.; Liong, M.; Zink, J. I.; Tamanoi, F. *Small* **2007**, *3*, 1341.

(87) He, X.; Wu, X.; Wang, K.; Shi, B.; Hai, L. *Biomaterials* **2009**, *2009*, 5601.

(88) Akbar, N.; Mohamed, T.; Whitehead, D.; Azzawi, M. *Biotechnol. Appl. Biochem.* **2011**, *58*, 353.

(89) Stober, W.; Fink, A. *J. Colloid Interface Sci.* **1968**, *26*, 62.

(90) Van Blaaderen, A.; Van Greest, J.; Vrij, A. *J. Colloid Interface Sci.* **1992**, *154*, 481.

(91) Guerrero-Martínez, A.; Pérez-Juste, J.; Liz-Marzán, L. M. *Adv. Mater.* **2010**, *22*, 1182.

(92) Bagwe, R. P.; Yang, C.; Hilliard, L. R.; Tan, W. *Langmuir* **2004**, *20*, 8336.

(93) Figueira, F.; Cavaleiro, J. A. S.; Tomé, J. P. C. *J. Porphyrins Phthalocyanines* **2011**, *15*, 517.

(94) Guo, X.; Guo, B.; Sun, X.; Zhang, Q.; Shi, T. *Chin. J. Chem.* **2011**, *29*, 363.

(95) Li, W.; Lu, W.; Fan, Z.; Zhu, X.; Reed, A.; Newton, B.; Zhang, Y.; Courtney, S.; Tiyyagura, P. T.; Li, S.; Butler, E.; Yu, H.; Ray, P. C.; Gao, R. *J. Mater. Chem.* **2012**, *22*, 12701.

(96) Qian, J.; Wang, D.; Cai, F.; Zhan, Q.; Wang, Y.; He, S. *Biomaterials* **2012**, *33*, 4851.

(97) Teng, I. T.; Chang, Y.-J.; Wang, L.-S.; Lu, H.-Y.; Wu, L.-C.; Yang, C.-M.; Chiu, C.-C.; Yang, C.-H.; Hsu, S.-L.; Ho, J.-a. A. *Biomaterials* **2013**, *34*, 7462.

(98) Wang, L.-S.; Wu, L.-C.; Lu, S.-Y.; Chang, L.-L.; Teng, I. T.; Yang, C.-M.; Ho, J.-a. A. *ACS Nano* **2010**, *4*, 4371.

(99) Vivero-Escoto, J. L.; Vega, D. L. *RSC Adv.* **2014**, *4*, 14400.

(100) Deng, X.; Xiong, L.; Lin, L.; Xiong, G.; Miao, X. *Photodiagn. Photodyn. Ther.* **2013**, *10*, 460.

(101) Liu, Z.-T.; Xiong, L.; Liu, Z.-P.; Miao, X.-Y.; Lin, L.-W.; Wen, Y. *Nanoscale Res. Lett.* **2014**, *9*, 319.

(102) Selvestrel, F.; Moret, F.; Segat, D.; Woodhams, J. H.; Fracasso, G.; Echevarria, I. M. R.; Bau, L.; Rastrelli, F.; Compagnin, C.; Reddi, E.; Fedeli, C.; Papini, E.; Tavano, R.; Mackenzie, A.; Bovis, M.; Yaghini, E.; MacRobert, A. J.; Zanini, S.; Boscaini, A.; Colombatti, M.; Mancin, F. *Nanoscale* **2013**, *5*, 6106.

(103) Perrier, M.; Gary-Bobo, M.; Lartigue, L.; Brevet, D.; Morère, A.; Garcia, M.; Maillard, P.; Raehm, L.; Guari, Y.; Larionova, J.; Durand, J.-O.; Mongin, O.; Blanchard-Desce, M. *J. Nanopart. Res.* **2013**, *15*, 1.

(104) Dongyu, L.; Hequn, Z.; Liliang, C.; Xinyuan, Z.; Jun, Q. *Opt. Quantum Electron.* **2015**, *47*, 3081.

(105) Barata, J. F. B.; Daniel-da-Silva, A. L.; Neves, M. G. P. M. S.; Cavaleiro, J. A. S.; Trindade, T. *RSC Adv.* **2013**, *3*, 274.

(106) Tu, J.; Wang, T.; Shi, W.; Wu, G.; Tian, X.; Wang, Y.; Ge, D.; Ren, L. *Biomaterials* **2012**, *33*, 7903.

(107) Ma, X.; Sreejith, S.; Zhao, Y. *ACS Appl. Mater. Interfaces* **2013**, *5*, 12860.

(108) Zhao, Y.-L.; Li, Z.; Kabehie, S.; Botros, Y. Y.; Stoddart, J. F.; Zink, J. I. *J. Am. Chem. Soc.* **2010**, *132*, 13016.

(109) Zhao, B.; Duan, W.; Lo, P.-C.; Duan, L.; Wu, C.; Ng, D. K. P. *Chem. Asian J.* **2013**, *8*, 55.

(110) Ke, X.; Wang, D.; Chen, C.; Yang, A.; Han, Y.; Ren, L.; Li, D.; Wang, H. *Nanoscale Res. Lett.* **2014**, *9*, 666.

(111) Nikoobakht, B.; El-Sayed, M. A. *Chem. Mater.* **2003**, *15*, 1957.

(112) Wu, C.; Xu, Q.-H. *Langmuir* **2009**, *25*, 9441.

(113) Wang, F.; Chen, X.; Zhao, Z.; Tang, S.; Huang, X.; Lin, C.; Cai, C.; Zheng, N. *J. Mater. Chem.* **2011**, *21*, 11244.

(114) Sun, S.; Zeng, H.; Robinson, D. B.; Raoux, S.; Rice, P. M.; Wang, S. X.; Li, G. *J. Am. Chem. Soc.* **2004**, *126*, 273.

(115) Zhao, Z.; Han, Y.; Lin, C.; Hu, D.; Wang, F.; Chen, X.; Chen, Z.; Zheng, N. *Chem. Asian J.* **2012**, *7*, 830.

(116) Liu, X.; Qian, H.; Ji, Y.; Li, Z.; Shao, Y.; Hu, Y.; Tong, G.; Li, L.; Guo, W.; Guo, H. *RSC Adv.* **2012**, *2*, 12263.

(117) Qiao, X.-F.; Zhou, J.-C.; Xiao, J.-W.; Wang, Y.-F.; Sun, L.-D.; Yan, C.-H. *Nanoscale* **2012**, *4*, 4611.

(118) Gary-Bobo, M.; Hocine, O.; Brevet, D.; Maynadier, M.; Raehm, L.; Richeter, S.; Charasson, V.; Loock, B.; Morère, A.; Maillard, P.; Garcia, M.; Durand, J.-O. *Int. J. Pharm.* **2012**, *423* 509.

(119) Hocine, O.; Gary-Bobo, M.; Brevet, D.; Maynadier, M.; Fontanel, S.; Raehm, L.; Richeter, S.; Loock, B.; Couleaud, P.; Frochot, C.; Charnay, C.; Derrien, G.; Smaïhi, M.; Sahmoune, A.; Morère, A.; Maillard, P.; Garcia, M.; Durand, J.-O. *Int. J. Pharm.* **2010**, *402* 221.

(120) David Brevet, M. G.-B., Laurence Raehm, Sebastien Richeter, Ouahiba Hocine, Kassem Amro, Bernard Loock, Pierre Couleaud, Ce´line Frochot, Alain Morere, Philippe Maillard, Marcel Garcia, Jean-Olivier Durand *Chem. Commun.* **2009**, 1475.

(121) Sperling, O.; Fuchs, A.; Lindhorst, T. K. *Org. Biomol. Chem.* **2006**, *4*, 3913.

(122) Yang, G.; Gong, H.; Qian, X.; Tan, P.; Li, Z.; Liu, T.; Liu, J.; Li, Y.; Liu, Z. *Nano Res.* **2015**, *8*, 751.

(123) Yang, S.; Li, N.; Liu, Z.; Sha, W.; Chen, D.; Xu, Q.; Lu, J. *Nanoscale* **2014**, *6*, 14903.

(124) Yao, X.; Chen, X.; He, C.; Chen, L.; Chen, X. *J. Mater. Chem. B* **2015**, *3*, 4707.

(125) Chen, X.; Yao, X.; Zhang, Z.; Chen, L. *RSC Adv.* **2014**, *4*, 49137.

(126) Vivero-Escoto, J.; Elnagheeb, M. *Nanomaterials* **2015**, *5*, 2302.

(127) Vivero-Escoto, J. L.; Taylor-Pashow, K. M. L.; Huxford, R. C.; Della Rocca, J.; Okoruwa, C.; An, H.; Lin, W.; Lin, W. *Small* **2011**, *7*, 3519.

(128) Hayashi, K.; Nakamura, M.; Miki, H.; Ozaki, S.; Abe, M.; Matsumoto, T.; Kori, T.; Ishimura, K. *Adv. Funct. Mater.* **2014**, *24*, 503.

(129) Zhao, Z. X.; Huang, Y. Z.; Shi, S. G.; Tang, S. H.; Li, D. H.; Chen, X. L. *Nanotechnology* **2014**, *25*, 285701.

(130) Siegel, R.; Naishadham, D.; Jemal, A. *A Cancer Journal for Clinicians* **2013**, *63*, 11.

(131) Ahmad, A. S.; Ormiston-Smith, N.; Sasieni, P. D. *Br J Cancer* **2015**, *112*, 943.

(132) Bonnett, R. *Chemical Society Reviews* **1995**, *24*, 19.

(133) Henderson, B. W.; Dougherty, T. J. *Photochemistry and Photobiology* **1992**, *55*, 145.

(134) Dolmans, D. E. J. G. J.; Fukumura, D.; Jain, R. K. *Nat Rev Cancer* **2003**, *3*, 380.

(135) Macdonald, I. J.; Dougherty, T. J. *Journal of Porphyrins and Phthalocyanines* **2001**, *05*, 105.

(136) Chatterjee, D. K.; Fong, L. S.; Zhang, Y. *Advanced Drug Delivery Reviews* **2008**, *60*, 1627.

(137) Idris, N. M.; Gnanasammandhan, M. K.; Zhang, J.; Ho, P. C.; Mahendran, R.; Zhang, Y. *Nature Medicine* **2012**, *18*, 1580.

(138) O'Connor, A. E.; Gallagher, W. M.; Byrne, A. T. *Photochemistry and Photobiology* **2009**, *85*, 1053.

(139) Hao, E.; Jensen, T. J.; Vicente, M. G. H. *Journal of Porphyrins and Phthalocyanines* **2009**, *13*, 51.

(140) Ma, L.; Moan, J.; Berg, K. *International Journal of Cancer* **1994**, *57*, 883.

(141) Kostenich, G. A.; Zhuravkin, I. N.; Zhavrid, E. A. *Journal of Photochemistry and Photobiology B: Biology* **1994**, *22*, 211.

(142) Ris, H. B.; Altermatt, H. J.; Inderbitzi, R.; Hess, R.; Nachbur, B.; Stewart, J. C.; Wang, Q.; Lim, C. K.; Bonnett, R.; Berenbaum, M. C. *British Journal of Cancer* **1991**, *64*, 1116.

(143) Montforts, F.-P.; Meier, A.; Haake, G.; Höper, F. *Tetrahedron Letters* **1991**, *32*, 3481.

(144) Silva, E. F. F.; Serpa, C.; Dąbrowski, J. M.; Monteiro, C. J. P.; Formosinho, S. J.; Stochel, G.; Urbanska, K.; Simões, S.; Pereira, M. M.; Arnaut, L. G. *Chemistry – A European Journal* **2010**, *16*, 9273.

(145) Hajri, A.; Wack, S.; Meyer, C.; Smith, M. K.; Leberquier, C.; Kedinger, M.; Aprahamian, M. *Photochemistry and Photobiology* **2002**, *75*, 140.

(146) Chen, Y.; Li, G.; Pandey, R. K. *Current Organic Chemistry* **2004**, *8*, 1105.

(147) Allen, C. M.; Sharman, W. M.; Van Lier, J. E. *Journal of Porphyrins and Phthalocyanines* **2001**, *05*, 161.

(148) Pereira, P. M. R.; Silva, S.; Cavaleiro, J. A. S.; Ribeiro, C. A. F.; Tomé, J. P. C.; Fernandes, R. *PLoS ONE* **2014**, *9*, e95529.

(149) Lukyanets, E. A. *Journal of Porphyrins and Phthalocyanines* **1999**, *03*, 424.

(150) Soares, A. R. M.; Neves, M. G. P. M. S.; Tomé, A. C.; Iglesias-de la Cruz, M. C.; Zamarrón, A.; Carrasco, E.; González, S.; Cavaleiro, J. A. S.; Torres, T.; Guldi, D. M.; Juarranz, A. *Chemical Research in Toxicology* **2012**, *25*, 940.

(151) Maeda, H. *Bioconjugate Chemistry* **2010**, *21*, 797.

(152) Biju, V. *Chemical Society Reviews* **2014**, *43*, 744.

(153) Dawidczyk, C. M.; Kim, C.; Park, J. H.; Russell, L. M.; Lee, K. H.; Pomper, M. G.; Searson, P. C. *Journal of Controlled Release* **2014**, *187*, 133.

(154) Pillai, G. *SOJ Pharmacy & Pharmaceutical Sciences* **2014**, *1*, 1.

(155) Gopalakrishna Pillai; Ceballos-Coronel, M. L. *SAGE Open Medicine* **2013**, *1*, 1.

(156) Wioleta, B.; Tito, T.; Tomás, T.; João, T. *Current Pharmaceutical Design* **2016**, *22*, 6021.

(157) Fei Yan, R. K. *Photochemistry and Photobiology* **2003**, *78*, 587.

(158) Agostinis, P.; Berg, K.; Cengel, K. A.; Foster, T. H.; Girotti, A. W.; Gollnick, S. O.; Hahn, S. M.; Hamblin, M. R.; Juzeniene, A.; Kessel, D.; Korbelik, M.; Moan, J.; Mroz, P.; Nowis, D.; Piette, J.; Wilson, B. C.; Golab, J. *A Cancer Journal for Clinicians* **2011**, *61*, 250.

(159) Allison, R.; Sibata, C. *Photodiagnosis and Photodynamic Therapy* **2010**, *7*, 61.

(160) Yoon, I.; Li, J. Z.; Shim, Y. K. *Clinical Endoscopy* **2013**, *46*, 7.

(161) Castano, A. P.; Demidova, T. N.; Hamblin, M. R. *Photodiagnosis and Photodynamic Therapy* **2004**, *1*, 279.

(162) Chen, X.; Hui, L.; Foster, D. A.; Drain, C. M. *Biochemistry* **2004**, *43*, 10918.

(163) Shiho HirohHirohara, S.; Obata, M.; Alitomo, H.; Sharyo, K.; Ando, T.; Yano, S.; Tanihara, M. *Bioconjugate Chemistry* **2009**, *20*, 944.

(164) Singh, S.; Aggarwal, A.; Thompson, S.; Tomé, J. P. C.; Zhu, X.; Samaroo, D.; Vinodu, M.; Gao, R.; Drain, C. M. *Bioconjugate Chemistry* **2010**, *21*, 2136.

(165) Hirohara, S.; Nishida, M.; Sharyo, K.; Obata, M.; Ando, T.; Tanihara, M. *Bioorganic & Medicinal Chemistry* **2010**, *18*, 1526.

(166) Hirohara, S.; Obata, M.; Alitomo, H.; Sharyo, K.; Ando, T.; Tanihara, M.; Yano, S. *Journal of Photochemistry and Photobiology B: Biology* **2009**, *97*, 22.

(167) Chen, X.; Hui, L.; Foster, D. A.; Drain, C. M. *Biochemistry* **2004**, *43*, 10918.

(168) Stober, W.; Fink, A. *Journal of Coloid and Interface Science* **1968**, *26*, 62.

(169) Shang, L.; Nienhaus, K.; Nienhaus, G. U. *Journal of Nanobiotechnology* **2014**, *12*, 5.

(170) Torchilin, V. *Advanced Drug Delivery Reviews* **2011**, *63*, 131.

(171) Biswas, S.; Torchilin, V. P. *Advanced Drug Delivery Reviews* **2014**, *66*, 26.

(172) Silva, S.; Pereira, P. M. R.; Silva, P.; Almeida Paz, F. A.; Faustino, M. A. F.; Cavaleiro, J. A. S.; Tome, J. P. C. *Chemical Communications* **2012**, *48*, 3608.

(173) Pereira, P. M. R.; Silva, S.; Ramalho, J. S.; Gomes, C. M.; Girão, H.; Cavaleiro, J. A. S.; Ribeiro, C. A. F.; Tomé, J. P. C.; Fernandes, R. *European Journal of Cancer* **2016**, *68*, 60.

(174) Pereira, P. M. R.; Silva, S.; Bispo, M.; Zuzarte, M.; Gomes, C.; Girão, H.; Cavaleiro, J. A. S.; Ribeiro, C. A. F.; Tomé, J. P. C.; Fernandes, R. *Bioconjugate Chemistry* **2016**, *27*, 2762.

(175) Bancirova, M. *Luminescence* **2011**, *26*, 685.

(176) Aruoma, O. I.; Halliwell, B.; Hoey, B. M.; Butler, J. *Free Radical Biology and Medicine* **1989**, *6*, 593.

(177) Vallet-Regi, M.; Rámila, A.; del Real, R. P.; Pérez-Pariente, J. *Chemistry of Materials* **2001**, *13*, 308.

(178) Slowing, I. I.; Trewyn, B. G.; Giri, S.; Lin, V. S. Y. *Advanced Functional Materials* **2007**, *17*, 1225.

(179) Muñoz, B.; Rámila, A.; Pérez-Pariente, J.; Díaz, I.; Vallet-Regí, M. *Chemistry of Materials* **2003**, *15*, 500.

(180) Siegel, R. L.; Miller, K. D.; Jemal, A. *CA: A Cancer Journal for Clinicians* **2016**, *66*, 7.

(181) Detty, M. R.; Gibson, S. L.; Wagner, S. J. *Journal of Medicinal Chemistry* **2004**, *47*, 3897.

(182) Cheng, S.-H.; Lee, C.-H.; Yang, C.-S.; Tseng, F.-G.; Mou, C.-Y.; Lo, L.-W. *Journal of Materials Chemistry* **2009**, *19*, 1252.

(183) Tu, H.-L.; Lin, Y.-S.; Lin, H.-Y.; Hung, Y.; Lo, L.-W.; Chen, Y.-F.; Mou, C.-Y. *Advanced Materials* **2009**, *21*, 172.

(184) Zhang, R.; Wu, C.; Tong, L.; Tang, B.; Xu, Q.-H. *Langmuir* **2009**, *25*, 10153.

(185) Brevet, D.; Gary-Bobo, M.; Raehm, L.; Richeter, S.; Hocine, O.; Amro, K.; Loock, B.; Couleaud, P.; Frochot, C.; Morere, A.; Maillard, P.; Garcia, M.; Durand, J.-O. *ChemComm* **2009**, 1475.

(186) Cheng, S.-H.; Lee, C.-H.; Chen, M.-C.; Souris, J. S.; Tseng, F.-G.; Yang, C.-S.; Mou, C.-Y.; Chen, C.-T.; Lo, L.-W. *Journal of Materials Chemistry* **2010**, *20*, 6149.

(187) Hocine, O.; Gary-Bobo, M.; Brevet, D.; Maynadier, M.; Fontanel, S.; Raehm, L.; Richeter, S.; Loock, B.; Couleaud, P.; Frochot, C.; Charnay, C.; Derrien, G.; Smaïhi, M.; Sahmoune, A.; Morère, A.; Maillard, P.; Garcia, M.; Durand, J.-O. *International Journal of Pharmaceutics* **2010**, *402* 221.

(188) Cindolo, L.; Benvenuto, G.; Salvatore, P.; Pero, R.; Salvatore, G.; Mirone, V.; Prezioso, D.; Altieri, V.; Bruni, C. B.; Chiariotti, L. *International Journal of Cancer* **1999**, *84*, 39.

(189) Carruthers, A.; DeZutter, J.; Ganguly, A.; Devaskar, S. U. *American Journal of Physiology - Endocrinology And Metabolism* **2009**, *297*, E836.

(190) Fernandes, R.; Hosoya, K.-i.; Pereira, P. *American Journal of Physiology - Cell Physiology* **2011**, *300*, C927.

(191) Chan, H. B. S.; Budd, P. M.; Naylor, T. d. *Journal of Materials Chemistry* **2001**, *11*, 951.

(192) Huang, X.; Li, L.; Liu, T.; Hao, N.; Liu, H.; Chen, D.; Tang, F. *ACS Nano* **2011**, *5*, 5390.

(193) Huang, X.; Teng, X.; Chen, D.; Tang, F.; He, J. *Biomaterials* **2010**, *31*, 438.

(194) Hao, N.; Yang, H.; Li, L.; Li, L.; Tang, F. *New Journal of Chemistry* **2014**, *38*, 4258.

(195) Frey, B. L.; Corn, R. M. *Analytical Chemistry* **1996**, *68*, 3187.

(196) Feifel, S. C.; Lisdat, F. *Journal of Nanobiotechnology* **2011**, *9*, 59.

(197) Suteewong, T.; Sai, H.; Bradbury, M.; Estroff, L. A.; Gruner, S. M.; Wiesner, U. *Chemistry of Materials* **2012**, *24*, 3895.

(198) Piao, Y.; Burns, A.; Kim, J.; Wiesner, U.; Hyeon, T. *Advanced Functional Materials* **2008**, *18*, 3745.

(199) Silva, S.; Pereira, P. M. R.; Silva, P.; Paz, F. A. A.; Faustino, M. A. F.; Cavaleiro, J. A. S.; Tome, J. P. C. *Chem Commun* **2012**, *48*, 3608.

(200) Lourenco, L. M.; Pereira, P. M.; Maciel, E.; Valega, M.; Domingues, F. M.; Domingues, M. R.; Neves, M. G.; Cavaleiro, J. A.; Fernandes, R.; Tome, J. P. *Chem Commun (Camb)* **2014**, *50*, 8363.

(201) Nyst, H. J.; Tan, I. B.; Stewart, F. A.; Balm, A. J. M. *Photodiagnosis and Photodynamic Therapy* **2009**, *6*, 3.

(202) Wolf, P.; Rieger, E.; Kerl, H. *Journal of the American Academy of Dermatology* **1993**, *28*, 17.

(203) Deda, D. K.; Araki, K. *Journal of the Brazilian Chemical Society* **2015**, *26*, 2448.

(204) van Straten, D.; Mashayekhi, V.; de Bruijn, H.; Oliveira, S.; Robinson, D. *Cancers* **2017**, *9*, 19.

(205) Rio, Y.; Salome Rodriguez-Morgade, M.; Torres, T. *Organic & Biomolecular Chemistry* **2008**, *6*, 1877.

(206) Venkatramaiah, N.; Pereira, P. M. R.; Almeida Paz, F. A.; Ribeiro, C. A. F.; Fernandes, R.; Tome, J. P. C. *Chemical Communications* **2015**, *51*, 15550.

(207) Auger, A.; Samuel, J.; Poncelet, O.; Raccurt, O. *Nanoscale Research Letters* **2011**, *6*, 328.